Journal of Research of the National Bureau of Standards Vol. 48, No. 2, February 1952 Research Paper 2291

Film-Rupture Mechanism of Stress Corrosion

Hugh L. Logan

The atmospherically formed protective films were removed by abrasion in an argon atmosphere from surfaces of an aluminum alloy, two brasses, a magnesium alloy, and low-carbon and stainless steels. The resulting surfaces were 0.12 to 0.76 volt more negative with respect to a calomel electrode than surfaces prepared and measured under normal atmospheric conditions. Appreciable changes in electrochemical solution potentials of notched specimens, stressed in tension, occurred at or just above stresses at which the true stress–true strain curves deviated from the modulus lines. These changes in potential were caused by rupturing of the protective films at the roots of the notches and were of the order of 0.16 to 0.70 volt at failure, depending on the material. Stress corrosion is postulated to occur in corrosive media, at stresses sufficient to rupture the protective film, by electrolytic action between the filmed (cathodic) and film-free (anodic) areas.

1. Introduction

Stress-corrosion cracking has been defined as the "spontaneous failure of metal by cracking under the combined action of corrosion and stress, residual or applied" [1].[1] Service failures have frequently resulted from residual stresses set up in the material or structure during fabrication. These stresses may result from the spinning or deep drawing of sheet brass, the work-hardening of aluminum-alloy tubing, the pressing of oversized bushings into aluminum-alloy fittings, the riveting or welding of steel structures, or even as the result of the application of excessive torques in the assembling of brass-pipe structures [2]. Stress-corrosion cracking may be either intercrystalline, as in aluminum alloys, alpha brass, and low-alloy steels, or transcrystalline, as is usually the case in magnesium-base alloys and the austenitic stainless steels.

It is agreed by most workers in the field that some degree of stress-corrosion cracking can be produced in many alloys and commercially pure metals by the proper combinations of stresses and corrosive media. The ASTM-AIMME Symposium on Stress-Corrosion Cracking of Metals [3], published in 1944, gives an excellent summary of work in the field to that date. A number of papers have also appeared in recent years [4 to 8, 10] that contain excellent bibliographies. For the most part, the data in the literature are from investigations of the relative susceptibilities of various materials to stress-corrosion cracking, susceptibilities of particular materials to stress corrosion in specific corrosive media, or susceptibilities of particular materials to stress corrosion after various mechanical or thermal treatments.

The purpose of this investigation was to study the mechanism of stress corrosion and not to determine the relative susceptibilities of various materials to stress corrosion. Recently the various theories of the mechanism of stress corrosion were summarized by Harwood [10]. Of these theories the "Generalized theory of stress corrosion" proposed by Mears, Brown, and Dix [11], the "Mechanical theory" of Keating [5], and the "Film rupture theory", or better, "Film rupture mechanism," are pertinent to the present paper. It is considered in this paper that the "Film rupture mechanism" and the "Mechanical theory" are logical parts of the Generalized theory.

In the Generalized theory, corrosion is postulated to occur by an electrochemical mechanism along localized paths that are anodic to the surrounding metal. There will be stress concentrations at the bases of localized corroded areas; the deeper the attack and . . . "the smaller the radius at the base of the path the greater would be the stress concentration. Such a condition would act to pull the metal apart along more or less continuous paths. At sufficient concentrations of stress, the metal might start to tear apart by mechanical action . . . the tearing action described above would expose fresh metal, unprotected by films, to the action of the corrosive environment. Because this freshly exposed metal is more anodic, an increase in current from the base of the localized path to the unaffected surface would be expected . . .". It is seen from this quotation that Mears and his coworkers [11] postulate a mechanism in which protective films on metal surfaces are ruptured. Keating [5] suggested that each advancing section of the crack in time encounters an obstacle in the form of a nonmetallic inclusion, lattice discontinuity, or unfavorably orientated grain boundary. In each case, the result may be reduction in the stress-concentration effect to a level at which cracking cannot proceed. Such a process would explain branching of stress-corrosion cracks, sudden changes in direction at grain boundaries, etc. Gilbert and Haden [12] report the results of an investigation on an aluminum alloy containing 7 percent of magnesium in which they found that the cracking process was not continuous but stepwise.

There are few published data from which the electrochemical solution potential of the freshly torn metal at the root of the crack can be estimated. Work at the National Bureau of Standards as early as 1940 showed that the solution potential of freshly quenched or freshly abraded 24S-T aluminum-alloy sheet was much more electronegative (anodic) than that of the same material permitted to stand for

[1] Figures in brackets indicate the literature references at the end of this paper.

some minutes before measurements were made [13]. Similar results were recently obtained at the Bureau on 18-percent-Cr–8-percent-Ni austenitic stainless steels. Mears and Brown [14] report a solution potential greater than −3.0 v for commercially pure aluminum from which the film was removed by scratching the surface with a glass stylus in the electrolyte. Druet and Jacquet [15] report values of −0.75 v for mechanically polished specimens containing 99.99 percent of aluminum (presumably with a protective film intact) and −1.384 v for the same material with measurements made immediately after electrolytic polishing.

The author is not aware of any data giving the magnitude of changes in solution potential produced by rupture of protective films on the metals or alloys that are particularly susceptible to stress corrosion. Such data are necessary to establish the validity of the so-called film rupture process in the generalized theory of stress corrosion. In the early phases of the investigation of the mechanism of stress corrosion, the following have been determined and are reported in this paper: (a) the electrochemical solution potentials of several alloys free from the protective effects of films,[2] and (b) relationships between the applied stresses and the electrochemical solution potentials of these alloys.

2. Materials and Methods of Test

The materials used in this investigation were 24S-T4 aluminum alloy, 70-percent-Cu–30-percent-Zn cartridge brass, 61-percent-Cu–36-percent-Zn–3-percent-Pb leaded brass, AZ31f magnesium alloy, low-carbon steel, and type 302 stainless steel. The chemical compositions are given in table 1. The aluminum alloy, the leaded brass, and the steels were obtained commercially. The magnesium alloy was supplied by the Dow Chemical Co., and the cartridge brass was made in the Bureau's Experimental Foundry from electrolytic copper and 99.99-percent zinc. Prior to machining of the specimens, the materials were heat treated as follows: (a) The aluminum-alloy stock was solution heat-treated at 920°±10° F, and quenched in water at approximately 70° F, (b) the cartridge brass was rolled to a diameter of about 0.62 in. and then annealed for 1 hour at 1,560° F, after which the Brinell hardness number was 66 and the grain size approximately 0.025 mm, (c) the low-carbon steel, originally in the cold-rolled condition, was heated to 1,625° F and cooled with the furnace, (d) the stainless steel was heated to 1,950° F and quenched in cold water. The magnesium alloy, in the form of an extruded rod ½ in. in diameter, and the leaded-brass rod, ½ in. in diameter, were used as received. The magnesium alloy evidently had been extruded at a sufficiently high temperature that the metal had recrystallized following extrusion. The leaded brass had a Brinell hardness number of 113 and a grain size of 0.015 to 0.025 mm. The tensile properties, as determined on subsize (0.355-in. diameter) ASTM round tensile specimens, are given in table 2.

When the protective film on 24S–T4 aluminum alloy is broken in air, it tends to repair itself quite rapidly. Therefore, specimens were prepared by abrading them with "400 aloxite" metallographic polishing paper, and all measurements were made in an argon atmosphere [3] in a dry box. In making measurements, drops of the desired electrolyte were placed on the prepared surface and brought into electric contact with a calomel electrode of the saturated KCl type by means of an agar-agar bridge. Potential measurements were made with a pH meter, or for values in excess of 1.3 v, with the pH meter in series with a L&N type K potentiometer.

It was recognized that the preparation of the specimen surfaces by abrasion left the surfaces to be measured in the cold-worked condition and might produce phase changes in the stainless steel. In some earlier work at the Bureau the author reduced the thickness of some 24S–T4 aluminum-alloy sheet approximately 5 percent without appreciable changing its solution potential. Druet and Jacquet [15] showed that severely cold-worked high-purity aluminum was only about 0.04 v more negative than the annealed material. The author has seen no data on

[2] It is recognized that contact of an electrolyte, at least with the aluminum and magnesium alloys studied, may produce a protective film on the metal surfaces.

[3] An analysis of the argon by the mass spectrograph method showed 0.2 percent of N_2 as the only detectable impurity.

TABLE 1. *Chemical composition of metals used*

Material	Al	C	Cr	Cu	Fe	Pb	Mn	Mg	Ni	P	Si	S	Zn
	%	%	%	%	%	%	%	%	%	%	%	%	%
24S aluminum alloy [a]	.....	.....	.....	3.9	0.4	.....	0.6	1.4	.....	.....	0.1	.....	.....
Cartridge brass	.....	.....	.....	69.4	.....	.....	.....	.....	.....	.....	.....	.....	[b] 30.6
Leaded brass	.....	.....	.....	61.2	.....	3.0	.....	.....	.....	.....	.....	.....	[b] 35.8
AZ31 magnesium alloy [a]	2.9	.....	.....	0.01	.003	.....	.4	.....	.....	.....	.03	.....	1.0
Low-carbon steel	.....	0.17	.....	.....	.....	.....	.81	.....	.....	0.005	.019	0.024	.....
Type 302 stainless steel [c]	.....	.072	19.17	.....	.....	.....	.38	.....	8.63	.017	.297	.013	.....

[a] Determined spectroscopically. [b] By difference. [c] Manufacturer's analysis.

TABLE 2. *Mechanical properties of metals used*

Material	Ultimate tensile strength	Yield strength	Elongation in 1.4 in.
	1,000 lb/in.²	*1,000 lb/in.²*	*Percent*
24S–T4 aluminum alloy	69.4	42.5	24
Cartridge brass	48.1	16.3	54
Leaded brass	54.6	43.6	28
AZ31f magnesium alloy	41.0	33.5	11
Low-carbon steel	54.7	31.5	40
Type 302 stainless steel	91.1	33.5	77

the effect of cold-work on the solution potentials of other materials studied nor no the effect of a phase change on the solution potential of the stainless steel.

Stress-electrochemical solution potential relationships were obtained on notched specimens made in accordance with the drawing in figure 1. The specimens were covered, except for the threaded ends, with two coats of Glyptal red enamel. After the enamel had dried it was cut through by means of a razor blade so as to expose an extremely narrow width of metal around the specimen at the root of the notch. The specimens were placed in cells in a tensile-testing machine, figure 2, with a calomel electrode placed directly in the cell if potassium chloride was used as the electrolyte or in a beaker connected to the cell by an agar-agar bridge if some other electrolyte was used. The specimens were stressed to failure in the corroding solution, and the electrochemical solution potentials that corresponded to given loads were determined either with a pH meter used as a vacuum-tube voltmeter or a Miller multimeter (used as a high-resistance potentiometer). The free cross-head speed of the testing machine was held between 0.05 and 0.10 in./min. In order to obtain true stress–true strain and load–true stress relationships, three or more additional notched specimens of each material were broken in the uncorroded condition.[4] True stress–electrochemical solution potential relationships were then obtained by combining load–true stress and load-electrochemical solution potential data.

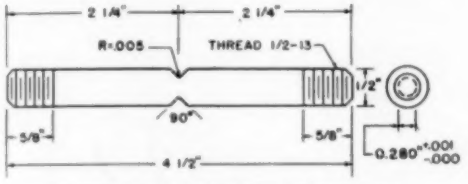

FIGURE 1. *Details of notched specimens.*

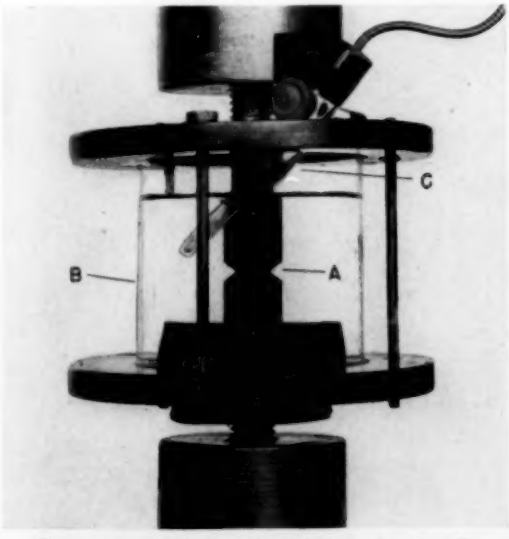

FIGURE 2. *Notched specimen (A) in place in cell, (B) in testing machine.*

Electrode (C) was placed directly in cell if potassium chloride was the corrodent, otherwise an agar-agar bridge was used.

3. Results and Discussion

3.1. Electrochemical Solution Potentials of the Metals

The different electrolytes used and the electrochemical solution potentials of the various materials, determined in air and in argon, are given in table 3. All values are in terms of a calomel electrode of the saturated KCl type and were determined at approximately 25° C. The values reported for atmospherically formed filmed surfaces were equilibrium values obtained by immersion of the prepared surfaces in their specific electrolytes; the values reported for the specimens prepared in argon were instantaneous maxima and not necessarily equilibrium values. These values are given inasmuch as they represent the conditions under which changes in electrochemical solution potential values reported in a later section of this paper were obtained.

TABLE 3. *Electrochemical solution potentials (with respect to calomel electrode of saturated KCl type) of materials with surfaces prepared and measurements made in air or argon*

Material	Electrolyte	Electrochemical solution potentials in—	
		Air	Argon
		Volt	*Volt*
24S–T4 aluminum alloy	KCl (saturated)	−0.67	−1.43
70%-Cu-30%-Zn brass	5% NH_4OH+ 5% $(NH_4)_2CO_3$	−.47	−0.96
61%-Cu-36%-Zn-3%-Pb brass	do	−.39	−.98
AZ31 magnesium alloy	3.5% NaCl+2% K_2CrO_4	−1.51	−1.645
Low-carbon steel	5% NH_4NO_3	−0.60	−0.72
Type 302 stainless steel	KCl (saturated)	−.28	−.78

The data indicate that, under normal atmospheric conditions, protective films are formed on the surfaces of these alloys. These filmed materials are in some cases as much as 0.76 v more electropositive than the same materials with surfaces prepared under argon. The largest differences in potential are found on the aluminum alloy, the brasses, and the stainless steel, all of which are relatively corrosion-resistant materials. Those materials that corrode more readily, such as low-carbon steel and the magnesium alloy, had very much smaller differences in potential between filmed and unfilmed surfaces.

In order to determine whether the difference in solution potential of the cartridge brass was due to the formation of an oxide film or to some other cause, the following investigation was carried out. A

[4] The use of notched specimens, of course, introduces stress concentrations of undetermined magnitude at the root of the notch. The maximum stress at the root of the notch is a function not only of the geometry of the specimen, but also of the applied stress. Although the radii of the notches used were small (approximately 0.005 in.), they were nevertheless large compared to those at the roots of stress-corrosion cracks in many materials.

specimen was placed in the dry box, and a surface was prepared and measured under argon. Approximately 20 percent of the argon was then replaced by dry oxygen, and additional measurements were made on the same surface. The experiment was repeated with wet oxygen, wet carbon dioxide, and dry ammonia gas. The results are given in table 4.

TABLE 4. *Electrochemical solution potentials of 70%-Cu–30%-Zn brass with surfaces prepared in an argon atmosphere and measurements made in a mixed atmosphere*

Electrolyte was 5% NH_4OH+5%$(NH_4)_2CO_3$

Atmosphere	Electrochemical solution potential
	Volt
Argon	−0.96
80% argon+20% dry O_2	−.45 to −.50
80% argon+20% wet O_2	−.45 to −.50
80% argon+20% wet CO_2	−.72 to −.78
80% argon+20% dry NH_3	−.53 to −.61
Air	−.47

It will be noted that in every case the solution potential was more positive after the addition of the second gas, the change being most marked in the case of oxygen, either dry or wet. In the atmosphere containing ammonia, the surface of the alloy adjacent to drops of liquid used in making the measurements became tarnished; its final potential was −0.31 v compared to −0.47 v for brass measured in air. Measurements made on the surfaces of brass specimens covered with a blue corrosion product after exposure to an atmosphere containing ammonia, carbon dioxide, air, and water vapor were 0.75 v more electropositive than film-free surfaces of the same alloy.

3.2. Stress–Electrochemical Solution Potential Relationships

The relationships between the true stresses and electrochemical solution potentials of the materials are shown in figures 3 to 8. The maximum values of the potentials were usually obtained just at the failure of the specimen as the result of the exposure of large areas of unfilmed material. These values are of course not shown on the figures but are given in table 5. In any measurement of electrochemical solution potentials the measured potentials are

TABLE 5. *Maximum change in electrochemical solution potential with stress.*

Material	Electrolyte	Change in electrochemical solution potential
		Volt
24S–T4 aluminum alloy	Saturated KCl	0.610
70%-Cu–30%-Zn Brass	5% NH_4OH+5% $(NH_4)_2CO_3$	.700
61%-Cu–36%-Zn–3%-Pb brass.	do	.510
AZ31 magnesium alloy	3.5% NaCl+2% K_2CrO_4	.240
Low-carbon steel	5% NH_4NO_3	.160
302 stainless steel	Saturated KCl	.315

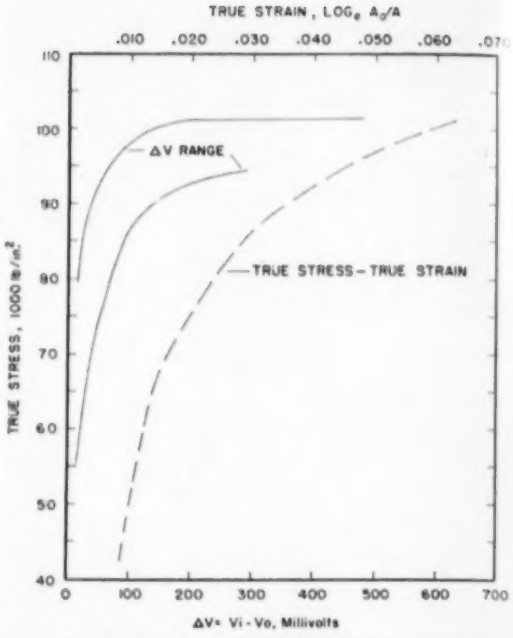

FIGURE 3. *True stress-electrochemical solution potential relationships for 24S–T4 aluminum alloy specimens.*

Corroding medium, saturated KCl. Data are from seven specimens.

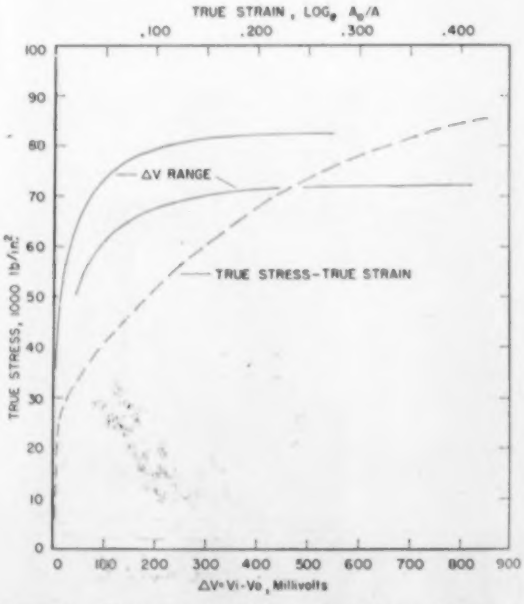

FIGURE 4. *True stress-electrochemical solution potential relationships for 70 percent* Cu–*30 percent* Zn *cartridge brass.*

Corroding medium, 5 percent NH_4OH +5 percent $(NH_4)_2CO_3$. Data are from seven specimens.

necessarily the integrated potentials over the entire area in contact with the electrolyte. It is therefore to be expected that potential measurements made on notched specimens of the same material may vary somewhat from specimen to specimen, hence the ranges of potential at given true stresses rather than average curves are shown in the graphs.

There was an appreciable change in the solution potential of the aluminum alloy (fig. 3) at stresses at which the true stress–true strain curve deviated from the modulus line, that is, at stresses at which plastic deformation had occurred. Marked changes in the potentials of the brass specimens (figs. 4 and 5) occurred at stresses that were 10,000 to 25,000 lb/in.^{2} above those at which the true stress–true strain curves deviated from the modulus line. The solution potential of the magnesium alloy changed appreciable at stresses only about one-third of those necessary to produce deviation from the modulus line (fig. 6). The yield point in the low-carbon steel was accompanied by a marked change in potential (fig. 7). Stresses sufficient to produce a deviation of the true stress–true strain curve from the modulus line for stainless steel also produced appreciable changes in the solution potential (fig. 8). The electrochemical solution potentials (except for the low-carbon steel) became increasingly more negative as the stresses were increased. For every material (except low-carbon steel) stresses were reached, as is seen in figures 3, 4, 5, 6 and 8, at which the slope of the true stress–potential curves decreased markedly, and the potential increased rapidly to the failure of the specimen.

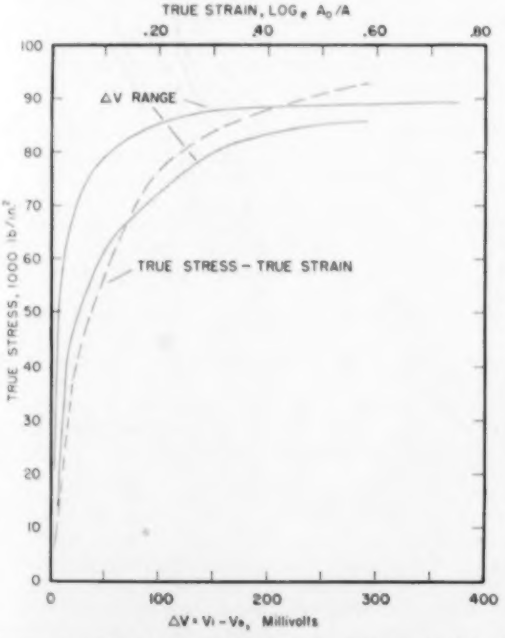

FIGURE 5. *True stress-electrochemical solution potential relationships for leaded brass.*

Corroding medium .5 percent NH_4OH +.5 percent $(NH_4)_2CO_3$. Data are from five specimens.

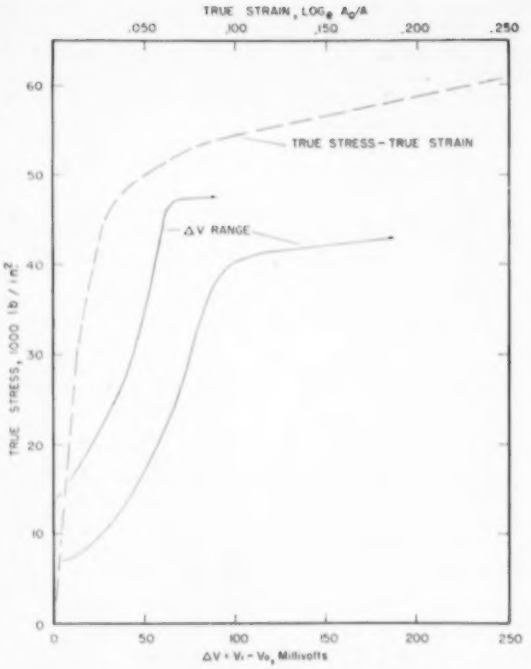

FIGURE 6. *True stress-electrochemical solution potential relationships for AZ31 magnesium alloy specimens.*

Corroding medium, 3.5 percent NaCl +2.0 percent K_2CrO_4. Data are from eight specimens.

It is postulated that during the loading of the specimens in tension the protective film is broken over minute areas of the surface. If the potential of the unprotected area alone could be measured, it would presumably be of the same order of magnitude as that determined on a film-free surface. The area where the film has been ruptured is very small compared with that of the filmed surface of a specimen, and consequently the measured potential differs by only a small amount from that obtained on an unbroken filmed surface. As the stresses are increased the ratio of the film free to the filmed surface of a specimen increases, and the solution potential becomes more negative, until at the instant of fracture the area of unfilmed surface may be very large compared to that of the filmed surface, and the potential may closely approach that of completely unfilmed material.

At a constant stress the protective film tends to repair itself. This was demonstrated by results obtained on aluminum-alloy specimens. After an appreciable change had been obtained in the solution potential during loading, the applied load was held constant, and within 1 minute the solution potential was the same as that of the unstressed specimen. After the specimens broke (exposing large unfilmed areas) the electrochemical solution potentials rapidly

assumed the same values as those of the filmed and unstressed materials.

Examination of the fractured surfaces of the notched specimens and the marked changes in the potentials of all of the materials except low-carbon steel at fracture indicated that the final failure had been almost instantaneous. In the low-carbon steel specimens, however, both the appearance of the fracture and the small change in potentials at failure indicated that prior to the final fracture, cracks had penetrated into the material from the roots of the notches and that the progression of fracture was not rapid and was probably discontinuous. Consequently, at failure the amount of freshly exposed unfilmed metal was too small to produce any marked change in the potential.

The data indicate that when the stresses are high enough to cause plastic deformation the atmospherically formed protective film will be broken and the exposed metal will become electronegative with respect to the filmed material. These film-free areas will, in general, be very small compared to the filmed areas. If such areas are connected to filmed areas by a conducting liquid, for example, by a drop of liquid containing dissolved gases or salts, a short-circuited electrolytic cell will be set up, the circuit being completed through the metal itself. As the film-free (anodic) area is generally very small compared with the filmed area, the current density over the anodic area will be high, and corrosion will proceed at a rapid rate until a readjustment of stresses permits reforming of the protective surface film. Corrosion will then become more general (or stress corrosion will proceed along different paths) until the stress concentration at the particular path under consideration again becomes sufficient to rupture the protective film. The author believes that successive breaks in the time-potential curves reported by Gilbert and Haden [12] indicate that such processes were occurring, probably at several points, on their test specimens.

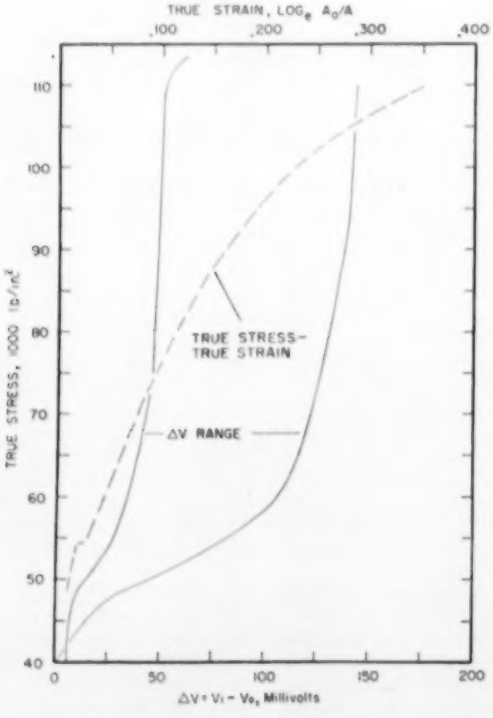

FIGURE 7. *True stress-electrochemical solution potential relationships for low-carbon steel.*

Corroding medium, 5-percent NH_4NO_3. Data are from nine specimens.

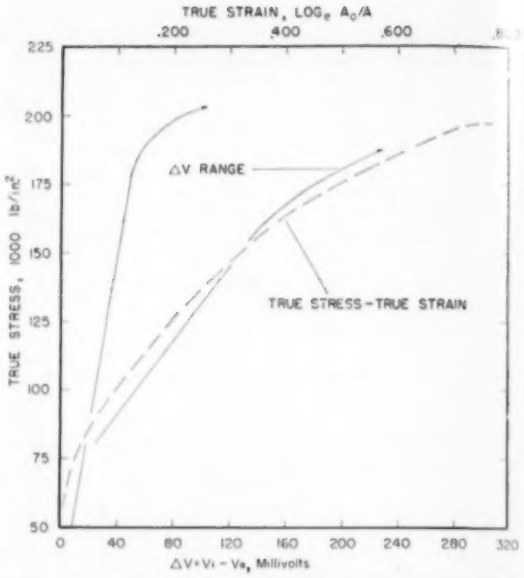

FIGURE 8. *True stress-electrochemical solution potential relationships for type 302 stainless steel specimens.*

Corroding medium, saturated KCl. Data are from six specimens.

The experiments reported in this paper confirm the general idea of the film-rupture mechanism suggested by Mears, Brown, and Dix. In the theory as first presented, it was postulated that tearing of the metal was necessary to expose film-free material. However, the present data indicate that film rupture occurs with comparatively small amounts of plastic deformation of the underlying material. When the film ruptures, stress corrosion may start in the film-free areas at stresses much below those normally required to tear the metal apart. Unless conditions permit film repair, stress corrosion may progress to cause complete failure in a relatively short time. If the film is restored and the stresses are not increased or readjusted, stress corrosion may cease. If, however, the stresses are readjusted by any means whatsoever, for example, by a change of external load or by corrosion, the film may again be broken and

stress corrosion proceed discontinuously to failure. The last process may be that which occurs in the transcrystalline type of stress corrosion.

4. Summary

As a part of a detailed study of the mechanism of stress corrosion, the electrochemical solution potentials of filmed and film-free surfaces and the true stress–electrochemical solution potential relationships for several alloys were determined.

The electrochemical solution potentials of surfaces, from which the atmospherically formed films had been removed by abrasion in an inert atmosphere, were 0.10 to 0.76 v more electronegative (with respect to a calomel electrode) than filmed surfaces of the same materials.

Appreciable changes in electrochemical solution potentials accompanied plastic deformation, and just prior to fracture the solution potentials were 0.16 to 0.70 v (depending on the alloy) more electronegative than the unstressed material.

The results of the investigation indicate that at stresses sufficiently high to produce failure of the protective film on metals, stress corrosion occurs in a corrosive medium by electrolytic action between film-free (anodic) and filmed (cathodic) areas. The process proceeds continuously or discontinously to failure, depending on whether or not the subsequent adjustment of stresses permits reforming of the protective film.

The author gratefully acknowledges the help of Thomas P. Royston, Jr., in obtaining the data presented in this paper.

5. References

[1] Metals Handbook, p. 14, 1948 ed. (Am. Soc. Metals, Cleveland, Ohio).
[2] W. B. Price, Am. Inst. Mining Engrs. **89,** 268 (1930).
[3] Symposium on Stress-Corrosion Cracking of Metals, Am. Soc. Testing Materials-Am. Inst. Mining Engrs., 1944 (Am. Soc. Testing Materials, Philadelphia, Pa.).
[4] U. R. Evans, Symposium on Internal Stresses in Metals and Alloys, Inst. Metals, p. 309 (1948).
[5] F. H. Keating, Symposium on Internal Stresses in Metals and Alloys, Inst. Metals, p. 329 (1948).
[6] E. Hugony, Alluminio **17,** 225 (1948).
[7] C. A. Zapffe, Trans. Am. Soc. Mech. Eng. **66,** 81 (1944).
[8] H. P. Croft and G. Sachs, Iron Age **151,** 47 (March 11, 1943); **151,** 62 (March 18, 1943).
[9] H. P. Croft, Proc. Am. Soc. Testing Materials **41,** 905 (1941).
[10] J. J. Harwood, Corrosion **6,** 249 and 290 (1950).
[11] R. B. Mears, R. H. Brown, and E. H. Dix, Jr., Symposium on Stress-Corrosion Cracking of Metals, Am. Soc. Testing Materials-Am. Inst. Mining Engrs., p. 329, 1944 (Am. Soc. Testing Materials, Philadelphia, Pa.).
[12] P. T. Gilbert and S. E. Haden, J. Inst. Metals **77,** 237 (May 1950).
[13] H. L. Logan, J. Research NBS **25,** 315 (1940) RP1328.
[14] R. B. Mears and R. H. Brown, Ind. Eng. Chem. **33,** 1001 (1941).
[15] Y. Druet and P. A. Jacquet, Metaux & Corrosion **22,** 139 (1947).

Washington, October 1, 1951.

Journal of Research of the National Bureau of Standards Vol. 48, No. 2, February 1952 Research Paper 2

A Note on the Bounds of the Real Parts of the Characteristic Roots of a Matrix[1]

P. Stein[2]

Two theorems are given for the bounds of the real parts of the characteristic roots of an $n\times n$ matrix, depending on the use of an arbitrary set of n positive numbers. The set is then specialized in several ways so as to lead to theorems for the bounds in terms of the elements of the matrix.

1. Fundamental Theorems

Let $A=(a_{ij})$ be an $n\times n$ matrix. Let M and m be the maximum and minimum real parts of its characteristic roots.

Let $u_1, u_2, \ldots, u_n$, be a set of positive numbers. In this note we prove the following two theorems:

Theorem A.

$$\text{(i)}\quad M\leqq\max_r\left\{\frac{1}{2}(a_{rr}+\bar{a}_{rr})+\frac{1}{2u_r}\sum_{\substack{s=1\\ s\neq r}}^{n}|a_{rs}+\bar{a}_{sr}|u_s\right\}$$

$$\text{(ii)}\quad m\geqq\min_r\left\{\frac{1}{2}(a_{rr}+\bar{a}_{rr})-\frac{1}{2u_r}\sum_{\substack{s=1\\ s\neq r}}^{n}|a_{rs}+\bar{a}_{sr}|u_s\right\}.$$

Theorem B. If the elements a_{rr} are real and the elements a_{rs}, $r\neq s$ are real and non-negative, then

$$\min_r\left(a_{rr}+\frac{1}{u_r}\sum_{\substack{s=1\\ s\neq r}}^{n}a_{rs}u_s\right)\leqq M\leqq\max_r\left(a_{rr}+\frac{1}{u_r}\sum_{\substack{s=1\\ s\neq r}}^{n}a_{rs}u_s\right).$$

Using these theorems and giving specific values to the set u_r, we obtain some further inequalities for M and m. These inequalities are numbered theorems 1 to 4. Theorem B is substantially a theorem of L. Collatz.[3]

To prove theorem A(i), we write $A=H+iK$, where H and K are Hermitian matrices whose elements h_{rs} and k_{rs} are given by

$$h_{rs}=\frac{a_{rs}+\bar{a}_{sr}}{2},\quad k_{rs}=\frac{i}{2}(\bar{a}_{sr}-a_{rs}). \tag{1}$$

It is known that the real parts of the characteristic roots of A are bounded above and below by the maximum and minimum characteristic roots (real) of H. Hence to prove A(i) it is sufficient to prove that the maximum characteristic root of H is less than the right-hand side of (i), and to prove A(ii) it is sufficient to prove that the minimum characteristic root is greater than the right-hand side of (ii).

Let λ and μ be the maximum and minimum characteristic roots of H. If x is a vector with n components, then h_{rr} is one value of x^*H_x/x^*x for all values of r, where x^* is the transpose of the conjugate of x. Hence $\lambda\geqq h_{rr}$, for all r, and $\mu\leqq h_{rr}$ for all r.

Let U be the diagonal matrix with elements $u_1, u_2, \ldots, u_n$. Let $B=U^{-1}HU$ and let its elements be b_{rs}. Then

$$b_{rs}=\frac{1}{u_r}h_{rs}u_s,\quad b_{rr}=h_{rr}. \tag{2}$$

As B is a transform of H, B and H have the same characteristic roots, so that λ and μ are characteristic roots of B. If α is any characteristic root of B, then α lies in at least one circle with center b_{rr} and radius

$$\sum_{\substack{s=1\\ s\neq r}}^{n}|b_{rs}|.$$

Thus we have

$$|\alpha-b_{rr}|\leqq\sum_{\substack{s=1\\ s\neq r}}^{n}|b_{rs}|$$

for at least one value of r.

As $\lambda-b_{rr}\geqq 0$, and $\mu-b_{rr}\leqq 0$, we have

$$\lambda\leqq b_{rr}+\sum_{\substack{s=1\\ s\neq r}}^{n}|b_{rs}|$$

for a least one value of r, and

$$\mu\geqq b_{rr}-\sum_{\substack{s=1\\ s\neq r}}^{n}|b_{rs}|$$

for at least one value of r. By (1) and (2), this completes the proof of theorem A.

Theorem B may be proved by a modification of the proof given by L. Collatz (see footnote 3), or alternatively, as follows.

Let $C=A+NE$, where E is the unit matrix, and N is a positive number so chosen that $a_{rr}+N>0$ for

[1] This work was performed under National Bureau of Standards contract with the University of California at Los Angeles, and was sponsored in part by the Office of Naval Research.
[2] University of Natal, South Africa, and University of California at Los Angeles.
[3] Math. Zeit. **48**, 221 (1942).

r. Let $D=U^{-1}CU$, where U is the diagonal matrix with elements $u_1, u_2, \ldots, u_n$.

The characteristic roots of C and D are the same, whereas the characteristic roots of A are those of C diminished by N.

If d_{rs} is an element of D, then $d_{rs}=(1/u_r)a_{rs}u_s$. Again the maximum positive root of a matrix with nonnegative elements is bounded above and below by the maximum and minimum values of the sums of elements of a row. The maximum positive root of such a matrix is also a root of maximum modulus, and so greater than the real part of any other root.

The sum of the rth row of the matrix D is

$$a_{rr}+N+\frac{1}{u_r}\sum_{\substack{s=1\\ s\neq r}}^{n}a_{rs}u_s.$$

Hence theorem B follows by subtracting N from each row.

2. The Case of Real Elements

In this section we shall suppose all the elements of A to be real. Let

$$R_r=\sum_{\substack{s=1\\ s\neq r}}^{n}a_{rs}, \quad C_r=\sum_{\substack{s=1\\ s\neq r}}^{n}a_{sr}.$$

Theorem 1. (i) *If* $a_{rs}+a_{sr}\geqq 0$, $r\neq s$, *if* $R_r+C_r>0$, *for all* r, *if* $a_{ii}\geqq a_{rr}$ *for all* r, *and* $a_{jj}\geqq a_{rr}$, $r\neq i$, *if* $R_p+C_p\geqq(R_r+C_r)$ *for all* r *and* $R_q+C_q\geqq R_r+C_r$, $r\neq p$, *then*

$$M\leqq\max\left(a_{ii}+\frac{R_q+C_q}{2}, \quad a_{jj}+\frac{R_p+C_p}{2}\right).$$

(ii) *If* $a_{mm}\leqq a_{rr}$ *for all* r *and* $a_{nn}\leqq a_{rr}$, $r\neq m$, *then*

$$m\geqq\min\left(a_{mm}-\frac{R_q+C_q}{2}, \quad a_{nn}-\frac{R_p+C_q}{2}\right).$$

To prove (i), we may suppose $i=1$, and let

$$\sigma=\frac{R_p+C_p}{2}, \quad \sigma^1=\frac{R_q+C_q}{2}.$$

We apply A (i), where we may leave out the modulus sign. We take $u_1=\sigma$ and

$$u_r=\frac{R_r+C_r}{2}, \qquad r\neq 1$$

$$a_{11}+\frac{1}{\sigma}\sum_{s=2}^{n}\frac{a_{1s}+a_{s1}}{2}u_s\leq a_{11}+\frac{R_1+C_1}{2\sigma}\max_{s\neq 1}u_s.$$

If

$$\frac{R_1+C_1}{2}=\sigma,$$

then

$$\max_{s\neq 1}u_s=\sigma';$$

if

$$\frac{R_1+C_1}{2}\neq\sigma,$$

then

$$\frac{R_1+C_1}{2}\leqq\frac{R_q+C_q}{2}=\sigma'$$

and

$$\max_{s\neq 1}u_s=\sigma.$$

Hence in either case

$$a_{11}+\frac{1}{\sigma}\sum_{s=2}^{n}\frac{a_{1s}+a_{s1}}{2}u_s\leqq a_{11}+\sigma'. \tag{3}$$

Again for $r\neq 1$, we have

$$a_{rr}+\frac{1}{u_r}\sum_{\substack{s=1\\ s\neq r}}^{n}\left(\frac{a_{rs}+a_{sr}}{2}\right)u_s\leqq a_{rr}+\max_{s\neq r}u_s\cdot\frac{1}{u_r}\sum_{\substack{s=1\\ s\neq r}}^{n}\left(\frac{a_{rs}+a_{sr}}{2}\right)$$
$$\leqq a_{rr}+\sigma. \tag{4}$$

From (3) and (4), part (i) of theorem 1 follows. Part (ii) of theorem 1 follows similarly from A(ii).

Theorem 2. *Let* a_{rr} *be real*, $a_{rs}\geqq 0$, $r\neq s$. (i) *If* $a_{ii}\geqq a_{rr}$, *for all* r, $a_{jj}\geqq a_{rr}$, $r\neq i$, *and* $R_p\geqq R_r$ *for all* r, $R_q\geqq R_r$, $r\neq p$, *then* $M\leqq\max\,(a_{ii}+R_q, a_{jj}+R_p)$. (ii) *If* $a_{mm}\leqq a_{rr}$ *for all* r, $a_{nn}\leqq a_{rr}$, $r\neq m$, *and* $R_p^1\leqq R_r$, *for all* r, $R_q^1\leqq R_r$, $r\neq p^1$, *then* $M\geqq\min\,(a_{mm}+R_q^1, a_{nn}+R_p^1)$.

The proof of this is similar to the proof of theorem 1 using theorem B, and may be omitted.

Theorem 3. *If* a_{rr} *is real and* $a_{rs}\geqq 0$, $r\neq s$, *then*

$$M\leqq\max_r\left(a_{rr}+\left\{\sum_{\substack{ij\\ i\neq j}}^{n}a_{ii}^2-\sum_{\substack{s=1\\ s\neq r}}^{n}a_{rs}^2\right\}^{\frac{1}{2}}\right).$$

We apply theorem B and take

$$u_r=\left(\sum_{\substack{s=1\\ s\neq r}}^{n}a_{rs}^2\right)^{\frac{1}{2}},$$

where we suppose $u_r\neq 0$. By the Hölder-Schwartz inequality

$$\frac{1}{u_r}\sum_{\substack{s=1\\ s\neq r}}^{n}a_{rs}u_s\leqq\frac{1}{u_r}\left(\sum_{\substack{s=1\\ s\neq r}}^{n}a_{rs}^2\right)^{\frac{1}{2}}\left(\sum_{\substack{s=1\\ s\neq r}}^{n}u_s^2\right)^{\frac{1}{2}}$$
$$=\left(\sum_{s=1}^{n}u_s^2-\sum_{\substack{s=1\\ s\neq r}}^{n}a_{rs}^2\right)^{\frac{1}{2}}.$$

The theorem follows from the definition of u_r.

Theorem 4. *If* a_{rr} *is real and* $a_{rs}\geqq 0$, $r\neq s$, *and if*

$$L_r=\left(\sum_{\substack{s=1\\ s\neq r}}^{n}a_{rs}^2\right)^{\frac{1}{2}}\neq 0,$$

then

$$M\leqq\max_r a_{rr}$$
$$+\min\left\{\left[\left(\sum_{s=1}^{n}L_s\right)^2-\max_r L_r^2\right]^{\frac{1}{2}}\left(\sum_{s=1}^{n}L_s\max_r L_r\right)^{\frac{1}{2}}\right\}.$$

We take $u_r = L_r^{\frac{1}{2}}$ and apply the Hölder-Schwartz inequality and obtain

$$\frac{1}{u_r}\sum_{\substack{s=1\\ s\neq r}}^{n} a_{rs}u_s \leqq L_r^{\frac{1}{2}}\left(\sum_{\substack{s=1\\ s\neq r}}^{n} L_s\right)^{\frac{1}{2}}$$

$$= \left\{L_r\left(\sum_{s=1}^{n} L_s - L_r\right)\right\}^{\frac{1}{2}} \tag{5}$$

$$< \max_r \left\{L_r \sum_{s=1}^{n} L_s\right\}^{\frac{1}{2}} \tag{6}$$

If $x, y > 0$, $x+y=a$, we have

$$a^2 - y^2 \geq a^2 - (a-x)^2 = 2ax - x^2 > ax - x^2.$$

Applying this to (5) we get

$$\left\{L_r\left(\sum_{s=1}^{n} L_s - L_r\right)\right\}^{\frac{1}{2}} \leqq \left(\sum_{s=1}^{n} L_s\right)^2 - \max_t L_t^2\Big\}^{\frac{1}{2}} \tag{7}$$

From (6) and (7) and theorem B the theorem follows.

Los Angeles, October 23, 1951.

Journal of Research of the National Bureau of Standards Vol. 48, No. 2, February 1952 Research Paper 2293

Chart for the TE_{11} Mode Piston Attenuator

Charles M. Allred

A nomogram is given and described that expedites the determination of the dependence of attenuation on frequency, conductivity, and radius in a cylindrical waveguide, TE_{11} mode, piston attenuator.

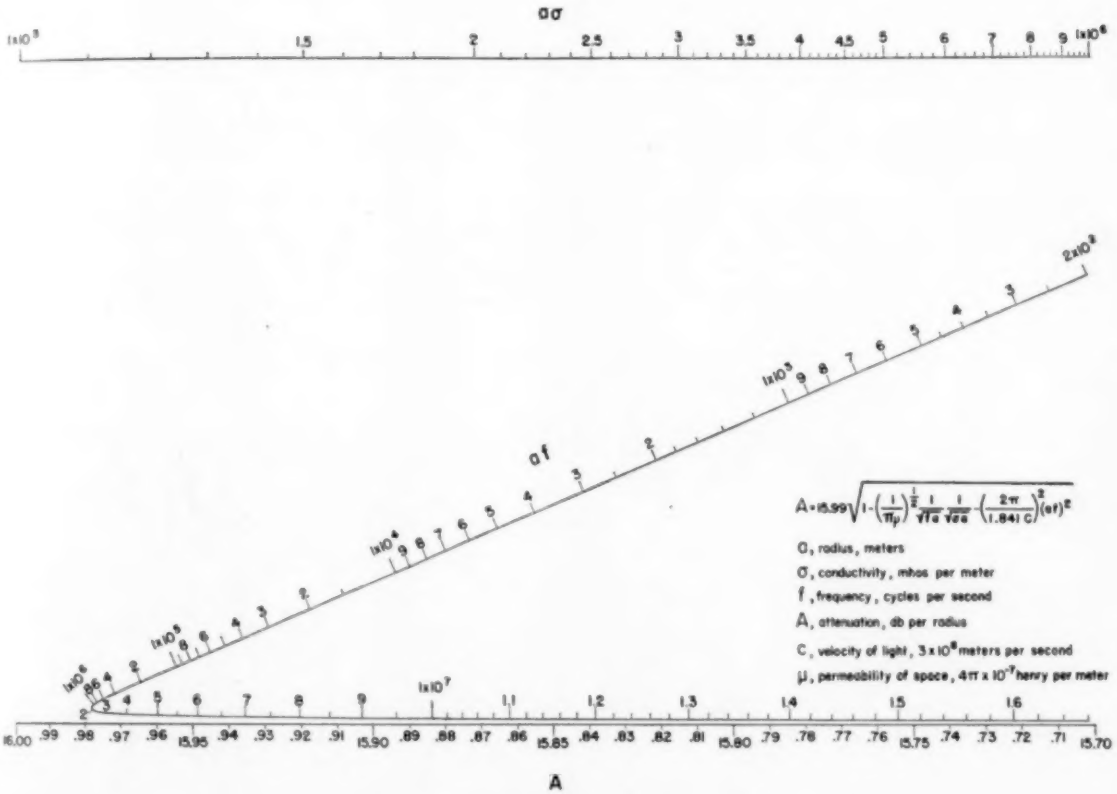

FIGURE 1. TE_{11} *mode piston attenuator chart.*

Piston attenuators (waveguide-below-cutoff) are extensively used as adjustable attenuators because of their desirable characteristics, namely, a linear decibel scale and potentially high accuracy.[1] However, their attenuation constant (decibels per radius of travel) is a slowly changing function of frequency. This variation is due to two factors: (1) the proximity of the operating frequency to the cutoff frequency, and (2) the frequency dependence of skin-depth, which alters the effective diameter of the attenuator.

The accompanying nomograph expedites the determination of the attenuation constant, A, for the most commonly used TE_{11} mode in a cylindrical guide. A good approximate functional relationship of A, the conductivity of the guide (nonmagnetic material), its radius, and the operating frequency is shown on the nomograph, and is the equation the nomograph solves. The effect of skin-depth is negligible for the TM_{01} mode, and a nomograph for this mode along with the TE_{11} mode for the case of infinite conductivity is already available.[2]

[1] R. E. Grantham and J. J. Freeman, A standard of attenuation for microwave measurements, Trans. Am. Inst. Elec. Engrs. **67**, 535 (1948).

[2] R. E. Lafferty, Piston attenuator chart. Electronics **21**, No. 2, 132 (1948).

This nomograph may be used in designing an attenuator to secure minimum frequency dependence over a given frequency range and to determine that dependence after its construction. To exemplify the latter, consider the radius $a=2$ cm, the conductivity $\sigma=1.5\times10^7$ mhos per meter, and the frequency $f=1\times10^6$ cycles per second; then $a\sigma=3\times10^5$ mhos, $af=2\times10^4$ meters per second, and the extension to the A scale of a straight line passing through the above points on the $a\sigma$ and af scales gives a value of 15.94 db per radius for A. In designing an attenuator, one simply chooses values of a and σ to place the operating point preferably on the right end of the $a\sigma$ scale and about the knee of the af scale.

WASHINGTON, October 29, 1951.

rnal of Research of the National Bureau of Standards Vol. 48, No. 2, February 1952 Research Paper 2294

Table of the Zeros and Weight Factors of the First Twenty Hermite Polynomials[1]

Herbert E. Salzer, Ruth Zucker, and Ruth Capuano

The chief use of this table of the zeros and weight factors of the Hermite polynomials is in the calculation of integrals over the interval $[-\infty, \infty]$, when the integrand is either the product of e^{-x^2} and a polynomial, or may be closely approximated by e^{-x^2} times a polynomial. The zeros and weight factors, $x_i^{(n)}$ and $\alpha_i^{(n)}$, respectively, together with the auxiliary quantities $\beta_i^{(n)}=\alpha_i^{(n)} \exp [(x_i^{(n)})^2]$, which are useful in computation, are all tabulated here for the first twenty Hermite polynomials. The zeros $x_i^{(n)}$ and $\beta_i^{(n)}$ are given to 13 or more decimals, and the weight factors $\alpha_i^{(n)}$ to 13 significant figures. Although other shorter tables have appeared, this present table will enable one to cope with problems requiring much higher degree and accuracy, both in problems involving direct quadratures and those arising in the numerical solution of linear integral equations for the range $[-\infty, \infty]$. Thus the use of this table in any direct quadrature can give exact accuracy as far as the 39th degree (the only inexactitude arising from the use of rounded values of $x_i^{(n)}$ and $\alpha_i^{(n)}$).

1. Introduction

The main purpose of the table of the zeros $x_i^{(n)}$ and weight factors ("Christoffel numbers") $\alpha_i^{(n)}$ of the Hermite polynomials is to provide the basic quantities that occur in the quadrature formula

$$\int_{-\infty}^{\infty} e^{-x^2} f(x)\,dx=\sum_{i=1}^{n} \alpha_i^{(n)} f(x_i^{(n)})+R_n, \tag{1}$$

where

$$R_n=\frac{n!\sqrt{\pi}f^{(2n)}(\xi)}{2^n (2n)(2n-1)\ldots(n+2)(n+1)}$$

for some ξ, $-\infty<\xi<\infty$ [2, p. 101–102, 369].[2]

When the integrand does not contain e^{-x^2} explicitly, but behaves like e^{-x^2} times a polynomial, instead of (1), there is

$$\int_{-\infty}^{\infty} F(x)\,dx=\int_{-\infty}^{\infty} e^{-x^2}[e^{x^2}F(x)]\,dx\cong\sum_{i=1}^{n}\alpha_i^{(n)}e^{x_i^{(n)2}}F(x_i^{(n)}). \tag{2}$$

For dealing with quadratures of the type in (2), it is convenient to follow the example of A. Reiz [1] and to tabulate also the quantities $\beta_i^{(n)}=\alpha_i^{(n)} \exp [(x_i^{(n)})^2]$. From the form of the remainder term R_n, (1) is seen to be exact (save for the use of rounded values of $x_i^{(n)}$ and $\alpha_i^{(n)}$) when $f(x)$ is a polynomial of at most the $(2n-1)$th degree.

2. Numerical Solution of Integral Equations

Besides problems involving direct quadratures, there are those arising in the numerical solution of linear integral equations of the second kind for integrals over the range $[-\infty, \infty]$, namely,

$$\phi(y)=f(y)+\lambda\int_{-\infty}^{\infty} f(x)K(y,x)\,dx. \tag{3}$$

By considering $e^{x^2} f(x)K(y,x)$ as a polynomial in x, and making use of (2) for $y=x_i^{(n)}$, $i=1, 2, \ldots, n$, the approximate solution of (3) is reduced to the solution of a set of only n linear equations for the (approximate values of) $f(x_i^{(n)})$. These values of $f(x_i^{(n)})$ can then be used in (2) to find $f(y)$ for any value of y. The advantage in the use of (2) instead of an equally spaced quadrature formula for solving (3) is that here only n points are needed to give accuracy obtainable by approximating $e^{x^2} f(x)K(y,x)$ as a polynomial of the $(2n-1)$th degree in x. For a full description of the method, including examples, see A. Reiz [1], especially p. 4 to 10, 16 to 21.

3. Important Properties of Hermite Polynomials

The Hermite polynomials may be defined by the formula

$$H_n(x)=(-1)^n e^{x^2}\frac{d^n}{dx^n}(e^{-x^2}), \tag{4}$$

or by the generating function

$$e^{-x^2+2xz}=\sum_{n=0}^{\infty} H_n(x)\frac{z^n}{n!}. \tag{5}$$

They are given explicitly by the formula

$$H_n(x)=\sum_{k=0}^{[n/2]}\frac{(-1)^k n!}{k!(n-2k)!}(2x)^{n-2k}. \tag{6}$$

The numerical values of the coefficients of $H_n(x)$ for the first 30 values of n are contained in H. E. Salzer [3]. The polynomials $H_n(x)$ satisfy the differential equation

$$H_n''(x)-2xH_n'(x)+2nH_n(x)=0, \tag{7}$$

[1] This project was sponsored in part by the Office of Air Research, AMC, USAF.

[2] Figures in brackets indicate the literature references at the end of this paper.

the recurrence formula

$$H_{n+1}(x)-2xH_n(x)+2nH_{n-1}(x)=0, \qquad n\geqq 2, \quad (8)$$

and the differential-recurrence formula

$$H_n'(x)=2nH_{n-1}(x). \quad (9)$$

The Hermite polynomials have the orthogonality property

$$\int_{-\infty}^{\infty} e^{-x^2}H_n(x)\,H_m(x)\,dx=\pi^{\frac{1}{2}}2^n n!\delta_n^m. \quad (10)$$

A most important consequence of (10) is (1), where the $\alpha_i^{(n)}$ are defined by

$$\alpha_i^{(n)}=\frac{1}{H_n'(x_i^{(n)})}\int_{-\infty}^{\infty}\frac{e^{-x^2}H_n(x)}{x-x_i^{(n)}}\,dx. \quad (11)$$

The $\alpha_i^{(n)}$ are also expressible in the following form [2, p. 344], [4, p. 311]:

$$\alpha_i^{(n)}=\frac{\pi^{\frac{1}{2}}2^{n+1}n!}{\{H_n'(x_i^{(n)})\}^2}, \quad (12)$$

which, from (9), can be written as

$$\alpha_i^{(n)}=\frac{\pi^{\frac{1}{2}}2^{n-1}(n-1)!}{n\{H_{n-1}(x_i^{(n)})\}^2} \quad (13)$$

the latter form being more convenient for computation.

4. Description of Tables

This table gives the zeros $x_i^{(n)}$, the weight factors $\alpha_i^{(n)}$ and $\beta_i^{(n)}$, for the first 20 Hermite polynomials. The absolute values of the zeros, $|x_i^{(n)}|$, are tabulated to 15 decimals for $n=1(1)13$, to 14 decimals for $n=14(1)16$, and to 13 decimals for $n=17(1)20$. To each nonvanishing $|x_i^{(n)}|$ there corresponds the two zeros $x_i^{(n)}=+|x_i^{(n)}|$ and $x_i^{(n)}=-|x_i^{(n)}|$. The weight factors $\alpha_i^{(n)}=\alpha_{n-i+1}^{(n)}$ are tabulated to 13 significant figures. For a given n, zeros having the same absolute value are associated with the same weight factor. The auxiliary quantities $\beta_i^{(n)}$ are tabulated to 13 decimals.

5. Method of Computation and Checking

Since $H_n(x)$ is an odd or even polynomial for n odd or even, respectively, it was convenient to change the variable to $X=4x^2$ and to calculate $X_i^{(n)}\equiv 4x_i^{(n)2}$, where the nonvanishing $X_i^{(n)}$ are the zeros of polynomials $A_{[n/2]}(X)$, n odd, and $B_{[n/2]}(X)$, n even, of degree $[n/2]$ in X. Thus the degree of the polynomials $A_{[n/2]}(X)$ and $B_{[n/2]}(X)$ did not exceed 10, and the coefficients were considerably smaller than those of $H_n(x)$. A first approximation to $X_i^{(n)}$ was obtained from E. R. Smith [5], which gives the zeros of

$$h_n(x)=(-1)^n e^{x^2/2}\frac{d^n(e^{-x^2/2})}{dx^n}$$

by taking twice the square of the latter. The polynomials $A_{[n/2]}(X)$ and $B_{[n/2]}(X)$ were tabulated for five or six values of X in the neighborhood of each $X_i^{(n)}$, at intervals of 0.0001 in X. The zeros $X_i^{(n)}$ were calculated by a formula for inverse interpolation given in H. E. Salzer [6], and then were checked by direct interpolation in the polynomials $A_{[n/2]}(X)$ and $B_{[n/2]}(X)$, using the Gregory-Newton formula with advancing differences. The accuracy of the zero $X_i^{(n)}$ was determined from the approximate relation:

$$\text{error in } X_i^{(n)}\cong\frac{0.0001}{\Delta}F(X_i^{(n)}),$$

where $F(X_i^{(n)})$ denotes either $A_{[n/2]}(X_i^{(n)})$ or $B_{[n/2]}(X_i^{(n)})$, and Δ is the difference between two consecutive entries of $F(X)$ on either side of $X_i^{(n)}$.

The values of $x_i^{(n)}$ were found from $x_i^{(n)}=\pm\frac{1}{2}\sqrt{X_i^{(n)}}$, and checked back by squaring to get $X_i^{(n)}=4x_i^{(n)2}$. Additional checks upon the $x_i^{(n)}$ were performed by calculating

$$\sum_{i=1}^{n} x_i^{(n)2}=\frac{n(n-1)}{2}, \quad (14)$$

$$\sum_{i=1}^{n}{}' x_i^{(n)}=(-1)^{(n-1)/2}\frac{(n+1)!}{((n+1)/2)!} \text{ for } n \text{ odd}, \quad (15a)$$

where $\sum'$ denotes the omission of the factor $x_i^{(n)}=0$, and

$$\prod_{i=1}^{n} x_i^{(n)}=(-1)^{n/2}\frac{n!}{(n/2)!} \text{ for } n \text{ even}. \quad (15b)$$

The weight factors $\alpha_i^{(n)}$ were calculated from (13), using

$$H_{n-1}(x_i^{(n)})=B_{[(n-1)/2]}(X_i^{(n)}) \text{ for } n \text{ odd},$$

and

$$H_{n-1}(x_i^{(n)})=\sqrt{X_i^{(n)}}\,A_{[(n-1)/2]}(X_i^{(n)}) \text{ for } n \text{ even}.$$

Formula (12) was used to check the $\alpha_i^{(n)}$, in the form

$$\alpha_i^{(n)}=\frac{\pi^{\frac{1}{2}}2^{n-3}n!}{\{X_i^{(n)}A'_{[n/2]}(X_i^{(n)})\}^2}, \text{ for } n \text{ odd}, \; i\neq\frac{1}{2}(n+1) \quad (12a)$$

and

$$\alpha_i^{(n)}=\frac{\pi^{\frac{1}{2}}2^{n-3}n!}{X_i^{(n)}\{B'_{[n/2]}(X_i^{(n)})\}^2}, \text{ for } n \text{ even}. \quad (12b)$$

Additional over-all checks upon $\alpha_i^{(n)}$ were performed, using (1) for $P(x)=1, x^2, x^4, \ldots, x^{2m}$, $2^m<2n-1<2^{m+1}$, and in a few cases for $P(x)=x^{2^m+2^p}$, $2^m+2^p<$

$k-1<2^{m+1}$, the left member of (1) equal to $\Gamma\left(k+\frac{1}{2}\right)$ for $P(x)=x^{2k}$. The choice of these different powers of x for $P(x)$ was to ensure that every significant figure of the $\alpha_i^{(n)}$ was covered in the checks.

The auxiliary quanitites $\beta_i^{(n)}$ were computed by multiplying the weight factors $\alpha_i^{(n)}$ by $e^{x_i^{(n)}/4}$, where the $e^{x_i^{(n)}/4}$ were obtained from the NBS tables of the exponential function [7] and were checked by the relation $\log \beta_i^{(n)}=\log \alpha_i^{(n)}+X_i^{(n)}/4$, where the logarithms were obtained from the NBS tables [8].

The functions $x_i^{(n)}$, $\alpha_i^{(n)}$, and $\beta_i^{(n)}$ were calculated to about two more places than are tabulated, and are available in manuscript form. All entries given here, which were obtained by rounding the manuscript table, are correct to within about a unit in the last place.

The functions in this present table were compared with those in three much shorter similar tables given by R. E. Greenwood and J. J. Miller [9], A. Reiz [1], and Z. Kopal [10], and the few errors of more than a unit in the last place in those three tables were noted and reported to the journal "Mathematical Tables and Other Aids to Computation." Also, the values of $X_i^{(n)}$ for $n=16$ upon the worksheets were compared with those in J. Barkley Rosser [11], with perfect agreement. Finally, the zeros in the table of the Harvard University Laboratory [28] were checked by calculating $\sqrt{2}|x_i^{(n)}|$, to give complete agreement.

6. Illustration

As an example of the use of (1) for quadratures, suppose that one wished to evaluate numerically, say to 13 places, the integral $\int_0^\infty e^{-t^2}J_0(t)\,dt$, where $J_0(t)$ denotes the Bessel function of order zero. It happens that that integral is known to be $\frac{1}{2}\sqrt{\pi}\,e^{-1/8}I_0(1/8)$, where $I_0(t)$ denotes the modified Bessel function of order zero (see [26, p. 394]). As the integrand $e^{-t^2}J_0(t)$ is even, and as $\alpha_i^{(n)}J_0(x_i^{(n)})=\alpha_{n-i+1}^{(n)}J_0(-x_i^{(n)})$, from (1), whenever n is even,

$$\int_0^\infty e^{-t^2}J_0(t)\,dt\cong\Sigma\alpha_i^{(n)}J_0(x_i^{(n)}), \tag{16}$$

where the summation covers only the positive values of $x_i^{(n)}$. In the present example the error in (16) (from the term R_n in (1) and the inequality $|J_0^{(n)}(x)|\leqq 1$) does not exceed 10^{-13} for n as small as 10. For the right member of (16), $J_0(x_i^{(10)})$ was computed to as many places as were sufficient to obtain $\alpha_i^{(n)}J_0(x_i^{(n)})$ to 13 places. The $J_0(x_i^{(10)})$ was calculated by interpolation in the Bessel function table of the Harvard Computation Laboratory [27]. The following are the results of these computations (the extra fourteenth place in $\alpha_i^{(10)}J_0(x_i^{(10)})$ was carried to avoid the cumulation of rounding errors):

i	$J_0(x_i^{(10)})$	$\alpha_i^{(10)}J_0(x_i^{(10)})$
6	0. 97081 99870 413	0. 59303 76541 6692
7	0. 74887 18398 349	0. 17983 30434 9660
8	0. 36515 41522 17	0. 01236 93757 8926
9	−0. 06452 02154 9	−0. 00008 66923 1312
10	−0. 37050 3331	−0. 00000 28308 0582

$$\sum_{i=6}^{10}\alpha_i^{(10)}J_0(x_i^{(10)})=0.78515\ 05503\ 338.$$

This answer differs by only a unit in the thirteenth place from the true value of $\frac{1}{2}\sqrt{\pi}\,e^{-1/8}I_0(1/8)$ which was found (employing the power series for $I_0(t)$) to be, to 13 decimals, 0.78515 05503 339.

7. Table of the Zeros and Weight Factors of the First Twenty Hermite Polynomials

$\lvert x_i^{(n)}\rvert$	$\alpha_i^{(n)}$	$\beta_i^{(n)}$
$n=1$	$n=1$	$n=1$
0. 00000 00000 00000	1. 7724 53850 906	1. 77245 38509 055
$n=2$	$n=2$	$n=2$
0. 70710 67811 86548	0. 88622 69254 528	1. 46114 11826 611
$n=3$	$n=3$	$n=3$
0. 00000 00000 00000	1. 1816 35900 604	1. 18163 59006 037
1. 22474 48713 91589	0. 29540 89751 509	1. 32393 11752 136
$n=4$	$n=4$	$n=4$
0. 52464 76232 75290	0. 80491 40900 055	1. 05996 44828 950
1. 65068 01238 85785	0. (1)81312 83544 725	1. 24022 58176 958
$n=5$	$n=5$	$n=5$
0. 00000 00000 00000	0. 94530 87204 829	0. 94530 87204 829
0. 95857 24646 13819	0. 39361 93231 522	0. 98658 09967 514
2. 02018 28704 56086	0. (1)19953 24205 905	1. 18148 86255 360

$\lvert x_i^{(n)} \rvert$	$\alpha_i^{(n)}$	$\beta_i^{(n)}$
$n=6$	**$n=6$**	**$n=6$**
0. 43607 74119 27617	0. 72462 95952 244	0. 87640 13344 362
1. 33584 90740 13697	0. 15706 73203 229	0. 93558 05576 312
2. 35060 49736 74492	0. (2)45300 09905 509	1. 13690 83326 745
$n=7$	**$n=7$**	**$n=7$**
0. 00000 00000 00000	0. 81026 46175 568	0. 81026 46175 568
0. 81628 78828 58965	0. 42560 72526 101	0. 82868 73032 836
1. 67355 16287 67471	0. (1)54515 58281 913	0. 89718 46002 252
2. 65196 13568 35233	0. (3)97178 12450 995	1. 10133 07296 103
$n=8$	**$n=8$**	**$n=8$**
0. 38118 69902 07322	0. 66114 70125 582	0. 76454 41286 517
1. 15719 37124 46780	0. 20780 23258 149	0. 79289 00483 864
1. 98165 67566 95843	0. (1)17077 98300 741	0. 86675 26065 634
2. 93063 74202 57244	0. (3)19960 40722 114	1. 07193 01442 480
$n=9$	**$n=9$**	**$n=9$**
0. 00000 00000 00000	0. 72023 52156 061	0. 72023 52156 061
0. 72355 10187 52838	0. 43265 15590 026	0. 73030 24527 451
1. 46855 32892 16668	0. (1)88474 52739 438	0. 76460 81250 946
2. 26658 05845 31843	0. (2)49436 24275 537	0. 84175 27014 787
3. 19099 32017 81528	0. (4)39606 97726 326	1. 04700 35809 767
$n=10$	**$n=10$**	**$n=10$**
0. 34290 13272 23705	0. 61086 26337 353	0. 68708 18539 513
1. 03661 08297 89514	0. 24013 86110 823	0. 70329 63231 049
1. 75668 36492 99882	0. (1)33874 39445 548	0. 74144 19319 436
2. 53273 16742 32790	0. (2)13436 45746 781	0. 82066 61264 048
3. 43615 91188 37738	0. (5)76404 32855 233	1. 02545 16913 657
$n=11$	**$n=11$**	**$n=11$**
0. 00000 00000 00000	0. 65475 92869 146	0. 65475 92869 146
0. 65680 95668 82100	0. 42935 97523 561	0. 66096 04194 410
1. 32655 70844 94933	0. 11722 78751 677	0. 68121 18810 667
2. 02594 80158 25755	0. (1)11911 39544 491	0. 72195 36247 284
2. 78329 00997 81652	0. (3)34681 94663 233	0. 80251 68688 510
3. 66847 08465 59583	0. (5)14395 60393 714	1. 00652 67861 724
$n=12$	**$n=12$**	**$n=12$**
0. 31424 03762 54359	0. 57013 52362 625	0. 62930 78743 695
0. 94778 83912 40164	0. 26049 23102 642	0. 63962 12320 203
1. 59768 26351 52605	0. (1)51607 98561 588	0. 66266 27732 669
2. 27950 70805 01060	0. (2)39053 90584 629	0. 70522 03661 122
3. 02063 70251 20890	0. (4)85736 87043 588	0. 78664 39394 633
3. 88972 48978 69782	0. (6)26585 51684 356	0. 98969 90470 923
$n=13$	**$n=13$**	**$n=13$**
0. 00000 00000 00000	0. 60439 31879 211	0. 60439 31879 211
0. 60576 38791 71060	0. 42161 62968 985	0. 60852 95837 033
1. 22005 50365 90748	0. 14032 33206 870	0. 62171 60552 868
1. 85310 76516 01512	0. (1)20862 77529 617	0. 64675 94633 158
2. 51973 56856 78238	0. (2)12074 59992 719	0. 69061 80348 378
3. 24660 89783 72410	0. (4)20430 36040 271	0. 77258 08233 517
4. 10133 75961 78640	0. (7)48257 31850 073	0. 97458 03956 399
$n=14$	**$n=14$**	**$n=14$**
0. 29174 55106 7256	0. 53640 59097 121	0. 58406 16905 220
0. 87871 37873 2940	0. 27310 56090 642	0. 59110 66670 432
1. 47668 27311 4114	0. (1)68505 53422 347	0. 60637 97391 261
2. 09518 32585 0772	0. (2)78500 54726 458	0. 63290 06064 723
2. 74847 07249 8540	0. (3)35509 26135 519	0. 67770 67591 924
3. 46265 69336 0227	0. (5)47164 84355 019	0. 75998 70873 976
4. 30444 85704 7363	0. (8)86285 91168 125	0. 96087 87030 257

$\lvert x_i^{(n)} \rvert$	$\alpha_i^{(n)}$	$\beta_i^{(n)}$
$n=15$	**$n=15$**	**$n=15$**
0. 00000 00000 0000	0. 56410 03087 264	0. 56410 03087 264
0. 56506 95832 5558	0. 41202 86874 989	0. 56702 11534 466
1. 13611 55852 1092	0. 15848 89157 959	0. 57619 33502 835
1. 71999 25751 8649	0. (1)30780 03387 255	0. 59302 74497 642
2. 32573 24861 7386	0. (2)27780 68842 913	0. 62066 26035 270
2. 96716 69279 0560	0. (3)10000 44412 325	0. 66616 60051 091
3. 66995 03734 0445	0. (5)10591 15547 711	0. 74860 73660 169
4. 49999 07073 0939	0. (8)15224 75804 254	0. 94836 89708 276
$n=16$	**$n=16$**	**$n=16$**
0. 27348 10461 3815	0. 50792 94790 166	0. 54737 52050 378
0. 82295 14491 4466	0. 28064 74585 285	0. 55244 19573 675
1. 38025 85391 9888	0. (1)83810 04139 899	0. 56321 78290 882
1. 95178 79909 1625	0. (1)12880 31153 551	0. 58124 72754 009
2. 54620 21578 4748	0. (3)93228 40086 242	0. 60973 69582 560
3. 17699 91619 7996	0. (4)27118 60092 538	0. 65575 56728 761
3. 86944 79048 6012	0. (6)23209 80844 865	0. 73824 56222 777
4. 68873 89393 0582	0. (9)26548 07474 011	0. 93687 44928 841
$n=17$	**$n=17$**	**$n=17$**
0. 00000 00000 000	0. 53091 79376 249	0. 53091 79376 249
0. 53163 30013 427	0. 40182 64694 704	0. 53307 06545 736
1. 06764 87257 435	0. 17264 82976 701	0. 53976 31139 085
1. 61292 43142 212	0. (1)40920 03414 976	0. 55177 73530 782
2. 17350 28266 666	0. (2)50673 49957 628	0. 57073 92941 245
2. 75776 29157 039	0. (3)29864 32866 978	0. 59989 27326 678
3. 37893 20911 415	0. (5)71122 89140 021	0. 64629 17002 129
4. 06194 66758 755	0. (7)49770 78981 631	0. 72874 83705 871
4. 87134 51936 744	0. (10)45805 78930 799	0. 92625 41399 895
$n=18$	**$n=18$**	**$n=18$**
0. 25826 77505 191	0. 48349 56947 255	0. 51684 58364 816
0. 77668 29192 674	0. 28480 72856 700	0. 52063 49466 761
1. 30092 08583 896	0. (1)97301 74764 132	0. 52858 94429 188
1. 83553 16042 616	0. (1)18640 04238 754	0. 54157 86786 621
2. 38629 90891 667	0. (2)18885 22630 268	0. 56127 90455 498
2. 96137 75055 316	0. (4)91811 26867 929	0. 59095 30034 631
3. 57376 90684 863	0. (5)18106 54481 093	0. 63763 01720 062
4. 24811 78735 681	0. (7)10467 20579 579	0. 71999 33831 053
5. 04836 40088 745	0. (11)78281 99772 116	0. 91639 35375 519
$n=19$	**$n=19$**	**$n=19$**
0. 00000 00000 000	0. 50297 48882 762	0. 50297 48882 762
0. 50352 01634 239	0. 39160 89886 130	0. 50461 53313 522
1. 01036 83871 343	0. 18363 27013 070	0. 50967 93750 983
1. 52417 06193 935	0. (1)50810 38690 905	0. 51863 31937 003
2. 04923 17098 506	0. (2)79888 66777 723	0. 53240 23605 516
2. 59113 37897 945	0. (3)67087 75214 072	0. 55269 46209 671
3. 15784 88183 476	0. (4)27209 19776 316	0. 58277 95297 628
3. 76218 73519 640	0. (6)44882 43147 223	0. 62965 66326 368
4. 42853 28066 038	0. (8)21630 51009 864	0. 71188 18743 371
5. 22027 16905 375	0. (11)13262 97094 499	0. 90719 87960 928
$n=20$	**$n=20$**	**$n=20$**
0. 24534 07083 009	0. 46224 36696 006	0. 49092 15006 667
0. 73747 37285 454	0. 28667 55053 628	0. 49384 33852 721
1. 23407 62153 953	0. 10901 72060 200	0. 49992 08713 363
1. 73853 77121 166	0. (1)24810 52088 746	0. 50967 90271 175
2. 25497 40020 893	0. (2)32437 73342 238	0. 52408 03509 486
2. 78880 60584 281	0. (3)22833 86360 163	0. 54485 17423 644
3. 34785 45673 832	0. (5)78025 56478 532	0. 57526 24428 525
3. 94476 40401 156	0. (6)10860 69370 769	0. 62227 86961 914
4. 60368 24495 507	0. (9)43993 40992 273	0. 70433 29611 769
5. 38748 08900 112	0. (12)22293 93645 534	0. 89859 19614 532

8. References

In addition to the references cited in the preceding text, there are mentioned here a few articles and books that cover many essential properties of Hermite polynomials. A detailed bibliography on Hermite polynomials is given in J. A. Shohat [12]. The standard work on the theory is G. Szegö [2].

[1] A. Reiz, On the numerical solution of certain types of integral equations, Arkiv. för Matematik, Astron. Fysik. **29A**, No. 29, 21 pp. (1943).

[2] G. Szegö, Orthogonal polynomials, Am. Math. Soc. Colloq. Pub. **23** (1939).

[3] H. E. Salzer, Coefficients for expressing the first thirty powers in terms of the Hermite polynomials, Math. Tables and Other Aids to Computation **3,** No. 23, 167 to 169 (1948).

[4] J. Deruyts, Sur le calcul approché de certaines intégrales définies, Bull. de l'Académie Royale de Belgique (3) **11,** 307 to 311 (1886).

[5] E. R. Smith, Zeros of the Hermitian polynomials, Am. Math. Monthly **43,** 354 to 358 (1936). Tabulates zeros of $(-1)^n e^{x^2/2} d^n(e^{-x^2/2})/dx^n$, which is $\sqrt{2}x_i^{(n)}$ for $n=1(1)27$, to 6*D*.

[6] H. E. Salzer, A new formula for inverse interpolation, Bull. Am. Math. Soc. **50,** No. 8, 513 to 516 (1944).

[7] Tables of the exponential function e^x, NBS AMS14 (1947).

[8] Table of natural logarithms, **I** to **IV,** NBS Mathematical Tables MT7, 9, 10, 12 (1941).

[9] R. E. Greenwood and J. J. Miller, Zeros of the Hermite polynomials and weights for Gauss' mechanical quadrature formula, Bull. Am. Math. Soc. **54,** No. 8, 765 to 769 (1948).

[10] Z. Kopal, A table of the coefficients of the Hermite quadrature formula, J. Math. Phys. **27,** 259 to 261 (1949).

[11] J. Barkley Rosser, Theory and application of $\int_0^x e^{-x^2}\,dx$ and $\int_0^x e^{-x^2}x^2\,dy\int_0^y e^{-x^2}\,dx$. Part I. Methods of computation (Mapleton House, Brooklyn, N. Y., 1948). On p. 166 there are tabulated $X_i^{(n)}=4x_i^{(n)2}$, for $n=16$, to 13 *D*.

[12] J. A. Shohat, A bibliography on orthogonal polynomials, Bull. Nat. Res. Council, No. 103 (1940). Lists over 2,000 articles, books, and theses, by 643 authors, on the subject of orthogonal polynomials. The topical index has a special section on Hermite polynomials, where more than 300 references are given.

[13] D. Jackson, Fourier series and orthogonal polynomials, Carus Mathematical Monographs, No. 6, Math. Assoc. Am. (1941). Chapters VII (general) and IX (on Hermite polynomials).

[14] W. Hahn, Die Nullstellen der Laguerreschen und Hermiteschen Polynome, Schriften des Mathematischen Seminars und des Instituts für angewandte Mathematik der Universität Berlin **1,** 213 to 244 (1933).

[15] W. Hahn, Bericht über die Nullstellen der Laguerreschen und der Hermiteschen Polynome, Jahresber. Deutschen Math. Verein. **44,** 215 to 236 (1934). This paper contains a good bibliography.

[16] J. Cossar and A. Erdélyi, Dictonary of Laplace transforms, Part 2B, Dept. of Scient. Res. and Exper. Admir. Comput. Serv., 82 to 83 (1945).

[17] H. Margenau and G. M. Murphy, The mathematics of physics and chemistry, 76 to 77, 117 to 122, 343 to 344 (D. Van Nostrand and Co., Inc., New York, N. Y., 1943).

[18] R. Courant and D. Hilbert, Methoden der mathematischen Physik, I, 76 to 77, 261, 294 to 295 (Springer, Berlin, 1931, reprinted by Interscience Publishers, 1943).

[19] M. Plancherel, Sur les valeurs asymptotiques des polynomes d'Hermite, Atti del Congresso Internazionale dei Matematici, Bologna **3,** 309 to 310 (1928).

[20] M. Plancherel and W. Rotach, Sur les valeurs asymptotiques des polynomes d'Hermite $H_n(x)=(-1)^n e^{x^2/2}d^n(e^{-x^2/2})/dx^n$. Commentarii Mathematici Helvetici **1,** 227 to 254 (1929).

[21] S. C. van Veen, Asymptotische Entwicklung und Nullstellenabschätzung der Hermiteschen Funktionen, Koninklijke Akademie van Wetenschappen te Amsterdam, Proc. Sec. Sci. **34,** No. 2, 257 to 267 (1931); and (larger article, same title) Mathematische Annalen **105,** 408 to 436 (1931).

[22] J. B. Russell, A table of Hermite functions, J. Math. Phys. **12,** 291 to 297 (1933). Tabulates $e^{-\frac{1}{2}x^2}H_n(x)$ for $n=0(1)11$, $x=0(.04)1(.1)4(.2)7(.5)8$, to 5*S*.

[23] N. Schwid, The asymptotic forms of the Hermite and Weber functions, Trans. Am. Math. Soc. **37,** 339 to 362 (1935).

[24] J. W. Glover, Tables of applied mathematics in finance, insurance, statistics, p. 392 to 411 (G. Wahr, Ann Arbor, Mich., 1923). Tabulates $(1/\sqrt{2\pi})d^n\left(e^{-\frac{1}{2}x^2}\right)/dx^n$ for $n=1(1)7$, $x=0(.01)4.99$, to 5*D*.

[25] J. I. Marcum, Tables of Hermite polynomials and the derivatives of the error function (RAND Corp., Santa Monica, Calif., Report P–90, 1948). Tabulates $(1/\sqrt{2\pi})d^n\left(e^{-\frac{1}{2}x^2}\right)/dx^n$ and the polynomials $e^{\frac{1}{2}x^2}d^n\left(e^{-\frac{1}{2}x^2}\right)/dx^n$ for $n=1(1)10$, $x=0(.01)12$, to 6*S*.

[26] G. N. Watson, A treatise on the theory of Bessel functions, 2d ed., (Cambridge Univ. Press, 1944).

[27] Harvard Computation Laboratory, Tables of the Bessel functions of the first kind of orders zero and one (Harvard Univ. Press, Cambridge, Mass., 1947).

[28] Harvard Computation Laboratory, Tables of the Error Function and of its First Twenty Derivatives, Harvard Univ. Press, Cambridge, Mass. (1952). Tabulates $\frac{1}{\sqrt{2\pi}}\int_0^x e^{-t^2/2}dt$ and $\phi^{(n)}(x)=\frac{1}{\sqrt{2\pi}}\frac{d^n}{dx^n}e^{-x^2/2}$, $n=0(1)20$, $x=0(.004)$ or $(.002)$ around 10.5, or less; 6D or 7S. Also, zeros of $\phi^{(n)}(x)$, or $\sqrt{2}\,|x_i^{(n)}|$, $n=1(1)20$; 10D.

WASHINGTON, May 14, 1951.

nal of Research of the National Bureau of Standards Vol. 48, No. 2, February 1952 Research Paper 2295

Film Dosimetry of Electrons in the Energy Range 0.5 to 1.4 Million Electron Volts[1]

J. Fleeman and F. S. Frantz, Jr.

Two types of films were exposed to electrons in the energy range 0.5 to 1.4 million electron volts. The film response was found to be linearly proportional to the dosage received and independent of the energy of the incident electrons in the measured energy range. The photographic density is further shown to be dependent on the amount of paper absorber surrounding the film. A step-wedge filter is suggested that would permit exptrapolation of densities to zero filter thickness.

1. Introduction

The recent advances in radioactivity leading to high-activity radiation sources has made the study of personnel monitoring increasingly important. For gamma rays, many of the techniques used earlier for X-rays have provided development guides. However, because high-activity electron sources have only recently become available, personnel monitoring systems for electrons are somewhat behind those for gamma rays. Several techniques, including photographic films similar to the film badges used for X-rays, have been suggested. In the film technique, the opacity of the processed film is a measure of the radiation received by it. However, each type of film requires a calibration curve relating the darkening of the film to the radiation exposure.

Monitoring techniques do not require a high accuracy as the short-time biological responses for low exposures are not appreciable, and in addition, there are considerable individual variations in radiation response. Usually an accuracy of 15 to 30 percent is acceptable.[2] It is therefore entirely feasible to determine the ionization produced in an air cavity by the radiation and from this to compute the dose delivered to the surrounding tissue. The theoretical and experimental factors involved in this computation are not accurately known, but it is estimated that the over-all accuracy of the computation is within 5 percent.

Because of the high attenuation in the body of the radiation from commonly available electron sources, the dose received near the surface of the skin is most important. However, as the skin has a dead layer averaging 7 mg/cm², there is no reason for measuring the dosage at lesser depths. Actually, because of electron scattering, the dosage may increase somewhat beyond this depth, but for moderate electron energies personnel monitoring dosages are measured at this depth.

Density-dosage curves for two films, Minimax Dental X-ray Film Extra Fast and du Pont Dosimeter type 552 single film packet,[3] when exposed to electrons of 0.5 to 1.4 million electron volts (Mev) and also to the beta rays from uranium, are presented in the present paper.

The polystyrene used in this experiment has an average atomic number and density close to that of human tissue. In addition, 7 mg/cm² of polystyrene is used to simulate the dead layer of tissue. Consequently, the correlation experiment reported here relates the darkening of the film previously mentioned when exposed to electron bombardment in terms of the energy dissipated in 7 mg/cm² of polystyrene, which is equivalent to the dead layer of human tissue. It must be clearly understood that the dosage is not the energy dissipated in the film but in the polystyrene. The two are related by way of the relative stopping powers of the materials.

2. Apparatus and Procedure

High-energy electrons produced in an electron accelerator [4] passed through a 20×10^{-4}-cm-thick aluminum window into an evacuated collimator, and thence through a second window into either an ionization chamber or into the film badge. A shutter near the first window permitted accurate control of the film exposure. Aluminum baffles in the collimator served to reduce the amount of scattered radiation incident on the film or ionization chamber and to make the main electron beam parallel. A carriage supported both the film-badge holder and the ionization instruments so that either could be accurately positioned in the electron beam (fig. 1).

The extrapolation-type ionization chamber [5] (fig. 2) was arranged so that the plates were perpendicular to the beam and the spacing could be varied. The plate upon which the electron beam was incident had a thickness of 7 mg/cm² of polystyrene. The collector plate size (1.04-cm diameter) was determined to be well within the area of uniform electron-beam intensity. An FP–54 electrometer located directly below the chamber measured the ionization current to this collector by indicating the voltage drop across a fixed resistor in the grid circuit.

[1] The work described here was sponsored by the Atomic Energy Commission.
[2] Civil Defense, Radiological Monitoring Instruments Specifications (Dec. 6, 1950).
[3] The Minimax dental film may be obtained from the Minimax Co., Chicago, Ill. The du Pont film was a specially prepared film packet used by the AEC and is no longer available.
[4] E. E. Charlton and H. S. Hubbard, Gen. Elec. Rev. **43,** 272 (1940).
[5] G. Failla, Radiology **29,** 202 (1937).

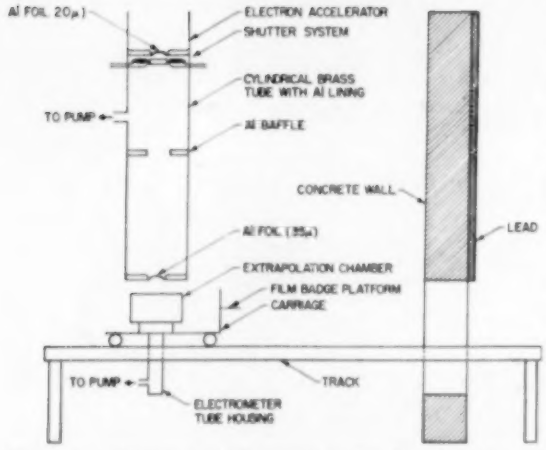

FIGURE 1. *Arrangement of apparatus showing the extrapolation chamber in position under the electron accelerator.*

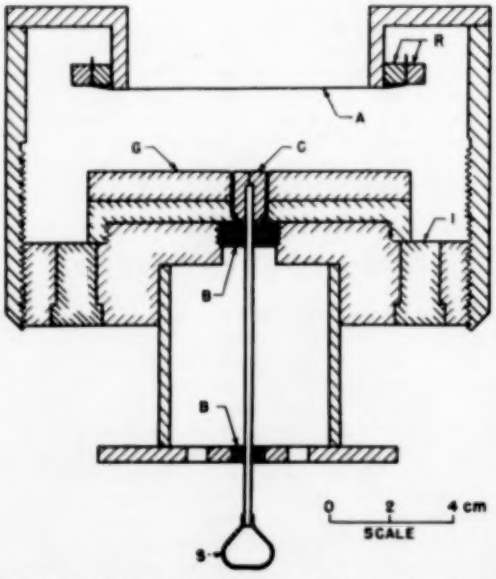

FIGURE 2. *Cross-sectional drawing of the extrapolation chamber.*

A, Accelerating electrode; B, amber bushings; C, collecting electrode; G, guard ring; R, Bakelite rings; S, phosphor bronze spring; I, Bakelite insulator.

It has recently been recommended [6] that electron dosages be expressed in terms of energy absorbed per gram of tissue at the position in question. It has been shown [7] that the energy, E_m, absorbed per gram of material is related to the number, J_m, of ion pairs produced in a small air cavity per gram of air by

$$E_m = sWJ_m,$$

where s is the stopping power of the material relative to air,[8] and W is the energy required to produce an ion pair (5.2×10^{-11} erg to within 3%). J_m is determined from the potential, V (volts), across the grid resistor, 4.56×10^8 ohms; the area of the collector, 0.855 cm²; the density of air at normal temperature and pressure, 0.00129 g/cm³; the actual air pressure, P (mm of Hg); the temperature, T (°K); the electronic charge, 1.60×10^{-19} coulomb; the time, t; and the plate separation, d (cm). Therefore,

$$E_m = \frac{(1.020)(5.20)(10^{-11})V(760)Tt}{(4.56)(10^8)(0.855)d(0.00129)P(273)(1.6)(10^{-19})}$$

$$= 1840\,\frac{VtT}{dP}.$$

Values of V were obtained experimentally for several different plate separations, d. The slope of the resulting curve gave V/d, and this, together with the pressure and temperature, gave the exposure rate, E_m/t.

Data were obtained at each 0.1 Mev in the range 0.5 to 1.4 Mev. The electron dosage rate was first determined at a given accelerating potential by the ionization chamber. The chamber was removed from the beam, and film were exposed to different dosages by timing the exposures. Ionization measurements were then repeated to determine the constancy of the dosage rate. For changes in dosage rates of less than 10 percent, average dosage rates were used; for changes larger than 10 percent, interpolated dosage rates were used.

Film exposures were also made on a large uranium plaque by placing the film directly on the tight 7 mg/cm² covering of the plaque. The dosage rate of the plaque had previously been measured [9] to be 20.1 (ergs/g)/hour at the surface of the covering by an extrapolation chamber method.

All films exposed at a given energy plus a control film were processed simultaneously. They were developed for 5 minutes in Eastman Liquid X-ray Developer and Replenisher at 20° C, fixed for 5 minutes at 20° C, washed for 30 minutes, and dried. Film density was determined on a calibrated Ansco-Sweet densitometer, model 11, for densities below 2.5 and on an Ansco color densitometer model 12 for higher densities.

3. Results and Discussion

Figures 3 and 4 show the results of the density-dosage determination of Minimax and du Pont 552 film, respectively. In each figure, two sets of curves are presented. The upper set are the data for the density-dosage relationship, using monoenergetic electrons, and the results are plotted, using the various values of the incident energy of the electrons as a parameter; the lower curve is the density-dosage relationship, using the uranium

[6] Recommendations of the International Commission on Radiological Units (London, 1950), Radiology **56,** 117 (1951). See also, U. Fano and L. S. Taylor, Radiology **55,** 743 (1950).

[7] L. H. Gray, Brit. J. Radiology **10,** 600 (1937).

[8] Computed values of s vary with electron energy, but 1.02 represents a mean value that is probably accurate to ±2% for the energy range of interest here.

[9] We are indebted to the New York Operation Office of AEC for the loan of this standard and for its calibration constant.

plaque. An examination of the data for monoenergetic electrons seems to indicate that the response of these films is independent of the energy. In order to establish this more accurately, the density was plotted against the energy by using several values of the dosage as a parameter (50, 100, and 150 ergs/g). By the method of least squares, it was determined that to within the accuracy of the results the density-dosage relationship is independent of the energy in the energy interval 0.5 to 1.4 Mev. These results can be understood in the following qualitative manner: The dosage to which a film has been exposed is essentially a measure of the amount of energy that has been expended by the electron in its traversal through a film. The main cause of this energy loss results from the inelastic scattering of the electrons by the atoms of the photographic emulsion. However, this process is the mechanism that accounts for the darkening of film. Consequently, to a first approximation, one expects a linear dependence of density upon dosage for electrons of sufficient energy to penetrate the film completely.

Pelc [10] has made the most intensive theoretical study of the action of X-rays and electrons on photographic film. He shows that the form of the density-dosage relationship is

$$D = D_0\ (1 - e^{-\epsilon r}),$$

where D_0 is the saturation density, and r is the dosage in roentgens. The quantity ϵ is a function of the mass of the undeveloped grains, the number of quanta required to affect a grain, and in the case of X-rays, the mass absorption coefficient of the silver-bromide grains. Expanding the quantity in the exponent, it will be observed that for small values of (ϵr) one must expect a linear function for the density-dosage relationship. In the low-density region, it will be observed that the density does indeed exhibit this linear relationship very well. This independence of the response of the film to electron energy and the linear dependence upon energy loss in the film is of the type to be expected from Pelc's results. As shown by these curves, the slope of the curve is determined only by the type of film used, that is, upon grain size, etc. For the du Pont 552 film only, there exists a slight amount of curvature for densities greater than 1.0. The saturation density for this film has been determined to be roughly 3.5; thus, the curvature that is observed results from the saturation properties of the film. For Minimax film, this curvature is not observed in the density range zero to six. In the low-energy region where the incident electrons are stopped in the film, the response of the film can be expected to be energy dependent.[11]

The lower curves of figures 3 and 4, respectively, show the response of Minimax and du Pont 552 film when exposed to uranium. These curves indicate a slope that is roughly one-half that of the corresponding curves obtained by using monoenergetic electrons in the previously mentioned energy interval. This difference in slope results from the difference in the energy spectrum to which the films have been exposed. The electrons from the uranium plaque have a continuous spectrum with a calculated most probable energy at roughly 0.1 Mev and an average in the neighborhood of 0.45 Mev. In the decay scheme of U^{238} there are six beta emitters of interest, UX_1, UX_2, RaB, RaC, RaD, and RaE.[12] Emitters UX_1 and RaC each have two possible modes of decay. For UX_1 the beta spectrum of one of the transitions has a maximum energy of 0.205 Mev and is 80 percent probable; the other has a maximum energy of 0.11 Mev and is 20 percent probable. For RaC, the end-point energies are 1.65 and 3.16 Mev with a probability of 80 percent and 20 percent, respectively. The remaining end-point energies are 2.3, 0.7, 0.029, and 1.16 Mev, respectively. From these data, semiempirical beta spectra[13] have been constructed for each of these transitions to determine a composite spectrum. In this manner, the above values of the most probable energy and average energy have been determined. The film itself is wrapped in two layers of paper whose total thickness is of the order of 25 mg/cm². From the curve of the composite U^{238} spectrum, it can be shown that the fractional number of electrons absorbed in the paper wrapping is of the order of 22 percent, so that the fractional loss of electrons due to their absorption by the paper covering is large for electrons from uranium and small for electrons from the monoenergetic

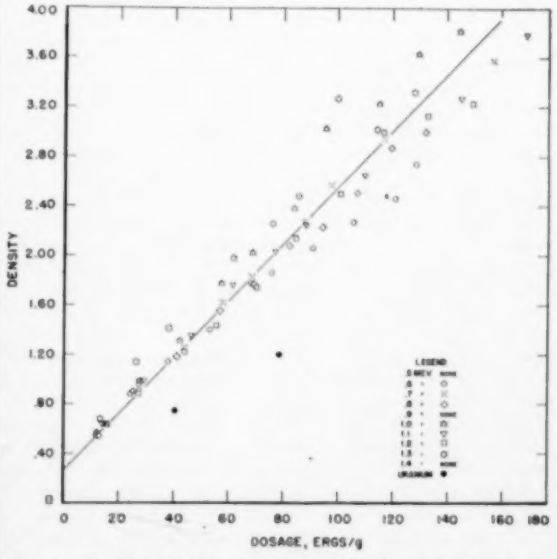

FIGURE 3. *Density-dosage curves for Minimax Dental X-ray film Extra Fast.*

[10] S. R. Pelc, Proc. Phys. Soc. **57**, 523 (1945).
[11] R. F. Baker, E. G. Ramberg, and J. Hillier, J. Applied Phys. **13**, 450 (1942); B. v. Borries, Z. Physik **119**, 498 (1942); Physik. Z. **43**, 190 (1947); H. F. Nissen, Z. Physik **122**, 573 (1944).
[12] Nuclear data, NBS Circular 499 (Sept. 1, 1950).
[13] L. D. Marinelli, R. F. Brinkerhoff, and G. J. Hine, Rev. Modern Phys. **19**, 25 (1947).

beam. Consequently, the reduced density of the film when exposed to the uranium plaque results from the loss of electrons by absorption, as well as the modification of the electron energy spectrum upon passage through the paper wrapping.

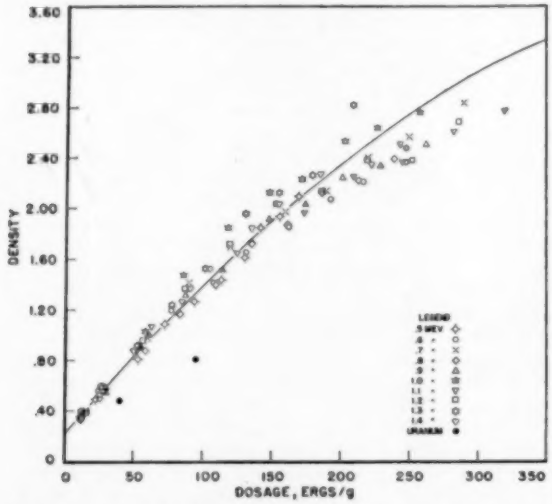

FIGURE 4. *Density-dosage curves for du Pont Dosimeter film type 552 single film packet.*

An auxiliary experiment was performed to determine the dependence of the Minimax dental film only upon the energy spectrum of the incident electrons. In addition to the paper wrapping normally present, aluminum absorbers of varying thickness were wrapped around the film, and the films were exposed to the uranium plaque until each received a surface exposure equal to 41.9 ergs/g of tissue-equivalent material. A set of data was obtained by using monoenergetic electrons at 0.6, 0.9, and 1.2 Mev. The results of this experiment are shown in figure 5. The upper curves are the results for the density of the film with aluminum absorbers when exposed to monoenergetic electrons at the three energies. The lower curve is the result for the identical experiment using the uranium plaque. For zero aluminum absorber, the density of the exposed film after background had been subtracted is approximately 0.52 for the lower curve. This value is to be compared with the density of 0.45 obtained from the corresponding point in figure 3 when the background of 0.25 is subtracted. In figure 5, the density of the film for zero aluminum absorber at 0.6 and 1.2 Mev is 1.10 and 0.87 respectively. Comparison with 0.9 Mev is omitted as no density-dosage information had been taken at this energy for Minimax film. The densities from figure 3 at a dosage of 41.9 ergs/g are 0.90 and 0.95 for the energies 0.6 and 1.2 Mev, respectively. The curves of figure 5 for the monoenergetic electrons give an average density of 0.97 for zero aluminum absorber. This value stands in good agreement with the value of 0.94 obtained from figure 3.

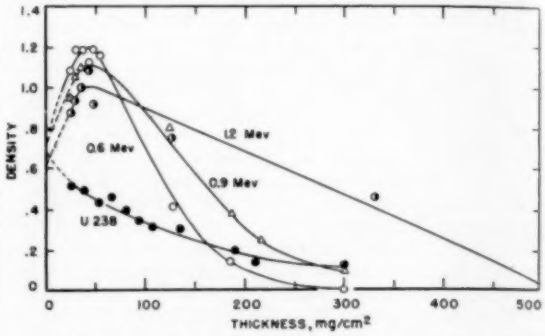

FIGURE 5. *Electron absorption curves by using aluminum absorbers.*

A, Thickness of paper covering the film. Penetration by electrons; dosage equals 41.9 ergs/g.

It is clear from the foregoing results that a simple determination of the density is not sufficient in order to determine uniquely the dosage to which the film has been exposed. In addition to the density, a knowledge of the energy spectrum of the electron beam would be required. In order to circumvent this limitation, a step-wedge type of filter could be used. A plot of the filter thickness against film densities would then permit extrapolation to a filter thickness of 7 mg/cm². Because the thinnest filter would have to be quite thick in order to make the packet light tight and because beta rays and electrons produce very different types of attenuation curves, the proposed filter would not give a high order of accuracy, but in many cases it may be sufficient for personnel monitoring.

The authors thank H. O. Wyckoff for the many helpful discussions during the course of the experiment; C. R. Horner, now with the Department of the Navy, who was chiefly responsible for the design of the extrapolation chamber and the FP–54 electrometer housing; and J. A. Simpson, for the design and construction of the electron extractor.

WASHINGTON, August 24, 1951.

al of Research of the National Bureau of Standards Vol. 48, No. 2, February 1952 Research Paper 2296

Thermal Converters as AC-DC Transfer Standards for Current and Voltage Measurements at Audio Frequencies

Francis L. Hermach

Thermal converters and associated equipment that are used as ac-dc transfer standards at the National Bureau of Standards for the precise measurement of current and voltage at power and audio frequencies are described. The standards and the equipment are primarily used to standardize a-c ammeters and voltmeters submitted to the Bureau for certification. The ac-dc transfer may be made with these thermal converters at currents from 1 milliampere to 50 amperes, voltages of 0.2 to 750 volts, with an accuracy of 0.01 percent at frequencies from 25 to 20,000 cycles per second.

The special tests to insure the required accuracy of the transfer standards are described, and the results are presented. A number of factors that limit the transfer accuracy of thermal converters have been discovered, and the results of special tests and theoretical work to evaluate these factors are discussed. The solutions, by an approximation method, of certain pertinent nonlinear differential equations governing the heating of a conductor by an electric current are given.

1. Introduction

The increasing use of electric energy for aircraft, induction furnaces, and induction heating, and the greater accuracy required in measurements in electronics, have led to increasing demands for the accurate standardization of ammeters and voltmeters at frequencies extending upward from power frequencies through the entire audio-frequency range. To meet these demands, special instruments have been developed at the National Bureau of Standards for the measurement of current and voltage over rather wide ranges. They make use of thermal converters [1] (often called thermoelements) like those incorporated in ordinary thermocouple instruments, but differ in the manner of reading and use. They may be used either directly to measure the ac-dc differences of ammeters and voltmeters, or with a suitable potentiometer and accessories to measure alternating currents and voltages. They were designed and are used primarily for testing electric instruments, at currents from 1 ma to 50 amp and voltages from 0.2 to 750 v, with an accuracy of 0.01 percent at frequencies from 25 to 20,000 c/s.

2. Transfer Principle

The basic electrical units are defined in terms of a concordant system of mechanical units and are realized by absolute electrical measurements carried out at national standardizing laboratories to fix the value of groups of standard cells and resistors. These standards are used in conjunction with a potentiometer to make measurements of direct voltage, current, and power. It has been known for a long time, but not sufficiently realized, that the measurement of the corresponding alternating-current quantities depends fundamentally on certain standard types of electric transfer instruments that ideally have the same response on direct and alternating current. If the instruments are calibrated on direct current at the time of each use and if the precision of reading is suitably increased, long-time stability, freedom from drift, small temperature influence, low losses, and other normally desirable characteristics become of secondary importance, and the instruments may be primarily designed and constructed to have the best possible frequency characteristic. For difference measurements such instruments need not have long scales in the ordinary sense, but rather may be designed for increased precision of reading by methods that would not be applicable to instruments intended for general service.

Special electrodynamic transfer instruments have long been used at the Bureau for accurate a-c measurements. These transfer standards are used largely to standardize (test) other instruments submitted to the Bureau for certification. There are two distinct types of such tests. For the "straight a-c test", the instrument under test and a transfer standard are connected to measure the same alternating electrical quantity (current, voltage, or power), which is adjusted to produce the desired deflection of the test instrument. The response of the standard instrument is observed, then the standard is transferred to direct current. The direct quantity is adjusted to give the same response of the standard and is then measured with a suitable potentiometer and accessories. For the so-called "ac-dc difference test", both instruments are connected to measure the same quantity first on alternating and then on direct current, which is in each case adjusted to give the same deflection of the test instrument. From the averaged difference in the response of the transfer standard, the ac-dc difference of the test instrument is computed. The second type of test can be made with somewhat higher accuracy than the first, and in conjunction

[1] Proposed AIEE definition 30.89.040: A thermal converter is a device that consists of one or more thermojunctions in thermal contact with an electric heater or integral therewith, so that the electromotive force developed at its output terminals by thermoelectric action gives a measure of the input current in its heater.

with a test on direct current gives more information about the performance of the test instrument. Because the ac-dc difference of an instrument depends upon geometrical factors that are relatively permanent, subsequent tests for checking the constancy of calibration need generally be made only on direct current. Occasionally transfer tests are made by using a selected low frequency (such as 60 c/s) as the reference in place of direct current.

An example of the accuracy with which such tests are made, laboratory standard instruments, with scales 12 in. long, are regularly standardized and certified at the Bureau to 0.05 of a scale division. For a 150-division instrument this requires an accuracy of measurement of 0.03 percent or better.

3. Development and Description of Electrothermic Transfer Standards

3.1. Choice of Standards

Several types of instruments were considered in choosing transfer standards to cover the full audio-frequency range. Electrodynamic instruments have been highly developed [1, 2, 3][2] at the Bureau for measurements at the commercially important power frequencies and can be used with proper corrections, up to about 2,000 c/s. However, unavoidable inductance and stray capacitance errors limit their useful frequency range and present little hope for the desired extension. Electrostatic instruments have been carefully studied [4, 5] at the National Physical Laboratory. They are useful over wide frequency ranges, but because of their low-torque–weight ratio at low voltage are not readily adaptable for either the low voltage or the current ranges desired in this application. Electrothermic instruments, which use an effect produced by the heating of a conductor carrying a current to be measured, seemed more promising. Of the several kinds, thermocouple instruments, in which the temperature rise of the conductor (heater) is measured by a thermocouple, seemed most feasible. Straight-wire heaters allow a wide frequency range, and the thermocouple measurements permit high precision of reading. The usual disadvantages of poor stability and large temperature influence are not important in their use as transfer instruments, and their low overload capacity is not a serious limitation in careful laboratory work. Fortunately, good thermal converters are commercially available. They have been used for measurements at frequencies up to about 65 Mc, with a d-c millivoltmeter as the indicator, and are generally considered in the ½- to 2-percent accuracy classes. So far as is known, they have not been previously studied for use as transfer instruments at the frequencies and the accuracies needed in this application.

For these reasons, commercial thermal converters were selected for study to determine their value as ac-dc standards in a wide-range audio-frequency transfer voltmeter. A careful experimental and theoretical study of their performance led to the purchase of additional commercial thermal converters of suitable ranges and the design and construction of equipment for using them as transfer standards for voltage and current.

[2] Figures in brackets indicate the literature references at the end of this paper.

3.2. Description of Transfer Standards

Each thermal converter purchased in the milliampere ranges is of the vacuum type, mounted in an evacuated glass bulb with supports of copper wire embedded in the glass. The conductor, heated by the current to be measured, is a short straight wire generally less than ½ cm long and often less than 0.001 in. in diameter. The heater alloy and dimensions are chosen to give a temperature rise of about 200° C at the center where the hot junction of the thermocouple is fastened by a ceramic bead. This bead provides electrical but not thermal insulation between the heater and thermocouple circuits, with a coupling capacitance less than 1 $\mu\mu$f and an insulation resistance greater than 50 megohms at 25° C.

Because high current sensitivity is not required, the thermal converters in the 1- to 50-amp ranges are not evacuated. The hot junction of the thermocouple is welded directly to the midpoint of a thin-walled tubular heater. These thermal converters are temperature compensated [6].

For current measurements, thermal converters in the series 1, 2, 5, 10, etc., with rated output electromotive forces of 10 mv were purchased, with ranges from 1 ma to 50 amp. Thermal converters of 7.5- and 30-ma ratings, with appropriate series resistors, are used for voltage measurements. Figures 1 and 2 show some of the thermal converters and the model A and model B voltmeter elements. It should be emphasized that the caption NBS on the nameplate sbown in figure 2 signifies only that the equipment was assembled for use at the National Bureau of Standards. All the thermal converters were purchased commercially, as were the components of the voltmeters. It should also be emphasized that the thermal converters shown in these figures are the transfer elements only. An indicator (to be discussed in the next section) is necessary for all measurements, and a potentiometer and accessories are also necessary, except for transfer tests of other instruments.

The model A voltmeter was developed as a prototype instrument to meet an immediate need for voltage measurements. It consists of a 30-ma thermal converter connected with its heater in series with a commercial decade resistance box, modified to have two 1,000-ohm-per-step decades, and a 100-, a 10- and a 1-ohm-per-step decade, all in series. As shown in figure 3, one end of the heater of the thermal converter is connected to the low-side terminal of the box, with the shield of the box connected to the other end of the heater and to the shield of the coaxial cable connecting the instrument to the circuit. The center lead of this cable is connected directly to the high-side terminal of the box.

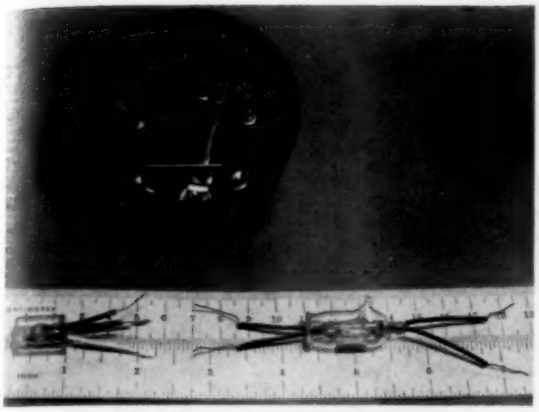

FIGURE 1. *Typical thermal converters.*

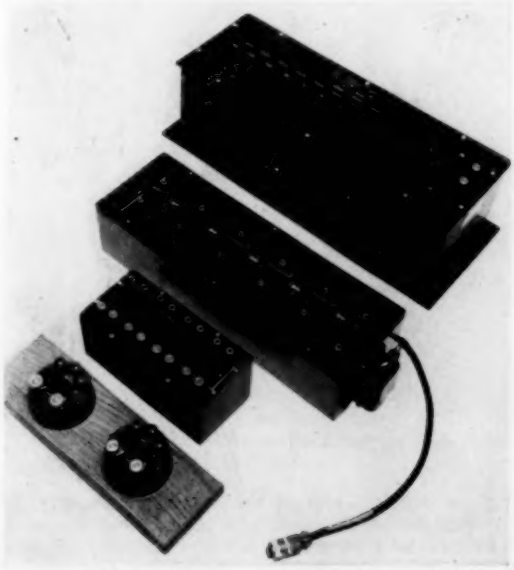

FIGURE 2. *Mounted thermal converters and the model A and model B voltmeter elements.*

Like the electrodynamic transfer standards used at lower frequencies, the series resistor is adjusted in use to give the same nominal current level for each measured voltage. This was chosen at 20 ma, resulting in a voltmeter having a constant 50 ohms/v and an upper range of 400 v. The model A voltmeter, described in some detail in an earlier paper [7] is now no longer used for routine measurements.

For the model B voltmeter, a built-in 7.5-ma thermal converter was used, with a fixed resistor having taps to give voltage ranges of 1.5, 3, 6, 7.5, 15, 30, 60, 75, 150, 300, 600, and 750v. The resistance cards for this instrument were purchased commercially, and the cards and thermal converter were mounted in a suitable shielded box with the shield connected to the low-side terminal of the instrument, as shown in figure 3. For both instruments the effects of capacitance currents and of the self-inductance of the resistors were carefully considered; the limiting factors are discussed in another section of this paper.

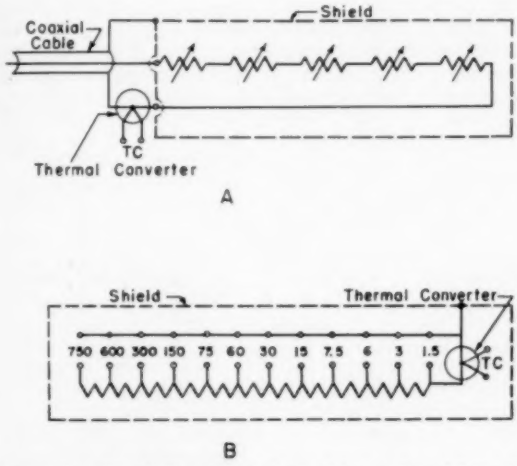

FIGURE 3. *Circuit diagrams of the model A and model B voltmeter elements.*

A, Model A voltmeter element; B, model B voltmeter element.

3.3. Indicator

Because of its convenience and portability, a millivoltmeter is generally used for measuring the emf in the usual thermocouple instrument. The precision of reading of the usual millivoltmeter is of course far too low for this application. For increased accuracy a potentiometer can be used to measure the thermocouple emf. However, if the thermal converter is used only as a transfer standard, the emf need not be measured in a "straight a-c" test; and in ac-dc difference tests it is only the small change in emf between the a-c and d-c settings that is significant. The change and the full emf with which it is compared need be measured with relatively low accuracy, provided the change is referred to a highly stable base value. Thus high sensitivity and high stability but only moderate accuracy in the measurement of emf are required of the indicator. For these requirements, a Lindeck potentiometer for providing the base value, used in conjunction with a suitable galvanometer, the deflection of which indicates the change, forms the ideal indicator. In a Lindeck potentiometer, based on Poggendorf's second principle [8], the emf to be measured is balanced by an adjustment of the current through a fixed resistor. At balance the voltage drop across the resistor, which is the product of the potentiometer current and the resistance, is equal to the measured emf. The current is ordinarily measured with a milliam-

meter, which generally sets the limit on the accuracy obtainable with this form of potentiometer.

Such a potentiometer has been incorporated in a panel constructed for the audio-frequency testing. It was designed to have adequate stability, freedom from changing extraneous electromotive force and the required ranges, with sufficient precision of reading. Its circuit is shown in the central portion of figure 4. The resistor, R, is made of manganin, and a special thermofree key [8] and copper binding posts are used in the electrothermally sensitive emf circuit. The components are mounted in the central part of the panel, as shown in figure 5, and are enclosed by a grounded metal shield. No other thermal precautions were found necessary. A reflecting wall-mounted galvanometer is used, with a voltage sensitivity (in the circuit) of 1 mm/μv. A No. 6 dry cell supplies the potentiometer current, which is adjustable from 0.2 to 1.2 ma. At these current levels, repeated tests have shown that the steady drift in the voltage across the four terminal resistor is less than 0.02 percent per hour, and that superposed fluctuations are much less than 0.01 percent. The four-terminal manganin resistor has taps at 0.1, 0.5, 2.5, 5, 10, and 25 ohms, giving milivolt ranges, at a current of 1 ma, of these same numerical values. The lowest range is used in transfer tests as a quick check of the potentiometer. With the thermocouple of the thermal converter connected to the "TC" posts of the potentiometer, but with no current through its heater, a galvanometer deflection of 10.0 cm to the left on the scale with the Lindeck set for 0.1 mv serves as a valuable partial check of the required accuracy and correctness of the Lindeck circuit.

3.4. Use of Instruments

These transfer standards are used almost solely for standardizing other a-c instruments. The necessary switching and control circuits for such tests have been incorporated in the panel shown in figure 5. In addition to these circuits and the Lindeck potentiometer, the panel contains the impedance-matching transformers for the high-voltage circuits used in testing voltmeters and the high-current circuits used in testing ammeters. The present transformers provide ranges up to 50 amp and 800 v, with a nominal input voltage of 150 v and a power level up to 100 w.

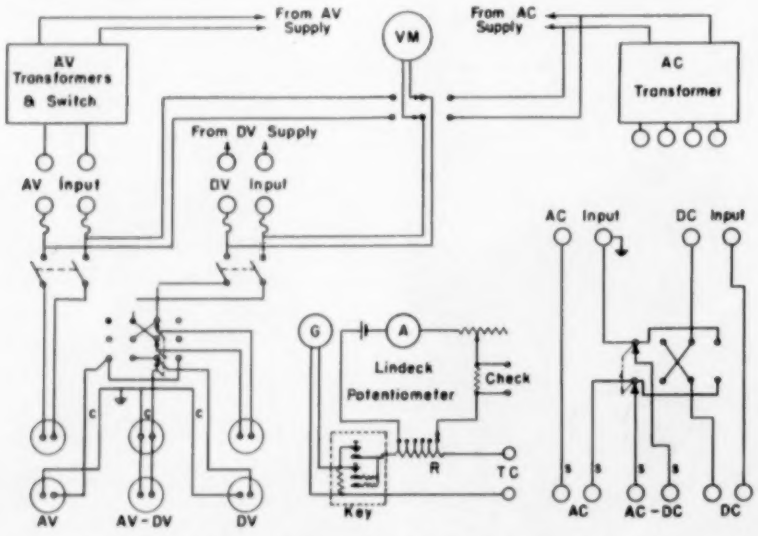

FIGURE 4. *Schematic diagram of circuits used for testing instruments.*
C signifies coaxial lead with shield grounded; S signifies shielded lead with shield grounded.

Motor-generator sets and voltage stabilizers are available for tests at 60 c/s and audio-frequency oscillators and power amplifiers for tests at other frequencies. Batteries, controlled by suitable adjustable resistance voltage dividers and series resistors, are used for the necessary direct-current sources. The potentiometer, standard cells, volt boxes, and resistors are those normally used for instrument testing and are periodically standardized to insure a continued accuracy of considerably better than 0.01 percent.

A schematic diagram of the major circuits and equipment on this panel is shown in figure 4. For an a-c test of an ammeter, the transfer thermoelement is connected to the AC-DC binding posts and its thermocouple to the TC posts on the panel. The test instrument is connected to the AC posts, and a suitable four-terminal standard resistor is connected to the DC posts for use in measuring the d-c current by means of a potentiometer. For low currents at the higher audio frequencies, shielded leads with the

shields grounded are used to minimize errors due to stray capacitance currents. The alternating current is adjusted for the desired deflection of the test instrument, and the Lindeck potentiometer is adjusted for an "on-scale" deflection of the galvanometer. The standard instrument is then switched to direct current, which is adjusted to give the same galvanometer deflection and is then measured with the external potentiometer. The direct current through the heater of the thermoelement is then reversed and the d-c measurement repeated.[3]

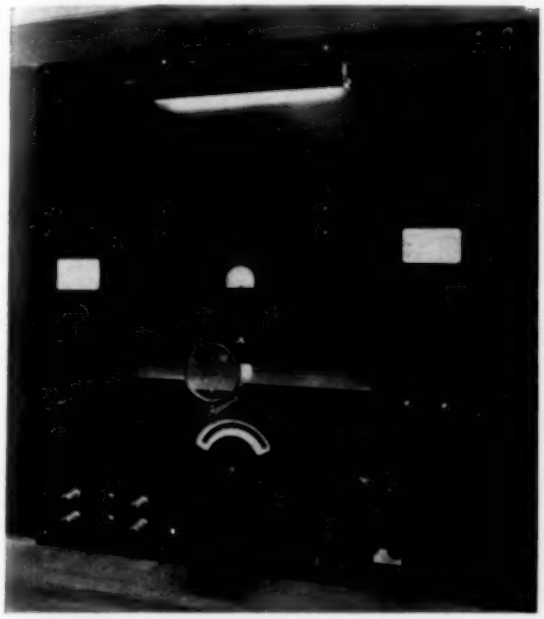

FIGURE 5. *Instrument testing panel, including Lindeck element.*

For an a-c test of a voltmeter, a similar procedure is used. The transfer standard is connected to the AV-DV receptacle on the panel with a coaxial lead, with due care to connect its thermal converter to the grounded shield of this lead, and the thermocouple is connected to the TC posts on the panel. The test instrument is connected to the circuit with a special twin lead consisting of two coaxial lines permanently paralleled at the instrument and connecting to the two AV receptacles on the panel. Similar leads of the same length are used to connect the high side of a volt box for use with the external potentiometer to measure the direct voltage, to the two DV receptacles. The use of these leads eliminates the effect of any stray magnetic field or lead resistance on the measurements.

This simple procedure is reliable only if the drift of the response of the standard instrument is negligibly small in the time taken for a series of such readings. This is fortunately true for each of the thermal converters used. After an initial warm-up period of a minute or so, the maximum observed drift under those laboratory conditions of any of the thermal converters tested was less than 0.5 percent per hour, and the average less than 0.05 percent per hour. If it were necessary, the effect of significant drift could be practically eliminated by using a deflection method as outlined for transfer tests, calibrating the standard instrument on direct current at the nominally correct current or voltage before and after each a-c setting.

For ac-dc difference or transfer tests, which are more frequent and usually more important than straight a-c tests, the test and standard instruments are connected in series to the AC-DC posts [4] in the case of ammeters, or in parallel with suitable coaxial leads to the AV-DV receptacles in the case of voltmeters. Suitable short leads are used to connect the two AV receptacles together and to connect the two DV receptacles together. The current or voltage is adjusted for the desired deflection of the test instrument, and the Lindeck potentiometer is adjusted for a deflection near the null position at the center of the galvanometer scale. The two instruments are then in quick succession connected to alternating, direct, reversed direct, and then alternating current. The current is adjusted to give the same deflection of the test instrument in each case. The resulting deflections of the galvanometer of the Lindeck potentiometer are observed with the potentiometer controls undisturbed. This procedure practically eliminates any effect of drift in either instrument, and errors in repeating the settings of the instrument under test can be made very small by using a low-power microscope and setting the image of the instrument pointer in coincidence with a cross-hair in the eyepiece. The control circuits have been arranged to facilitate switching, and with two observers the procedure is rapid even with moderately fluctuating voltages as only one of the two instruments is set to a given deflection.

From the average of the deflections on alternating and on direct current, the ac-dc difference of the test instrument is readily computed by a simple formula.[5]

4. Evaluation of Transfer Performance

The ac-dc difference of each transfer standard must be known to the full accuracy desired in the measurements to be made. As, in a sense, there are no absolute transfer standards, such an evaluation essentially consists of four steps.

1. Choice of a type of instrument that theory indicates is suitable over the desired ranges.
2. Study of all known effects that can cause such an instrument to depart from this ideal.
3. Construction and use of an instrument in such a way that these effects, by computation or direct tests of the separate components, are negligible or known.

[3] Such reversed d-c readings are common practice for highest accuracy with all types of ac-dc instruments.

[4] One terminal of the heater is connected to the post that is grounded on alternating current.

[5] The formulas used in computing the results of the a-c and transfer tests are developed in appendix 1.

4. Comparison of actual transfer performance of the standard with that of some other instrument, preferably of a quite different type, whose performance has also been evaluated.

The evaluation of these electrothermic transfer standards was considered of primary importance because of the high order of accuracy demanded in this application. The unique facilities of the Bureau made this quite feasible, particularly for step 4, which is necessary to guard against errors from unsuspected causes. Prototype instruments such as these, in which previously available ranges are greatly extended, cannot be directly compared with other types of standards over their full range. The evaluation therefore consisted of the study, computations, and special tests of steps 2 and 3 during the design and construction of these instruments and their panel, the intercomparisons of thermal converters of adjacent current ranges in the series, the comparison at low frequencies of selected thermal converters with the electrodynamic transfer standards at the Bureau, and the comparison of these thermal converters with certain portable hot-wire and electrostatic instruments also available.

A thermal converter can be used as a transfer standard for alternating-current measurements over the range of frequencies for which the response characteristic, $E=f(I)$, is the same as with direct current, where E is the output emf, and I the current through the heater of the thermal converter. For a voltmeter element consisting of a resistor in series with a thermal converter, the magnitude of the effective impedance $Z=V/I$ must also be equal to the effective resistance on direct current, where V is the applied voltage. In addition to these two requirements for instrument testing, the fundamental principle that the standard and the instrument under test "see" exactly the same quantity must be carefully observed.

The response characteristic of the types of thermal converters used were believed to be suitable at frequencies far higher than those used in this application, and their direct-current and low-frequency responses were verified by special tests described in other sections. The effective impedance of each voltmeter element was approximately computed from inductance and capacitance data supplied by the manufacturer of the resistance cards, and was verified by special tests to be described later. The capacitance and resistance of the Lindeck potentiometer to ground were measured and found to be 1,600 $\mu\mu$f and 10,000 megohms at an ambient relative humidity of 40 percent. Thus the computed stray currents are sufficiently small so that no appreciable fraction of the currents measured will be diverted through the thermocouple at audio frequencies when one end of the heater is grounded. The use of shielded leads where necessary, the avoidance of a ground between the test instrument and the standard in the current circuits, and the use of the special coaxial lines in the voltage circuits assure that the fundamental principle is observed even at the smallest current and voltage in the present ranges.

The comparison tests of step 4 were planned to give maximum possible assurance against errors due to unsuspected causes. Each comparison consisted of repeated careful transfer (ac-dc difference) tests, as described in section 3.4. The 1-, 2- and 5-amp thermal converters were compared with the NBS electrodynamic transfer ammeter at selected frequencies from 25 to 200 c/s. The model A voltmeter was compared with the NBS suppressed-zero electrodynamic voltmeter at frequencies of 30 and 60 c/s and voltages from 20 to 240 v. Both of these electrodynamic instruments have been carefully studied [1, 2]. They can be read with a precision of better than 0.005 percent. The results of these comparisons, corrected for the small known transfer errors of the electrodynamic instruments, are shown in table 1. They are estimated to be accurate to 0.005 percent or better. The results of these tests disclosed that the model A voltmeter and the electrodynamic voltmeter were in excellent agreement at these frequencies.

TABLE 1. *Results of comparisons of thermal converters with other types of instruments*

Thermal converter range	Other instrument	Test current or voltage	Comparative ac-dc difference								
			25 c/s	30 c/s	60 c/s	100 c/s	200 c/s	1,000 c/s	10,000 c/s	15,000 c/s	20,000 c/s
amp		*amp*	%	%	%	%	%	%	%	%	%
1	Electrodynamic ammeter	0.4	−0.001	.....	+0.001	−0.001	−0.002	.....	.....	.....	.....
1	do	1	−.053	.....	.....	−.008	−.001	.....	.....	.....	.....
1	do	1.2	−.067	.....	−.013	−.008	−.005	.....	.....	.....	.....
2	do	0.8	−.022	.....	−.001	+.001	+.001	.....	.....	.....	.....
2	do	2	−.115	.....	−.025	−.009	+.001	.....	.....	.....	.....
2	do	2.4	−.154	.....	−.035	−.015	−.002	.....	.....	.....	.....
5	do	4	−.004	.....	−.006	−.005	.....	.....	.....	.....	.....
5	do	5	−.010	.....	.....	−.005	.....	.....	.....	.....	.....
5	do	6	−.011	.....	−.018	−.008	.....	.....	.....	.....	.....
5	Hot-wire ammeter	4	.....	.....	.....	.....	.....	.....	.....	.....	−0.006
	do	5	.....	.....	.....	.....	.....	−.007	−0.004	.....	−.002
		v									
Model A voltmeter	Electrodynamic voltmeter	20	.....	.....	−.004	.....	.....	.....	.....	.....	.....
Do	do	50	.....	.....	−.005	.....	.....	.....	.....	.....	.....
Do	do	120	.....	−0.002	.....	.....	.....	.....	.....	.....	.....
Do	do	150	.....	.....	−.003	.....	.....	.....	.....	.....	.....
Do	do	240	.....	.....	−.002	.....	.....	.....	.....	.....	.....
Do	Electrostatic voltmeter	150	.....	+.004	.....	−.002	.....	+.004	−.004	.....	−.002
Do	do	300	.....	+.004	.....	−.004	.....	−.010	.....	−0.008	+.009

They disclosed significant disagreements between the ampere-range thermal converters and the electrodynamic ammeter, which were considered to be due to a low-frequency error in the 1- and 2-amp thermal converters and a small error independent of frequency in the 5-amp thermal converter.

The model A voltmeter was also compared with two new high-grade portable pivoted electrostatic voltmeters, having scales over 5 in. long, at selected frequencies from 30 to 20,000 c/s. For increased precision a low-power microscope was focused on the pointer of the electrostatic instrument under test. This instrument was always set to the same deflection and was tapped lightly before each reading. Repeated sets of careful readings were taken at each frequency, and all tests were at the full-scale deflection of the electrostatic instrument. Because of these repeated readings and the favorable conditions, the averaged results are estimated to be accurate to 0.01 percent. The results, as shown in table 1, verify the absence of capacitance errors in the thermal voltmeter. Direct comparisons at the higher frequencies could not be made at lower voltages, but calculations indicate that skin effect and the effect of inductance should be considerably less than 0.01 percent at 20,000 c/s.

Similarly, the 5-amp thermal converter was compared with a high-quality portable 5-amp hot-wire ammeter at frequencies from 25 to 20,000 c/s. The results, as shown in table 1, indicate excellent agreement at frequencies of 1,000 c/s and above. Tests at lower frequencies showed very puzzling discrepancies, which, in a separate investigation, were traced to vibration errors [6] in the hot-wire instrument. For that reason the results at frequencies less than 1,000 c/s are not shown in this table.

A plus sign in table 1 indicates that with equal response of the thermal converter on direct and alternating currents the response of the other instrument was greater on alternating than on direct current.

Each thermal converter was compared with the next higher- and lower-range thermal converter in the series at two currents and at selected frequencies from 25 to 20,000 c/s. The results of each of these comparisons at the higher of the two currents at which tests were made are shown in table 2. They are estimated to be accurate to somewhat better than 0.01 percent, with very little possibility of systematic error. A plus sign in the table indicates that with equal response of the lower-range thermal converter on alternating and on direct currents, the response of the higher-range thermal converter was greater on alternating than on direct currents. This series of tests was made to extend stepwise the results of low-frequency comparisons with the electrodynamic ammeter, and to indicate any high-frequency effects that might well be expected to differ in different thermal converters.[7] The group

[6] Electromagnetic forces between the hot wire and its closely adjacent iron mounting plate resulted in vibration of the wire because the plate was magnetized by the damping magnet of the instrument. This vibration caused additional cooling and thus an error that was as large as 0.2 percent at certain frequencies.

[7] The percentage errors due to any high-frequency effects would be expected to be independent of the current level and could thus be evaluated by these tests

TABLE 2. *Results of intercomparisons of thermal converters*

Thermal converter ranges	Test current	Comparative ac-dc difference					
		25 c/s	100 c/s	400 c/s	1,000 c/s	10,000 c/s	20,000 c/s
	ma	%	%	%	%	%	%
1 to 2 ma	1.2	0.000			0.000		+0.006
2 to 5 ma	2.4	+.006			+.003		−.003
5 to 10 ma	6	+.004			.000		.000
10 to 20 ma	12	.000			+.004		−.006
20 to 30 ma[a]	24	+.001		−0.003	−.001		.000
30[a] to 50 ma	36	+.004			.000		.000
50 to 100 ma	60	+.024	+0.028		+.036		+.027
100 to 200 ma	100	−.046			−.044	−0.050	−.049
200 to 500 ma	240	+.026					+.039
500 to 1,000 ma	600	−.002			−.002	+.002	+.002
	amp						
1,000 ma to 1 amp	1.2	+.034			−.065	−.056	−.065
1 to 2 amp	1	−.028	−.002		−.002	−.002	+.001
2 to 5 amp	2	−.123	−.011		+.003	+.004	+.009
5 to 10 amp	5	−.008	−.006		−.006	−.007	−.004
10 to 20 amp	10	−.010	−.010		−.008	−.012	−.009
20 to 50 amp	20	−.014	−.015	−.014	−.018	−.035	

[a] This 30-ma thermal converter was the one used in the model A voltmeter.

of tests disclosed small discrepancies independent of frequency in a few thermal converters, and verified the absence of any high-frequency errors in the thermal converters tested. However, they could not be used to assign numerical values to the errors of individual thermal converters in the milliampere range as the differences were found to depend upon the current. The concluding series of tests to evaluate these errors were comparisons of a shunted thermal converter with each of those pairs of thermal converters that showed discrepancies in the previous intercomparisons. The model A voltmeter was shunted with a bifilar resistor of computed skin effect and time constant for tests at currents from 1 to 40 amps, and with a suitable high-quality audio-frequency decade resistance box for tests at lower currents. The results are shown in table 3 and are estimated to be accurate to better than 0.01 percent. A positive sign in this table indicates that with equal

TABLE 3. *Results of comparisons of selected thermal converters with shunted model A thermal voltmeter*

Thermal converter range	Test current	Comparative ac-dc difference		
		25 c/s	100 c/s	400 c/s
ma	*ma*	%	%	%
50	60	−0.003		
100	70		−0.043	
	100		−.062	
	120	−.065		−0.065
200	240	−.010	+.002	+.002
500	200	−.044		−.042
	400	−.056		−.054
	600	−.068	−.070	−.069
1,000	400	−.041		
	600		−.060	
	800	−.061	−.059	
amp	*amp*			
10	5	−.004		−.006
	10		−.014	−.015
	12	−.018		−.020
20	10	−.003		−.006
	20		−.015	−.017
50	24	−.023		−.024
	20	−.008		−.010
	40	−.010	−.010	−.010

response of the thermal converter on alternating and on direct current the response of the shunted model A voltmeter was greater on alternating than on direct current. The results of tests of the 1-, 2- and 5-amp thermal converters, duplicating those with the electrodynamic ammeter, are not shown in the table. The average difference between eight such duplicate results obtained with this ammeter and with the shunted model A voltmeter was 0.004 percent, and the largest difference was 0.013 percent. A few additional check tests of these thermal converters with the shunted voltmeter were made at other frequencies but are not tabulated.

The results of all these tests were combined to assign reliable values of ac-dc difference, δ, to each thermal converter in the series from 1 ma to 50 amp and to the model A voltmeter. These values were less than 0.01 percent for the model A voltmeter and for all the thermal converters of ranges less than 100 ma. The values for the other converters (rounded off to the nearest 0.005%) are shown in table 4.

TABLE 4. *Observed percentage ac-dc differences of thermal converters (to the nearest 0.005 percent)*

(a) Differences independent of frequency

Converter range	Percentage of rated current					
	40	50	60	80	100	120
ma						
1 through 50	(*)	(*)	(*)	(*)	(*)	(*)
100	.....	.....	−0.030	.....	−0.060	−0.065
200	(*)	(*)	(*)	(*)	(*)	(*)
500	−0.045	.....	.....	−0.055	.....	−.070
1000	−.040	.....	−.060	−.060	.....	.....
amp						
5	.000	.....	.000	−.005	−.010	−.015
10	.....	−0.005	.....	.....	−.015	−.020
20	.....	−.005	.....	.....	−.045	−.025
50	−.010	.....	.....	−.010	.....	.....

(b) Differences dependent upon frequency

Converter range	Test current	Frequency (cycles per second)			
		25	60	100	200
amp	*amp*				
1	0.4	−0.040	0.000	0.000	0.000
	1.0	−.055	.....	−.010	.000
	1.2	−.065	−.015	−.010	−.005
2	0.8	−.020	.000	.000	.000
	2.0	−.120	−.025	−.010	.000
	2.4	−.155	−.035	−.015	.000

* Less than 0.01 percent throughout.

The model B voltmeter, which was developed to give a wider voltage range and greater convenience of use than the model A, was compared with the model A voltmeter at rated voltage on each range up through the 300-v range and at 400 v on the higher ranges, at selected frequencies from 30 to 20,000 c/s. The results are shown in table 5 and represent directly the ac-dc difference, δ, of the model B voltmeter. They disclosed significant but not unexpected errors for the higher voltage ranges at the higher frequencies.

TABLE 5. *Results of comparisons of model A and model B thermal voltmeters*

Range of model B	Voltage	ac-dc difference of model B voltmeter				
		25 c/s	1,000 c/s	5,000 c/s	15,000 c/s	20,000 c/s
Volts		%	%	%	%	%
3 through 75	Rated	(*)	(*)	(*)	(*)	(*)
150	do	.....	.....	.....	.....	+0.013
300	do	.....	.....	.....	.....	+.024
600	400	.....	.....	+0.014	+0.044	+.054
750	400	+0.003	+0.011	+.028	+.064	+.082

* Less than 0.01 percent, 25 to 20,000 c/s each range.

As a result of these extensive series of tests, the transfer performance of each of this first set of thermal converters and of each of the two voltmeters was uniquely determined. Small but significant ac-dc differences of both known and unsuspected causes were found. Corrections for these differences can readily be applied when these thermal converters are used as transfer standards. However, an investigation of such differences is an especially important objective of a development such as this. As a result of such an investigation, a number of factors that limit the transfer accuracy of an electrothermic instrument were discovered and evaluated, with the results given in the following sections.

5. D-C Response

In all measurements with a transfer standard the average of the d-c response of the standard for the two directions of current is taken as the reference upon which the a-c measurements are based. For all three types of such standards, the reversed d-c average gives a better basis than does the response for one direction alone as effects that lead to small differences in response for the two directions of direct current are reduced to the second order of smallness when the average is taken.

Reversal differences may be expected in a contact thermal converter because of the flow of heater current through the hot junction of the thermocouple. This can cause a voltage drop in the thermocouple circuit, which may lead to second-order errors because of the nonlinearities of the thermal and electric circuits. This cause of reversal difference is minimized by the special constructions used in most high-range thermal converters, and is eliminated by the use of the small insulating bead between the heater and the thermocouple in the low-range thermal converters. Surprisingly, however, early tests of the first thermal converters purchased for the model A voltmeter showed appreciable reversal differences (up to 0.2%) even in these insulated-heater thermal converters. It was soon realized that this was probably due to thermoelectric effects in the heater circuit. Peltier and Thomson heating of the heater can cause dissymmetry in the temperature rise of the heater, and thus cause differences in the emf of the thermocouple unless the hot junction is exactly at the

midpoint of the heater.[8] This supposition was verified by an analysis of the data, which showed that the differences were larger in those thermal converters with heaters having larger thermoelectric effects. Further verification was secured by tests of special thermal converters, constructed by one of the manufacturers [9] at the Bureau's request, with the hot junction of each deliberately and considerably off-center. The reversal differences were much larger, and the signs and magnitudes were found to be roughly in agreement with calculations based on thermoelectric data for the alloys used.

Early intercomparisons of these few thermal converters indicated that no significant ac-dc differences should be expected, even with rather large reversal differences from this cause, provided that the average for the two directions of current is taken as the d-c response. However, intercomparisons and tests of the much larger number of thermal converters later purchased for current measurements showed that a good proportion had measurable ac-dc differences, all of the same sign and independent of frequency. This suggested a d-c error, for which these thermoelectric efforts seemed the most likely cause. This was investigated theoretically (see appendix 2) by considering the temperature rise of a homogeneous conductor heated by an electric current and cooled solely by conduction to two relatively massive terminals; i. e. by neglecting, for simplification, radiation and convection losses and the heat abstracted by the attached thermocouple.

With only the normal joule, or resistance, heating, and with the terminals of the conductor at equal and fixed temperature, the temperature distribution along the conductor is parabolic, and the temperature rise at the midpoint is, as Goodwin showed,[10] equal to

$$\theta_d = \frac{V_e^2}{8\rho k}, \tag{1}$$

where V_e is the voltage drop across the conductor, and ρ and k are the electrical resistivity and thermal conductivity, respectively. In addition, however, there is Peltier heating or cooling at the junctions of dissimilar metals (the two junctions between the heater and its two supports) and Thomson heating along each half of the wire. Unlike joule heating, these are dependent upon the direction of the current flow and can thus cause a dissymmetry of the temperature distribution along the conductor, which reverses when the direct current through the conductor is reversed. On alternating current, even at the low frequencies in which we are interested, the reversal of current occurs so rapidly that the thermal inertia of the wire prevents any such dissymmetry, and the temperature distribution is unchanged by these thermoelectric effects. Calculations show (see appendix 2) that with direct current the temperature rise at the midpoint of the conductor, where the hot junction of the thermocouple is attached, is unaffected by the Peltier heating, for completely symmetrical construction of a thermoelement. They show, however, that it is changed by Thomson heating, and becomes, approximately,[11]

$$\theta_t = \theta_d\left[1-\frac{4}{3}\left(\frac{\sigma\theta_d}{V_e}\right)^2\right], \tag{2}$$

where θ_t is the midpoint temperature rise in the presence of Thomson heating, in ° C; θ_d, the rise without Thomson heating; σ, the Thomson voltage coefficient in volts-degree $^{-1}$, V_e, the voltage across the conductor in volts.

This was derived by considering σ a constant, whereas both experimental results and the electron theory of metallic conduction indicate that $\sigma = BT$, where B is a constant and T is the absolute temperature. However, a solution by a perturbation method,[12] of the nonlinear equation that results when $\sigma = BT$, shows that the above results give a sufficiently close approximation for the temperature rise of about 200 deg C encountered in typical thermal converters. Thus eq 2 shows that an ac-dc difference, or transfer error, should be expected in a thermal converter, and enables the approximate calculation of this error. Such calculations have been made for some common metals and some of the alloys used as heaters in thermal converters, on the assumption of a 200 deg C rise at the midpoint, and a voltage drop of 0 .2 v at rated currents.[13] The results, converted to ac-dc difference for the same temperature rise, rather than temperature difference for the same current, are shown in table 6. For the computation of these results, the Thomson coefficient σ was considered to be equal to $B(\theta_0+2/3\theta_d+273)$, where B is the second derivative of the characteristic curve of emf versus temperature for a thermocouple composed of the indicated metal and lead.[14] θ_0 is the ambient temperature in deg C. The results show approximately the errors to be expected for these materials.

TABLE 6. *Calculated ac-dc difference at rated current due to Thomson effects in thermal converter heaters*

Metal	B	ac-dc difference
	$v/°C^2$	*Percent*
Copper	$+0.8\times10^{-4}$	<0.005
Platinum	−3.2	−.013
Manganin	−0.08	<.005
Constantan (60 Cu-40 Ni)	−7.3	−.064
90 Ni-10 Cr	−3.2	−.013
85 Pt-15 Ir	−2.1	−.005

[8] This dissymmetry has actually been utilized to measure the Thomson effect. See [9].

[9] M. Rosenfield, of the Field Electrical Instrument Co., who first showed that the reversal differences were dependent upon the type of heater material.

[10] See [6]. In addition to this classic paper, Goodwin has written an excellent series of articles on "Thermal problems relating to measuring and control services", which appeared in Weston Eng. Notes, 1948–50 (Weston Electrical Instrument Corp., Newark, N. J.).

[11] At other points along the conductor the average temperature rise for the two directions of direct current is also changed by Thomson heating.

[12] This method was suggested by Chester Snow.

[13] From eq 1, a series of thermal converters having similar thermocouples and the same rated output emf at rated current, and having heaters that obey the Weidemann-Franz law will all have the same temperature rise and the same voltage drop across the heater. The temperature rise is about 200 deg C, and the voltage drop about 0.2 v at rated current for most thermal converters.

[14] This weighted average absolute temperature gives results in closer agreement with those computed by the more exact method than does the unweighted average, $\theta_0+1/2\theta_d+273$.

The results may be compared with the observed ac-dc differences shown in table 4. From information supplied by the manufacturers, the 1-, 2-, 5-, 10-, 20-, 50-, and 200-ma thermal converters have heaters of either carbon, nickel-chromium, or platinum-rhodium-ruthenium alloys. The observed ac-dc differences of these converters were less than 0.01 percent. The 100-, 500- and 1,000-ma thermal converters had heaters of constantan (Advance). The observed differences for these converters (at rated current) were close to the calculated value of −0.06 percent. The 1- and 2-amp converters, of platinum-iridium, had observed differences (from table 4,b) less than 0.005 percent, except at low frequencies, also close to the calculated values. The 5-, 10-, 20- and 50-amp converters, of a special platinum–3-percent-copper alloy, had differences of −0.010 to −0.015 percent. Thus the agreement between the computed and observed values serves as excellent verification of this source of error in transfer thermal converters. Very fortunately, the error is significantly large only for materials having unusually large thermoelectric effects, such as constantan. However, this does lead to the interesting conclusion that for operation at a low temperature a thermal converter should have large thermoelectric effects in the thermocouple, but that for the highest transfer accuracy it should have very small thermoelectric effects in the heater.

Additional experimental verification of this cause of transfer error was secured by constructing[15] at the Bureau two 5-amp thermal converters differing only in that one had a heater of manganin and the other of constantan. These were 5-amp thermal converters with a small Borax bead between the hot junction of a copper-constantan thermocouple and the center of the heater wire, to eliminate contact effects. Careful ac-dc difference tests with the standard electrodynamic ammeter as the reference established agreement within 0.005 percent for the manganin element and indicated an ac-dc difference of −0.06 percent for the constantan element at an emf of about 5 mv.

As a result of this work, a second set of thermal converters in the 1- to 1,000-ma range was purchased under specifications prohibiting heaters of constantan or similar alloys. All of these converters were found to have ac-dc differences less than 0.01 percent at audio frequencies.

6. Low-frequency Response

It has long [10] been known that there is a low-frequency limit to the correct rms response of a thermal converter, for reasons analogous to those causing a similar low-frequency limit in all other types of transfer instruments. Below this limit the response characteristic $E=f(I)$ is not independent of frequency (except for symmetrical square waves), and may be expected to be in error by an amount that is inversely proportional to the square of the frequency. As table 4, b, shows, such an error was observed for the 1- and 2-amp thermal converters.

[15] These thermal converters were constructed by E. S. Williams.

When a constant direct current is applied, the heater of a thermal converter reaches a constant temperature. When an alternating current is applied (after the transient state is over) the temperature of the heater varies cyclically about a mean value, with an amplitude that decreases with increasing frequency because of the thermal capacity of the element. At frequencies high enough so that the cyclic variations are negligible, the temperature rise of the heater is independent of frequency (provided that at very high frequencies the skin effect and electromagnetic radiation are negligible and that standing waves do not alter the temperature distribution). However, at lower frequencies the mean value, to which the d-c instrument or potentiometer connected to the thermocouple responds, may not be the same because of nonlinearities in the thermal and electric circuits. These nonlinearities are caused principally by radiation losses, the dependence upon temperature of the electrical resistivity and the thermal conductivity of the heater, and the curvature of the emf versus temperature characteristic of the thermocouple. A theoretical evaluation of these effects for the conditions in a thermal converter, in which most of the cooling is by conduction to the heater, is difficult, but does serve as a guide in determining the approximate limiting frequencies for an arbitrarily chosen error and for determining which factors influence that error. Such an approximate analysis has been carried out by a perturbation method (see appendix 3). The results show that the average (time average) temperature rise at the midpoint of a conductor heated by a sinusoidal electric current and cooled solely by conduction to massive terminals is approximately

$$\theta_{ac}=\theta_{dc}\left[1+\frac{h}{2}\theta_{dc}q^2\right] \tag{3}$$

and that the percentage *ac-dc* difference of a thermal converter having the hot junction of a thermocouple fastened to the midpoint of such a heater is approximately

$$\delta=-25H\theta_{dc}q^2 \tag{4}$$

where

θ_{ac} = the midpoint temperature rise in degrees centigrade on alternating current of rms value I amperes

θ_{dc} = the midpoint temperature rise in degrees centigrade for the same value of direct current.

$h=\alpha-\beta-2NT_0^3$, where α is temperature coefficient of electrical resistivity.

β = the temperature coefficient of thermal conductivity of the conductor,

$N=p\zeta K/ak$.

p and a = the perimeter and area of the cross section of the conductor, respectively.

ζ = the emissivity.

K = the Stefan-Boltzmann constant in watts-cm^{-2}-(deg K)$^{-4}$

k = the thermal conductivity in watts-cm^{-1}-deg^{-1}

T_0=the ambient temperature in degrees Kelvin

$q=d/\omega l^2$ and is (approximately) the ratio of the crest value of the cyclic fluctuation of temperature at the midpoint to the average temperature rise at the midpoint

$\omega=2\pi f$, where f is the frequency of the applied current in cycles per second.

d=the thermal diffusivity of the heater material in $cm^2\text{-}sec^{-1}$.

l=one-half the length of the conductor in centimeters.

$H=h+B/2A$, where A and B are the constants in the emf-temperature characteristic for the thermocouple itself, that is, in the expression, $E=A\theta+(B/2)\theta^2$

These equations indicate the factors upon which the low-frequency error depends. They show that the temperature rise can correctly be used as a measure of the rms alternating current, at frequencies high enough so that the second term in the bracket of eq 3 is negligible for the accuracy desired; in other words, at frequencies for which the heater integrates reasonably well. This is true even if the thermal and electrical conductivities of the heater are dependent upon temperature. As a corollary, these equations show that a thermal converter correctly indicates rms response, except at low frequencies, even though its response characteristic $E=f(I)$ is not quadratic.

The above equations are valid only at frequencies for which the second term in the brackets of eq 3 is small compared to 1.

Equation 4 may be used to calculate approximately the frequencies for which ac-dc differences may be expected to cause an error of an arbitrarily chosen value. This has been done for some typical materials for an error of 0.1 percent, a temperature rise of 200° C, and a typical heater length of 0.4 cm. The results are shown in table 7.[16]

TABLE 7. *Frequencies for which the computed ac-dc difference is 0.1 percent*

[TC-A signifies a thermocouple of Chromel P and Alumel, and TC-B a thermocouple of copper and constantan, for which $B/2A=-0.1\times10^{-3}$ and $+0.9\times10^{-3}$, respectively]

Heater material	Approximate temperature coefficient		Thermal diffusivity	Frequency for $\delta=0.1$[a]	
	Electrical resistivity	Thermal conductivity		TC-A	TC-B
	%/°C	%/°C	$cm^2\text{-}sec^{-1}$	c/s	c/s
Copper	+3.9×10⁻³	−0.2×10⁻³	1.1	60	70
Platinum	+3.5	+.5	.25	12	14
Manganin	<.1	+2.7	.075	3	2
Constantan	<.1	+2.3	.064	3	2
80 Ni-20 Cr	.1	[b]+3.5	.038	2	2
Carbon	−.5	+.4	.2	5	1

[a] For a heater 0.4 cm long with a temperature rise of 200° C.
[b] Estimated from Lorenz' Law.

[16] The effect of radiation losses has been neglected in preparing this table. In general, this effect is significant only in the very low and very high range thermal converters.

It is evident that the most significant factor in the error term of eq 4 is the length of the heater as the error is dependent upon the fourth power of this quantity.[17] It is of interest to note that the lengths, $2l$, of the heater of the 1- and 2-amp thermal converters are only 0.28 and 0.19 cm, respectively, and that the length of each of the higher-range thermal converters is about 0.5 cm. The value of H can be determined from the departure from "square law" of the characteristic equation $E=f(I)$ of a thermal converter. For these thermal converters it was considerably less than the factor given for platinum in table 7. The estimated frequencies for a 0.1-percent error, on the assumption that the diffusivity of the platinum-iridium alloy used in these thermal converters is the same as that of platinum, were about one-half the observed values.

7. High-Frequency Response

As these thermal converters are inherently suitable at frequencies up to 100 Mc or more, the upper-frequency limit is set by the circuits in which they are used. The precautions indicated in section 4 are sufficient to control capacitance and leakage currents in tests of ammeters at frequencies considerably higher than the 20,000 c/s established as the present upper limit by the demand for this testing service. The actual upper-frequency limit has not been established.

The magnitude of the effective impedance sets the upper frequency limit for the model A and the model B voltmeters. For an accuracy of 0.01 percent at 20,000 c/s, a time constant of less than 1×10^{-7} and a skin effect less than 0.01 percent are necessary for the impedance of each step of the model A and each range of the model B instruments. The time constant of each decade of the model A voltmeter was computed from the inductance and direct-capacitance values furnished by the manufacturer of the resistance box used. This was less than 5×10^{-8} for each decade. The skin effect was also negligible for each decade. The resistance box is connected as a three-terminal resistor, with the shield connected to the grounded side of the line. For this connection the errors caused by the capacitance currents to the shield are much less than those that would occur if the shield were connected to a resistor terminal. They are significant only for the two 1,000-ohms-per-step decades. The effects of the capacitance of the resistance cards and switch studs of these decades to the shield were computed from the manufacturer's capacitance figures of about 10 $\mu\mu f$ per decade by considering the capacitance as distributed along a uniform transmission line, composed of resistance elements and short-circuited at the end. From the usual transmission line formulas, the magnitude of

[17] For a given heater alloy, the low-frequency range can be extended by using longer heaters, with proportionately greater cross-sectional area to give the same temperature rise for the same current. If solid heaters are used, the improved low-frequency performance will be accompanied by increased error due to skin effect at high frequencies.

the current at the short-circuited end was computed as approximately

$$|I| = \frac{V}{R}[1 - 0.0056\,(\omega CR)^2], \qquad (5)$$

where

V = the applied voltage
I = the current at the short-circuited end
R = the resistance in the circuit
C = the total capacitance to shield of the windings in use
$\omega = 2\pi f$.

At 20,000 c/s for a capacitance of 30 $\mu\mu$f this is changed by less than 0.005 percent at 20,000 ohms, the maximum setting. The effect of the capacitance (about 10 $\mu\mu$f) of each rather large switch blade to the shield was separately computed, and found to be less than 0.005 percent at 20,000 c/s. Thus it was concluded that the errors of this voltmeter should be a maximum of 0.01 percent at the highest settings and frequencies used, and less at lower settings and frequencies. The performance at the top settings was verified by the tests outlined in section 4.

The impedance of the model B voltmeter was similarly computed, and only the capacitance to the shield was found to be significant. As a rough but adequate approximation this may be considered the same for each step, which leads to the approximation of considering the capacitance as distributed along a nonuniform transmission line composed of resistance elements and short-circuited at the end. The effective impedance was computed by a perturbation method,[18] on the rough assumption that the resistance per unit length was proportional to the square of the electrical distance from the output end. The magnitude of the current at the short-circuited end was found to be approximately

$$|I| = \frac{V}{R}[1 - 0.0022\,(\omega CR)^2]. \qquad (6)$$

From the measured capacitance of 50 $\mu\mu$f and the total resistance of 100,000 ohms for the 750-v range, the change in current was computed as -0.09 percent at 20,000 c/s, which is in very good agreement with the observed results of table 5. Moderately good agreement for the other ranges was also obtained, but the change in current was not observed to increase in proportion to the square of the frequency as indicated by eq 6. However, the agreement is good enough to show that the ac-dc difference of this instrument is due to capacitance currents to the shield. These currents cannot easily be reduced in a shielded multirange instrument of reasonable size. (A shield is desirable to control the currents.) They could be compensated by connecting appropriate capacitors across sections of the resistors, but this seems less desirable than the procedure of applying small corrections and has not been done in the model B voltmeter. Much of the capacitance is that between the binding posts of each range (see fig. 2) and between the high-side binding post and the top shield. This shield is brought as close as 2.5 cm to the row of high-side posts.

[18] See appendix 4.

8. Other Effects

The intercomparisons of insulated-heater thermal converters disclosed an unsuspected ac-dc difference that was dependent upon the voltage between the heater and ground and upon the heater current of each of these elements. This was traced to a very small leakage current flowing through the ceramic bead between the heater and thermocouple and then through the stray capacitance of the Lindeck potentiometer to ground. This current caused additional heating of the bead and thus an error as on direct current the insulation resistance of the Lindeck was much higher than the capacitive reactance, even at 20 c/s. In addition, the ceramic bead of each of these thermal converters exhibited marked dielectric absorption, so that its a-c resistance was much less than its d-c resistance. For a typical thermal converter at rated current a leakage current of 0.7 μa resulted from a difference of 50 v between the heater and ground, resulting in a power dissipation of 35 μw in the bead. This was sufficient to cause a 0.2-percent error, which was proportional to the square of the voltage difference and was very markedly dependent upon the heater current.[19] The reactance of a capacitance as small as 100 $\mu\mu$f is less than the computed bead resistance, even at a frequency as low as 50 c/s, so that in almost any application this source of error makes it necessary to maintain the heater near ground potential.

9. Other Applications

This equipment was designed for the testing of other instruments. Portability and the ease of making other a-c measurements were not considered to be important. However, the thermal converters and voltmeter elements are readily portable and have been used, with a small portable millivolt potentiometer as the indicator, for measurements at other locations. For measurements of current or voltage to 0.01 percent, it is necessary to use a transfer method, calibrating the thermal converter or voltmeter on direct current at the time of use. For a more moderate accuracy of about 0.1 percent, it should be feasible to use a low-range thermal converter, shunting it for current measurements and adding a series resistor for voltage measurements. Only the thermal converter itself need be transferred to direct current if the resistances of the shunts and the series resistor are properly adjusted. Thus d-c sources of extended range, volt boxes, etc., should be unnecessary. The whole apparatus could be built in a convenient case, containing a small potentiometer for the measurements of the current through or the voltage across the thermal converter heater.

[19] This was due to the marked decrease in the resistance of the ceramic bead with an increase in temperature. With a fixed voltage across the bead, the error was in some cases proportional to the tenth power of the heater current.

A suitable low-range thermal converter should also make feasible an a-c potentiometer with an inherent accuracy of 0.01 percent. The basic circuit for a polar form of such a potentiometer (to measure the magnitude but not the components or phase angle of an alternating voltage) is shown in figure 6. With the switch thrown to direct-current the potentiometer is standardized in the usual manner, and the deflection of the indicator of the thermal converter is observed. The switch is then thrown to alternating current, which is adjusted for the same deflection of this indicator. The circuit is surely not new, but a proved thermal converter makes possible a convenient transfer with accuracies comparable to those of a d-c potentiometer. The other basic limitation remains that any a-c potentiometer measures only the fundamental component of the unknown voltage. However for an alternating quantity having a harmonic content as large as 2 percent, the rms value differs from the fundamental by only 0.02 percent. Audio-frequency oscillators and amplifiers with amplitude distortion much less than this are now available. Such an oscillator could be used to supply the potentiometer directly and to supply the test circuit through an amplifier preceded by a suitable phase-shift network.

10. Summary

The electrothermic transfer standards used at the Bureau for the precise measurement of voltage and current at audio frequencies, and designed primarily for the standardization of electric instruments, have been described. The extensive tests to establish the transfer performance of the standards have been outlined, and the results have been given. The causes of the observed ac-dc differences have been outlined and the errors evaluated. The equations governing the temperature rise of a conductor heated by an electric current and cooled by conduction to relatively massive terminals have been solved to establish the steady-state midpoint temperature rise on direct current with Peltier and Thomson heating, as well as the ordinary resistance heating, in order to obtain the d-c error of a thermal converter. The equations have been solved to establish the average midpoint temperature rise on alternating current, in order to obtain the low-frequency error of a thermal converter in which the electrical and thermal conductivities of the heater are temperature dependent, in which some loss of heat occurs by radiation, and in which the characteristic of the thermocouple is nonlinear. Possible applications and modifications of the equipment for measurements under less stringent conditions have been suggested, and the application to an a-c potentiometer of excellent inherent accuracy has been diagrammed.

The results of this work establish the excellence of thermal converters as transfer standards of highest accuracy, comparable over wide ranges with that obtainable with other types of standards at much narrower ranges. The requirements for such standards are feasible and the manner of use to insure such accuracy not unreasonable. The cost of the required number of standards and the equipment is not prohibitive. Thus electrothermic instruments may be ranked on a par with electrodynamic and electrostatic instruments for a-c measurements of the highest accuracy.

As a result of this work, thermal converters of negligible or small known transfer error are now available as transfer standards with which the transfer performance of other thermal converters may be evaluated at the NBS to 0.01 percent at audio frequencies.

The author acknowledges the help of Murray Blitz, who made most of the intercomparisons described in section 4 of this report and checked all the tables and equations, and of Earl Williams, who constructed all the equipment and assisted with the measurements.

11. References

[1] F. K. Harris, A suppressed-zero electrodynamic voltmeter, BS J. Research **3,** 445 (1929) RP105.
[2] J. H. Park and A. B. Lewis, Standard electrodynamic wattmeter and ac-dc transfer instrument, J. Research NBS **25,** 545 (1940) RP1344.
[3] F. B. Silsbee, Composite-coil electrodynamic instruments, BS J. Research **8,** 217 (1932) RP411.
[4] C. C. Patterson, E. H. Rayner, and A. Kinnes, The use of the electrostatic method for the measurement of power, J. Inst. Elec. Engrs. (London) **51,** 294 (1913).
[5] R. S. J. Spilsbury and A. Felton, The electrostatic voltmeter as a dc-ac transfer instrument, J. Inst. Elec. Engrs. (London) **89-II,** 129 (1942).
[6] W. N. Goodwin, Jr., The compensated thermocouple ammeter, Trans. Am. Inst. Elec. Engrs. **55,** 23–33 (1936).
[7] F. L. Hermach, A precision electrothermic voltmeter for measurements between 20 and 20,000 cycles, Trans. Am. Inst. Elec. Engrs. **67,** 1224 (1948).
[8] H. B. Brooks and A. W. Spinks, A multi-range potentiometer and its application to the measurement of small temperature differences, BS J. Research **9,** 781 (1932) RP506.
[9] G. Borelius, Bestimmung des Thomsoneffektes aus dem thermischen Gleichgewicht in einem strömdurchflossenen Drahte, Ann. Physik **63,** 845 (1920).
[10] M. G. Lloyd, Elec. Rev. & Western Elec. **58,** 65 (Jan. 14, 1911).

Appendix 1. Development of Working Equations

By definition, the percentage ac-dc difference of an instrument is the percentage difference in the quantity required to give the same response on alternating and direct current. It is

$$\delta = 100\,\frac{Q_{ac}-Q_{dc}}{Q_{dc}}, \tag{7}$$

where Q is the quantity (current, voltage, or power) that the instrument measures.

In a "straight a-c test" the direct current or voltage is adjusted to give the same response of the transfer standard observed on alternating current. The direct current or voltage is measured with the potentiometer and its accessories. Therefore, from the above definition,

$$Q_{ac} = Q_{dc}\left(1+\frac{\delta_a}{100}\right), \tag{8}$$

where Q_{dc} is the quantity measured with the potentiometer, δ_s is the ac-dc difference of the transfer standard, and Q_{ac} is the a-c value required for the observed deflection of the test instrument.

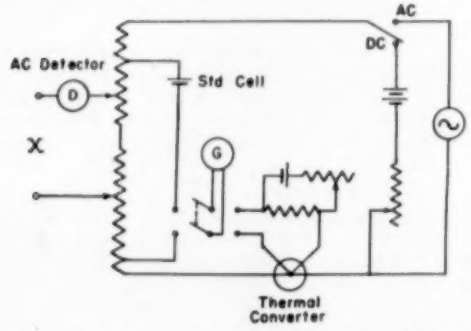

FIGURE 6. *Elementary form of Polar a-c potentiometer.*

When a thermal converter is used for transfer tests the small percentage difference, δ_t, between the values required for the same indication of the test instrument on alternating and direct current is determined from the resulting deflection of the Lindeck galvanometer. Therefore, for each transfer thermal converter, the small percentage difference in output emf resulting from a small percentage difference in heater current must be evaluated. This relationship may be expressed as

$$\frac{\Delta E}{E}=n\,\frac{\Delta I}{I}, \tag{9}$$

where E is the output voltage, I the heater current, and n a number that is generally close to 2, but may range from from 1.5 to 2.2. The characteristic, n, may be evaluated on direct current by measuring with a potentiometer the small percentage differences in E resulting from small percentage differences in heater current successively set with a potentiometer at selected current levels, then computing n by the above expression and plotting n versus E. The characteristic need not be determined with an accuracy better than 1 percent and is relatively permanent.

If the Lindeck potentiometer shown in figure 3 is used to measure E and ΔE in millivolts in a transfer test, then at balance $E=V_p$,[20] the voltage drop across the four-terminal resistor. If the galvanometer deflection D, is directly proportional to the current through the galvanometer[21] and if the potentiometer voltage is unchanged during a determination,

$$\Delta E=\frac{\Delta D R_p}{S},$$

where ΔD is the difference in galvanometer deflection corresponding to a difference ΔE in the applied emf, R_p is the resistance of the galvanometer circuit, and S is the current sensitivity of the galvanometer in centimeters per milliampere on the scale. In the Lindeck potentiometer used in this setup, the galvanometer sensitivity is adjusted so that numerically

$$\frac{100R_p}{S}=1.$$

These relationships may be combined with eq 9 to give

$$100\,\frac{\Delta I}{I}=\frac{\Delta D}{nV_p}. \tag{10}$$

[20] An accuracy of 1 percent is sufficient for this measurement.

[21] The use of a straight instead of cylindrical scale introduces an error that can be shown to be less than 1 percent if the galvanometer-to-scale distance is at least three times the scale length.

Therefore, for a transfer test of an ammeter with a thermal converter that has no transfer error, the required ac-dc difference of the test instrument is by eq 7 and 10

$$\delta_T=100\left(\frac{I_{ac}-I_{dc}}{I_{dc}}\right)=\frac{D_{ac}-D_{dc}}{nV_p}, \tag{11}$$

where the alternating and direct currents are adjusted for the same response of the test instrument, and the resulting galvanometer deflections are D_{ac} and D_{dc}, respectively.

If the transfer thermal converter has a percentage ac-dc difference, δ_s, at the current and frequency at which the test is made, then the ac-dc difference of the instrument under test is, to the desired order of approximation,

$$\delta_T=100\left(\frac{I_{ac}-I_{dc}}{I_{dc}}\right)=\frac{D_{ac}-D_{dc}}{nV_p}+\delta_s. \tag{12}$$

Similarly, for a voltmeter test,

$$\delta_T=100\left(\frac{V_{ac}-V_{dc}}{V_{dc}}\right)=\frac{D_{ac}-D_{dc}}{nV_p}+\delta_s, \tag{12}$$

in which δ_s is the percentage ac-dc difference of the range (or setting) of the standard voltmeter used.

In this deflection method of using the Lindeck potentiometer for rapid transfer tests, the resistance of the circuit seen by the galvanometer must be constant to better than 1 percent. The resistance of the thermocouple of each thermal converter has been adjusted to the same value so that the simplified formulas may always be used. The temperature coefficient of the resistance of the Lindeck circuit has been computed as less than 0.1 percent per deg C, and computations show that the resistance seen by the galvanometer is changed by less than 0.2 percent by the adjustable battery circuit, for all ranges of the potentiometer except the topmost.

Appendix 2. Effect of Peltier and Thomson Heating

The problem is to find the steady-state temperature rise of a uniform conductor of length $2l$ and uniform cross-sectional area, a, carrying a constant current, I, and cooled solely by conduction to its terminals. The joule heating of a length dx occurs at the time rate $I^2\rho dx/a$ watts, where ρ is the electric resistivity in ohm-cm. The difference in the heat conducted per second across the two ends of this differential element is $ak(d^2\theta/dx^2)dx$ watts where k is the thermal conductivity in watts-cm^{-1}-degrees^{-1}, and θ is the temperature of the element in deg C. Equating these and dividing by dx gives the differential equation governing the temperature of the conductor

$$ak\frac{d^2\theta}{dx^2}+\frac{I^2\rho}{a}=0, \tag{14}$$

which is of the form

$$\theta''=-b, \tag{14a}$$

where $b=I^2\rho/a^2k$.

If the terminals remain at equal temperatures θ_0, and if the origin is at the midpoint of the conductor, the boundary conditions are $\theta=\theta_0$ at $x=\pm l$. The solution, by direct integration and application of these conditions, is

$$\theta-\theta_0=\frac{b}{2}(l^2-x^2)$$

and at the midpoint

$$\theta_m-\theta_0=\frac{bl^2}{2}=\theta_d. \tag{15}$$

If the terminals are of different metal than the conductor, Peltier heating and cooling (proportional to the first power of the current) may occur at the junctions of the conductor with the terminals. These will be equal and opposite in sign at the two terminals, and, if we can assume complete thermal symmetry, their effect will be to raise the tempertaure of

terminal by a small amount $\Delta\theta$ and to lower the other by equal amount. The differential equation then has as its boundary conditions, $\theta=\theta_0+\Delta\theta$ at $x=+l$ and $\theta=\theta_0-\Delta\theta$ at $-l$. The solution is

$$\theta-\theta_0=\frac{b}{2}(l^2-x^2)+\frac{\Delta\theta x}{l}, \tag{16}$$

and is therefore unchanged at the midpoint.[22] Of course, complete thermal symmetry is never attained, so that Peltier heats may cause a change in the midpoint temperature. However, for massive terminals the temperature changes, $\Delta\theta$, are very small, so that Peltier heating need not be considered significant.

Thomson heating occurs in homogeneous conductors having a temperature gradient in the direction of the current flow. For the one-dimensional case here considered, the Thomson heat in an element of length dx having a temperature difference dy is $\sigma I d\theta$ watts where σ is the Thomson voltage coefficient. Experiment and theory indicate that σ is proportional to the absolute temperature, but, as the Thomson heating is small compared to the joule heating, we might, as a first approximation, consider σ constant. Equation 14 then becomes

$$ak\frac{d^2\theta}{dx^2}+\frac{I^2\rho}{a}+\sigma I\frac{d\theta}{dx}=0, \tag{17}$$

which is of the form

$$\theta''+c\theta'+b=0 \tag{17a}$$

with the boundary conditions $\theta=\theta_0$ at $x=\pm l$, where $c=\sigma I/ak$. The steady-state solution of this eq is

$$\theta-\theta_0=\frac{bl}{c}\left(\frac{1}{\tanh q}-\frac{e^{-q}}{\sinh q}\right)-\frac{bx}{c},$$

where $q=cl<<1$. At the midpoint, where $x=0$

$$\theta_m-\theta_0=\frac{bl^2}{q}\left(\frac{\cosh q-1}{\sinh q}\right).$$

Expanding the hyperbolic functions gives, by neglecting higher-order terms,

$$\theta_m-\theta_0=\theta_l=\frac{bl^2}{2}\left(1-\frac{q^2}{12}\right)=\theta_d\left(1-\frac{q^2}{12}\right). \tag{18}$$

By substituting the values for b and c and noting that $2I\rho l/a=V$, the voltage drop across the conductor, eq 1 and 2 of the text can be obtained. They show that Thomson heating causes a small (second order of smallness) decrease in the temperature rise at the midpoint of the conductor, and can thus lead to a transfer error in a thermal converter. However, the approximation of considering σ a constant is a drastic one, and a more accurate approach will be to consider $\sigma=BT$, where B is a constant,[23] and T is the absolute temperature. Equation 17 then becomes

$$ak\frac{d^2T}{dx^2}+\frac{I^2\rho}{a}+BIT\frac{dT}{dx}=0,$$

which is of the form

$$T''+wTT'+b=0, \tag{19}$$

with the boundary conditions $T=T_0$ at $x=\pm l$, where $w=BI/ak$

This is a nonlinear equation and very difficult to solve. Chester Snow showed that it could be reduced to a Ricatti and then to a Bessel equation, but suggested an approximation or perturbation method to give the desired results more simply and directly. The answer is not significantly different from that of eq 18. The method is powerful, however, and was used later in evaluating other perturbing effects, so that it will be outlined here. The Thomson heating, which is much smaller than the Joule heating, can be considered as perturbing the temperature distribution of the conductor. Its effect can be approximated by solving the differential equation without the perturbing term, then substituting the result, and its derivatives as necessary, in the perturbing term only, and solving the resulting equation.

Without the Thomson heat term, eq 19 becomes

$$T''=-b$$

with the boundary condition given, the solution of which is

$$T_1-T_0=\frac{b}{2}(l^2-x^2),$$

where the subscript 1 indicates the first approximation. Placing this value of T_1 and T_1' in the perturbing term of 19, reduces this to a linear equation,

$$T_2''=-b-\frac{wb^2x^3}{2}+wbx(T_d+T_0),$$

where $T_d=bl^2/2$, the solution of which is

$$T_2-T_0=\frac{b}{2}(l^2-x^2)-\frac{wb^2x^5}{40}+\frac{wb}{6}(T_d+T_0)x^3-$$
$$wT_d\left(\frac{7}{30}T_d+\frac{T_0}{3}\right)x$$

At $x=0$ this reduces to T_1-T_0 as only first-order terms are given, so that the process must be repeated to find the second-order term indicated by eq 18. The algebra rapidly becomes very lengthy and tedious, but the procedure is straightforward, and the resulting temperature rise at the midpoint is found to be approximately

$$T_2-T_0=T_d[1-3.4\times10^{-2}z_d^2-10.5\times10^{-2}z_0z_d-8.3\times10^{-2}z_0^2], \tag{20}$$

where $z_0=wT_0l$, and $z_d=wT_dl$

Appendix 3. Low-Frequency Error of a Thermoelement

The problem is to find the steady-state average (over an integral number of cycles) temperature rise at the center of a uniform conductor of length, $2l$, and cross-sectional area, a, carrying a sinusoidal current and cooled chiefly by conduction to massive terminals that are at fixed and equal temperatures. Assume that the current remains sinusoidal and that only Joule heating of the conductor occurs. If all the cooling is by conduction to the terminals, the differential equation governing the temperature of the conductor is, under these assumptions,

$$ak\frac{\partial^2\theta}{\partial x^2}+\frac{i^2\rho}{a}=ams\frac{\partial\theta}{\partial t}, \tag{21}$$

with the boundary condition $\theta(\pm l,t)=0$, where

θ = temperature in deg C
i^2 = the square of the instantaneous value of the current = $I^2(1-\cos 2\omega t)$
I = rms value of the current
$\omega=2\pi f$, and f is the frequency of the current in cycles per second
t = time in seconds
m = density of the conductor in grams-cm^{-3}
s = thermal capacity of the conductor in joules-grams^{-1}-deg C^{-1}.

[22] Since Peltier heating depends upon the junction temperature, a second-order change in midpoint temperature may occur.
[23] $B=d^2E/dT^2$, where E is the emf of a thermocouple composed of the metal in question and a metal such as lead, which has very small Thomson heating.

The procedure will be to consider ρ and k constant and to solve for the periodic steady-state temperature rise, then to approximate ρ and k as $\rho=\rho_0(1+\alpha\theta)$ and $k=k_0(1+\beta\theta)$, to introduce radiation loss, and to solve the resulting equation by the perturbation method just outlined. For the cases considered $\alpha\theta$ and $\beta\theta$ are considerably less than 1, and radiation loss is much less than the Joule heating of the conductor.

With α and $\beta=0$, eq 21 is the form

$$\frac{\partial^2\theta}{\partial x^2}-g\frac{\partial\theta}{\partial t}=-b(1-\cos 2\omega t)$$

where $g=ms/k_0$, and $b=I^2\rho_0/a^2k_0$.
Let $\theta=u(x,t)+\psi(x)$. Then

$$\frac{\partial^2\theta}{\partial x^2}=\frac{\partial^2 u}{\partial x^2}+\frac{\partial^2\psi}{\partial x^2}$$

Let $\partial^2\psi/\partial x^2=-b$. Then $\psi=-(bx^2)/2+c_1x+c_2$
Applying boundary conditions gives

$$\theta(+l,t)=u(+l,t)+\psi(l)=0$$

$$\theta(-l,t)=u(-l,t)+\psi(-l)=0.$$

We may take $\psi(l)=\psi(-l)=0$.
Then $\psi=b/2(l^2-x^2)$ and eq 22 becomes

$$\frac{\partial^2 u}{\partial x^2}-g\frac{\partial u}{\partial t}=b\cos 2\omega t,$$

with $u(\pm l,t)=0$.

From complex number theory if u is harmonic in time, it can be represented by the real part of $Ue^{j2\omega t}$, where U is a complex function of the real variable x, and $j=\sqrt{-1}$. Similarly, $b\cos 2\omega t$ can be represented by the real part of $be^{j2\omega t}$, where b is a real number. Substituitng these quantities and the appropriate derivatives in eq 23 and dividing by $e^{j2\omega t}$ results in

$$\frac{d^2U}{dx^2}-j2\omega gU=b, \tag{24}$$

with $U=0$ when $x=\pm l$. The solution of this is

$$U=-\frac{b}{\mu_2}\left[1-\frac{\cosh\mu x}{\cosh\mu l}\right], \tag{25}$$

where $\mu=\sqrt{j2\omega g}$. At the midpoint

$$U=-\frac{b}{\mu^2}\left[1-\frac{1}{\cosh\mu l}\right]\approx j\frac{b}{2\omega g},$$

as at the frequencies we are interested in $\cosh\mu l>>1$. Therefore, $u=$ real part of $Ue^{j2\omega t}=$ real part of

$$\left\{\frac{jb}{2\omega g}(\cos 2\omega t+j\sin 2\omega t)\right\}\approx-\frac{b}{2\omega g}\sin 2\omega t.$$

So that, to this approximation, at the midpoint

$$\theta_{m1}=\frac{bl^2}{2}\left(1-\frac{1}{\omega gl^2}\sin 2\omega t\right)=\theta_d(1-q\sin 2\omega t), \tag{26}$$

where $\theta_d=bl^2/2$ and $q=1/\omega gl^2$. Note that q is the crest value of the cyclic temperature fluctuation divided by the average temperature rise at midpoint.

In general, $U=U_a+jU_b$, where U_a and U_b are functions of x, so that $u=U_a\cos 2\omega t-U_b\sin 2\omega t$
and

$$\theta_1=\frac{b}{2}(l^2-x^2)+U_a\cos 2\omega t-U_b\sin 2\omega t. \tag{27}$$

Thus the average value over an integral number of cycles of the temperature rise is the same as that found in appendix 2 for the same numerical value of direct current, so that under these conditions the temperature rise of the conductor can be used as a measure of the current without ac-dc error.

We shall now consider that $\rho=\rho_0(1+\alpha\theta)$ and $k=k_0(1+\beta\theta)$ and that some small fraction of the total heat is lost by radiation. If p is the perimeter of the heater in centimeters, then the heat radiated per second from the surface of a differential length, d_x, of the heater is

$$dH_r=p\zeta K(T^4-T_0^4)dx,$$

where ζ is the emissivity of the heater material, a numerical constant, and K is the Stefan-Boltzmann constant in watts-cm^{-2}(deg K)$^{-4}$. T is the absolute temperature of the element; T_0 is the absolute temperature of the surroundings. Introducing these terms in eq 22 gives, as $\beta\theta<1$,

$$\frac{\partial^2\theta}{\partial x^2}-g(1-\beta\theta)\frac{\partial\theta}{\partial t}=-b(1-\cos 2\omega t)(1+\eta\theta)+\frac{p\zeta K}{ak}(T^4-T_0^4) \tag{28}$$

where $\eta=\alpha-\beta$. The perturbing terms are

(1) $$+\beta g\theta\frac{\partial\theta}{\partial t}$$

(2) $$-b(1-\cos 2\omega t)\eta\theta$$

(3) $$\frac{p\zeta K}{ak}(T^4-T_0^4).$$

As these perturbing terms are relatively small, the solution will differ by only a small amount from that given by eq 27. Hence a sufficient expression for these small terms will be given by substituting the known values of the dependent variables y from eq 27, and its derivatives as necessary, in these perturbing terms. When this is done, it is found that the first of these terms reduces to functions of x, each multiplied by sin $n\omega t$ or cos $n\omega t$, where $n=2$, 4. The second reduces to similar harmonic terms plus the terms $-b[\eta P-(\eta U_a/2)]$, where $P=(l^2-x^2)b/2$. The third term becomes unnecessarily complex. It can be simplified by making the further approximation that for this term

$$T-T_0=\theta_r=P(1-q\sin 2\omega t),$$

and

$$T^4-T_0^4=(T_0+\theta_r)^4-T_0^4\approx 4\theta_rT_0^3+6\theta_r^2T_0^2,\ \theta_r<T_0$$

and also that $k=k_0$. With these approximations, this term reduces to harmonic terms plus the terms

$$4NT_0^3P+6NT_0^2P^2\left(1+\frac{q^2}{2}\right),$$

where $N=p\zeta K/ak_0$.
Thus eq 28 becomes

$$\frac{\partial^2\theta}{\partial x^2}-g\frac{\partial\theta}{\partial t}=-b\left(1+\eta P-\frac{\eta U_a}{2}\right)+2NT_0^3P\left[2T_0+3P1+\left(\frac{q^2}{2}\right)\right]+\sum_{n=2}^{n=4}(F_n\cos n\omega t+G_n\sin n\omega t), \tag{29}$$

where F_n and G_n are known functions of x alone. We again let $\theta(x,\ t)=u(x,\ t)+\psi(x)$ and set $\partial^2\psi/\partial x^2$ equal to the terms independent of t in eq 29, so that

$$\frac{\partial^2 u}{\partial x^2}-g\frac{\partial u}{\partial t}=\sum_{n=2}^{n=4}(F_n\cos n\omega t+G_n\sin n\omega t) \tag{30}$$

For each frequency of the harmonic driving terms in the right-hand side of this equation, the solution of the equation which vanishes at the end points will be of the form $U_a \cos n\omega t - U_b \sin n\omega t$, where U_a and U_b are functions of x. The average value, over an integral number of cycles of the lowest frequency, will therefore vanish. Since this is a linear equation, the solution is the sum of such solutions and will therefore also vanish. Thus the average value of θ, which we are interested in, is equal to $\psi(x)$.

Evaluation $\psi(x)$ in the same manner as before gives for the value of ψ at the midpoint where $x=0$,

$$\psi(0)=\theta_d\left[1+\frac{5}{6}\eta\theta_d-\frac{\eta U_{a2}(l)}{l^2}-\frac{5}{3}NT_0^3l^2-\frac{11}{5}NT_0^3\theta_d l^2\left(1+\frac{q^2}{2}\right)\right] \tag{31}$$

where

$$U_{a2}(x)=\int_0^x dx_2\int_0^{x_2}U_a(x_1)dx_1$$

and on the assumptions that $U_{a2}(-l)=U_{a2}(l)$ and $U_{a2}(0)=0$.

The required expression for U_a can be evaluated from eq 25 and 27 by noting that

$$\mu x=\sqrt{j2\omega g}\;x=\gamma x+j\gamma x \text{ and } \mu l=\mu l+j\gamma l,$$

where $\gamma=\sqrt{\omega g}$, so that $\cosh \mu x=\cosh \gamma x \cos \gamma x+j \sinh \gamma x \sin \gamma x$, and $\cosh \mu l=\cosh \gamma l \cos\gamma l+j \sinh \gamma l \sin \gamma l$. At the frequencies we are interested in $\mu l>5$, so that

$$\cosh \mu l \approx \frac{e^{\gamma l}}{2}(\cos \gamma l+j \sin \gamma l).$$

Since $u=$ real part of

$$Ue^{j2\omega t}=re\left\{\frac{jb}{2\omega g}\left[1-\frac{\cosh \mu x}{\cosh \mu l}\right]e^{j2\omega t}\right\}=U_a \cos 2\omega t-U_b \sin 2\omega t,$$

it will be found that

$$U_a=\frac{b}{\omega g e^{\gamma l}}[\sinh \gamma x \sin \gamma x \cos \gamma l-\cosh \gamma x \cos \gamma x \sin \gamma l].$$

Performing the desired integration results in

$$U_{a2}=-\frac{b}{2\omega g\gamma^3 e^{\gamma l}}(\cos \gamma l \cosh \gamma x \cos \gamma x+\sin \gamma l \sinh \gamma x \sin \gamma x).$$

From which

$$U_{a2}(l)=U_{a2}(-l)\approx -\frac{b}{4\omega^2 g^2} \text{ and } U_{a2}(0)<<U_{a2}(l).$$

Therefore, eq 31 becomes

$$\psi(0)=\theta_{ac}=\theta_d\left[1+M+\left(\frac{\eta}{2}-\frac{11}{10}NT_0^3l^2\right)\theta_d q^2\right]=\theta_d\left[1+M+\frac{h}{2}\theta_d q^2\right], \tag{32}$$

where M is equal to the remaining terms in eq 31 and $h\approx\eta-2NT_0^3l^2$.

By the same procedure, eq 28 can be solved for the d-c case by considering $\partial\theta/\partial t=0$ and $i=I_s$ a constant of the same numerical value as the rms value of the alternating current. The temperature rise at the midpoint will be found to be

$$\theta_{ac}=\theta_d[1+M]. \tag{33}$$

Thus the temperature rise on direct current is the same as on alternating current when the frequency is high enough so that the third term in the brackets of eq 32 is sufficiently small compared to unity. Therefore the temperature rise at the midpoint on alternating current is

$$\theta_{ac}=\theta_{dc}\left[1+\frac{h\theta_{dc}q^2}{2(1+M)}\right]\approx\theta_{dc}\left[1+\frac{h}{2}\theta_{dc}q^2\right] \tag{34}$$

if M is small compared to unity.

If the hot junction of the thermocouple is fastened to the midpoint of the heater, the emf of the couple may be represented by

$$E=A\theta_m+\frac{B}{2}\theta_m^2,$$

where θ_m is the temperature of the hot junction in deg C, and A and B are constants to be evaluated at the temperature of the cold junction. On direct current $\theta_m=\theta_{dc}$ and

$$E=A\theta_{dc}\left[1+\frac{B}{2A}\theta_{dc}\right].$$

On alternating current of the same rms value, θ_m may be considered to be closely enough for these purposes

$$\theta_m=\theta_{dc}\left[1+\frac{h}{2}\theta_{dc}q^2\right](1-q \sin 2\omega t).$$

The average value of emf over an integral number of cycles of alternating current is then (to the desired accuracy, and if $(B/2A)\,\theta_{dc}$ is small compared to unity)

$$E_A=A\theta_{dc}\left(1+\frac{B}{2A}\theta_{dc}\right)\left[1+\left(\frac{h}{2}+\frac{B}{4A}\right)\theta_{dc}q^2\right].$$

From these expressions

$$\frac{E_a-E_d}{E_d}=\frac{H}{2}\theta_{dc}q^2$$

where $H=h+B/2A$.

For table 7, it is desired to compute the frequency at which the ac-dc difference of a thermal converter due to this effect is equal to 0.1 percent. From eq 7 and 9 and for $n=2$ the difference in current for the same emf is one-half the difference in emf for the same current, and is opposite in sign. Therefore the percentage ac-dc difference, δ, is approximately

$$\delta=-25H\theta_{dc}q^2=\frac{-25H\theta_{dc}d^2}{(2\pi f)^2l^4},$$

where in addition to the symbols already defined, $d=1/g=k_0/ms$ and is the thermal diffusivity in appropriate units.

Appendix 4. Effect of Shield Capacitance on the Model B Voltmeter

We may approximate the effects of capacitance to the shield of this voltmeter by considering the voltmeter as consisting of a transmission line of $r_s=r_0x^2$ ohms per unit length, having a constant capacitance c_0 farads per unit length to the shield, with a sinusoidal voltage of rms value V volts applied to the high-resistance end. The other end may be considered short-circuited, since the thermal converter, which is connected between the low-resistance end and the ground post, is of low resistance. The shield is also connected to this ground post. We wish to find the magnitude of current, I_0, at the short-circuited end. For an element of length dx at a distance x from this end, we have

$$\frac{dV}{dx}=Ir_s=Ir_0x^2 \text{ and } \frac{dI}{dx}=j\omega c_0V, \tag{35}$$

where dV is the rms voltage drop across the element, and dI is the rms current from the element to the shield. Differentiating the first of these and substituting the values of I and dI/dx in the resulting expression gives

$$\frac{d^2V}{dx^2}-\frac{2}{x}\frac{dV}{dx}-\lambda^3x^2V=0, \tag{36}$$

subject to the boundary conditions $V=0$ at $x=0$ and $V=V_s$ at $x=l$ and where $\lambda^3=j\omega c_0r_0$.

When $\lambda=0$ this becomes, with the same boundary conditions,

$$\frac{d^2V}{dx^2}-\frac{2}{x}\frac{dV}{dx}=0,$$

the solution of which is

$$V_1=\frac{V_a x^3}{l^3}.$$

We now put this value of V in the perturbing term containing λ^2 in eq 36, to get

$$\frac{d^2V}{dx^2}-\frac{2}{x}\frac{dV}{dx}=\frac{\lambda^2 V_a x^5}{l^3}.$$

The solution of this, with the same boundary conditions, is

$$V_2=\frac{V_a x^3}{l^3}\left(1-\frac{\lambda^2 l^4}{28}\right)+\frac{\lambda^2 V_a x^7}{28 l^3}.$$

As $\lambda^2=j\omega c_0 r_0$, we will need to repeat this process to secure terms in λ^4, for we are interested in the magnitudes of V and I. Putting the above value of V_2 in the last term of eq 36 and solving as before gives

$$V_3=\frac{V_a x^3}{l^3}\left(1-\frac{\lambda^2 l^4}{28}+8.8\times10^{-4}\lambda^2 l^4\right)+\frac{\lambda^2 V_a x^7}{28 l^3}\left(1-\frac{\lambda^2 l^4}{28}\right)+\frac{\lambda^4 V_a x^{11}}{2464 l^3} \tag{37}$$

From eq 35

$$I=\frac{1}{r_0 x^2}\frac{dV}{dx}. \tag{38}$$

Performing the indicated differentiation of eq 37 and substituting in 38, and noting that the total resistance is $R=r_0 l^3/3$ leads to

$$I=\frac{V_a}{R}\left[1-\frac{\lambda^2 l^4}{28}+8.8\times10^{-4}\lambda^2 l^4+\frac{\lambda^2 x^4}{12}\left(1-\frac{\lambda^2 l^4}{28}\right)+\frac{\lambda^4 x^8}{672}\right].$$

Solving for I_0 at $x=0$, and noting that the total capacitance is $C=c_0 l$ gives

$$I_0=\frac{V_a}{R}\left[1-j0.107\omega CR-7.9\times10^{-3}(\omega CR)^2\right].$$

Since the terms in the bracket are small compared with unity

$$|I_0|=\frac{V_a}{R}\left[1-0.0022(\omega CR)^2\right].$$

WASHINGTON, August 16, 1951.

nal of Research of the National Bureau of Standards Vol. 48, No. 2, February 1952 Research Paper 2297

Some Nonnegative Trigonometric Polynomials Connected With a Problem in Probability

Eugene Lukacs[1] and Otto Szász[2]

Let $0<b_1<b_2< \ldots <b_n$ be integers and let $g(\theta)$ be the Vandermonde determinant formed from $b_1^2, b_2^2, \ldots, b_n^2$ with the first row replaced by $\sin^2(b_i\theta/2)$ $(i=1, \ldots, n)$. The function $g(\theta)$ is then a cosine polynomial. In connection with a problem in probability, the question arose as to when $g(\theta)$ is a nonnegative trigonometric polynomial. This question is answered for six classes of such trigonometric polynomials.

In a previous paper [3] we gave a necessary condition that a polynomial without multiple roots must satisfy in order that its reciprocal be the Fourier transform of a distribution function. Imposing a further restriction on the polynomials it is easy to derive the following condition:

The reciprocal of a polynomial whose roots are all single and have the same imaginary part is the Fourier transform of a distribution function if and only if

(1) The polynomial has one purely imaginary root ai $(a\neq 0)$ and n pairs of complex roots $\pm b_k+ai$ $(0<b_1<b_2< \ldots <b_n,\ k=1, 2, \ldots, n)$.

(2) The determinant

$$\begin{vmatrix} \sin^2\frac{b_1\theta}{2}, & \sin^2\frac{b_2\theta}{2}, \ldots, & \sin^2\frac{b_n\theta}{2} \\ b_1^2, & b_2^2, \ldots, & b_n^2 \\ \cdot & \cdot \quad \cdots & \cdot \\ \cdot & \cdot \quad \cdots & \cdot \\ \cdot & \cdot \quad \cdots & \cdot \\ b_1^{2(n-1)}, & b_2^{2(n-1)}, \ldots, & b_n^{2(n-1)} \end{vmatrix} \geq 0 \text{ for all } \theta.$$

This condition follows easily from formula (4.4) of the reference cited in footnote 3. It is therefore of some interest to study this determinant and to investigate for what values of $b_1, b_2, \ldots, b_n$ it is a nonnegative function of θ.

In this paper we consider this determinant only for integer values of the b_i and show that it represents for certain configurations of the b_i a nonnegative trigonometric polynomial. Certain relations for generalized Vandermonde determinants of odd integers are also obtained.

We introduce first some notations. Let $0<b_1<b_2< \ldots <b_n$ be n integers and

$$V_k = \begin{vmatrix} b_1^{2k}, & b_2^{2k}, \ldots, & b_n^{2k} \\ b_1^2, & b_2^2, \ldots, & b_n^2 \\ \cdot & \cdot \quad \cdots & \cdot \\ \cdot & \cdot \quad \cdots & \cdot \\ \cdot & \cdot \quad \cdots & \cdot \\ b_1^{2(n-1)}, & b_2^{2(n-1)}, \ldots, & b_n^{2(n-1)} \end{vmatrix} \quad (1)$$

the generalized Vandermonde determinant formed from the numbers $b_1^2, b_2^2, \ldots, b_n^2$ with the exponents $k, 1, 2, \ldots, (n-1)$. Clearly $V_1=V_2= \ldots = V_{n-1}=0$, while V_0 is the ordinary Vandermonde determinant of the numbers $b_1^2, \ldots, b_n^2$. Denote further by Δ_m the minor of the element in the first row and m-th column of V_0 so that $V_0=\sum_{m=1}^{n}(-1)^{m-1}\Delta_m$.

In this paper we study the function

$$g(\theta)=2\begin{vmatrix} \sin^2\frac{b_1\theta}{2}, & \sin^2\frac{b_2\theta}{2}, \ldots, & \sin^2\frac{b_n\theta}{2} \\ b_1^2, & b_2^2, \ldots, & b_n^2 \\ \cdot & \cdot \quad \cdots & \cdot \\ \cdot & \cdot \quad \cdots & \cdot \\ \cdot & \cdot \quad \cdots & \cdot \\ b_1^{2(n-1)}, & b_2^{2(n-1)}, \ldots, & b_n^{2(n-1)} \end{vmatrix}$$

$$= V_0+\sum_{m=1}^{n}(-1)^m\Delta_m\cos b_m\theta \quad (2)$$

For the discussion of $g(\theta)$ we need the following lemmas:

Lemma 1. If $b_1, b_2, \ldots, b_n$ are integers, the determinant (2) can be factored so that

$$g(\theta)=(1-\cos\theta)^n A(\cos\theta), \quad (3)$$

where $A(x)$ is a polynomial in x of degree b_n-n.

Lemma 2. If $b_1, b_2, \ldots, b_n$ are odd integers we have

$$g'(\theta)=\sin\theta\,(1-\cos^2\theta)^{n-1}B(\cos\theta)=(\sin\theta)^{2n-1}B(\cos\theta), \quad (4)$$

where $B(x)$ is a polynomial in x of degree b_n-2n+1.

To prove lemma 1 we differentiate (2) with respect to θ and then set $\theta=0$. This shows that

$$\left.\begin{aligned} g^{2j-1}(0)&=0 && \text{for } j=1, 2, \ldots \text{ ad inf.} \\ g^{2j}(0)&=0 && \text{for } j=0, 1, 2, \ldots (n-1) \\ g^{2k}(0)&=(-1)^{k-1}V_k && \text{for } k=n, (n+1), \ldots \text{ad inf.} \end{aligned}\right\} \quad (5)$$

[1] National Bureau of Standards and Our Lady of Cincinnati College.
[2] University of Cincinnati and National Bureau of Standards.
[3] E. Lukacs and O. Szász, Certain Fourier transforms of distributions, Canadian J. Math. **3**, 140 to 144 (1951).

From (5) we obtain the expansion of $g(\theta)$ into a series

$$g(\theta)=\sum_{k=n}^{\infty}(-1)^{k-1}\frac{V_k}{(2k)!}\theta^{2k}. \tag{6}$$

On the other hand, (2) indicates that $g(\theta)$ is a cosine polynomial of degree b_n which vanishes for $\theta=0$. Therefore it has the form

$$g(\theta)=\beta_1(1-\cos\theta)+\beta_2(1-\cos\theta)^2+\ \ldots \\ +\beta_{b_n}(1-\cos\theta)^{b_n} \tag{7}$$

Comparing (6) and (7) it is seen that $\beta_1=\beta_2=\ \ldots\ =\beta_{n-1}=0$ so that $(1-\cos\theta)^n$ is a factor of $g(\theta)$; this establishes lemma 1.

To prove lemma 2 we assume that all the $b_i (i=1, 2, \ldots, n)$ are odd numbers. It follows then from (2) that

$$g(\pi-\theta)=2V_0-g(\theta), \tag{8}$$

therefore

$$g'(\pi-\theta)=g'(\theta). \tag{9}$$

From (3) we have

$$g'(\theta)=(1-\cos\theta)^{n-1}\sin\theta[nA(\cos\theta)- \\ (1-\cos\theta)A'(\cos\theta)].$$

Substituting this into (9) we obtain

$$(1-\cos\theta)^{n-1}\sin\theta[nA(\cos\theta)-(1-\cos\theta)A'(\cos\theta)]$$

$$=(1+\cos\theta)^{n-1}\sin\theta[nA(-\cos\theta)- \\ (1+\cos\theta)A'(-\cos\theta)].$$

This shows that $nA(\cos\theta)-(1-\cos\theta)A'(\cos\theta)$ and therefore also $g'(\theta)$ has the factor $(1+\cos\theta)^{n-1}$. This completes the proof of lemma 2.

If we introduce as a new variable

$$x=\cos\theta \tag{10}$$

and write

$$P(x)=g(\arccos x) \tag{11}$$

we have from lemma 1

$$P(x)=(1-x)^nA(x), \tag{12}$$

and similarly from lemma 2

$$P'(x)=-(1-x^2)^{n-1}B(x). \tag{13}$$

We substitute next the expansion (6) into (8) and see that

$$2V_0-\sum_{k=n}^{\infty}(-1)^{k-1}\frac{V_k}{(2k)!}\theta^{2k}=\sum_{k=n}^{\infty}(-1)^{k-1}\frac{V_k}{(2k)!}(\pi-\theta)^{2k} \tag{14}$$

Differentiating (14) and setting $\theta=0$ we obtain from this equation a number of relations for generalized Vandermonde determinants formed of odd integers

$$\left.\begin{aligned} &2V_0=\sum_{k=n}^{\infty}(-1)^{k-1}\frac{V_k}{(2k)!}\pi^{2k} \\ &\sum_{k=n}^{\infty}(-1)^{k-1}\frac{V_k}{(2k-m)!}\pi^{2k}=0 \\ &\qquad\text{for } m=1, 2, \ldots (2n-1) \\ &\sum_{k=n+m}^{\infty}(-1)^{k-1}\frac{V_k\pi^{2k}}{(2k-2n-2m)!} \\ &\qquad=(-1)^{n+m}\pi^{2(n+m)}V_{n+m} \\ &\qquad\text{for } m=0, 1, 2, \ldots \text{ad inf.} \\ &\sum_{k=n+m+1}^{\infty}(-1)^{k-1}\frac{V_k\pi^{2k}}{(2k-2n-2m-1)!}=0 \\ &\qquad\text{for } m=0, 1, 2, \ldots \text{ad inf.} \end{aligned}\right\} \tag{15}$$

In the following we discuss several configurations of the integers $b_1, b_2, \ldots, b_n$, which lead to non-negative trigonometric polynomials $g(\theta)$, the results are given in statements, labelled (A) (B) . . . (F).

(A) If the b_i are the first n consecutive integers, that is if $b_i=i$ for $i=1, 2, \ldots, n$, then the trigonometric polynomial $g(\theta)$ is nonnegative.

Proof: From lemma 1 we see $g(\theta)=A(1-\cos\theta)^n$, where A is a constant. Hence $A=2^{-n}g(\pi)$; from (2) it is seen that $g(\pi)=V_0+\sum_{m=1}^{n}\Delta_m$. Therefore $A>0$ and consequently $g(\theta)$ nonnegative for all values of θ.

(B) If the b_i are the first n consecutive odd integers, that is, if $b_i=2i-1$ for $i=1, 2, \ldots, n$ then the trigonometric polynomial $g(\theta)$ is nonnegative.

Proof: Since $b_n=2n-1$ the polynomial $B(x)$ of lemma 2 reduces to a constant B. From (13) we have $P'(x)=-B(1-x^2)^{n-1}$ or, in view of $P(1)=0$, $P(x)=B\int_x^1(1-t^2)^{n-1}\,dt$.

Formulae (11) and (2) show then that $P(0)=g(\pi/2)=V_0>0$, hence

$$B=\frac{P(0)}{\int_0^1(1-t^2)^{n-1}dt}>0.$$

Therefore $P(x)\geq 0$ for $|x|\leq 1$. This completes the proof of statement (B) since the inequalities $P(x)\geq 0$ for $|x|\leq 1$ and $g(\theta)\geq 0$ for all θ are equivalent.

(C) If $b_n=n+1$, that is if the numbers $b_1, \ldots, b_n$ are obtained from the first consecutive $(n+1)$ integers by omitting the integer k $(1\leq k\leq n)$ then the trigonometric polynomial $g(\theta)$ is nonnegative if and only if $2k^2\geq(n+1)$.

Proof: In this case $P(x)$ has degree $(n+1)$ so that according to lemma 1 $A(x)$ is a linear function.

$$A(x)=a+bx. \tag{16}$$

The substitution (10) transforms $\cos k\theta$ into $T_k(x)$ where $T_k(x)$ is the k-th Tchebicheff polynomial of the first kind. Formulae (2), (3) and (16) show that

$$A(x)=(1-x)^n(a+bx)=V_0+\sum_{m=1}^{n}(-1)^m\Delta_m T_{b_m}(x). \quad (17)$$

The coefficients a and b of $A(x)$ can be determined from (17), after some elementary computations it is seen that

$$A(x)=2^n\Delta_n\left[x+\frac{n(n+1)+k^2}{(n+1)^2-k^2}\right]. \quad (18)$$

In the interval $|x|<1$ the functions $A(x)$ and $P(x)=(1-x)^n A(x)$ have the same sign so that it is sufficient to determine when $A(x)$ is nonnegative in $|x|<1$. From (18) it is seen that $A(x)\geq 0$ in $|x|<1$ if and only if $n(n+1)+k^2\geq(n+1)^2-k^2$, that is if $2k^2\geq n+1$.

(D) If the b_i $(i=1, 2, \ldots, n)$ are all odd numbers and if $b_n=2n+1$ so that $b_1, b_2, \ldots, b_n$ are obtained from the first $(n+1)$ odd integers by omitting the k-th odd integer $2k-1$ $(1\leq k\leq n)$, than the trigonometric polynomial $g(\theta)$ is nonnegative if either one or the other of the following conditions is satisfied

$$k\geq\frac{1}{2}\left(1+\sqrt{1+2n}\right) \quad \text{(i)}$$

$$k<\frac{1}{2}\left(1+\sqrt{1+2n}\right), \quad \text{(ii)}$$

but

$$\frac{n-2k(k-1)}{2[n(n+1)-k(k-1)]}\leq z_n^2,$$

where z_n is the root of the equation

$$\int_{-z}^{1}(1-t^2)^{n-1}(t^2-z^2)dt=0 \quad (19)$$

which falls into the interval (0, 1).

If neither (i) nor (ii) is satisfied, then the function $g(\theta)$ assumes also negative values. Moreover it is possible to simplify (ii) for large n by proving the *Corollary to statement (D)*.

If for large n and $k<[1+\sqrt{1+2n}]/2$ also

$$\sqrt{\frac{\left(n+\frac{1}{2}\right)[n-2k(k-1)]}{2[n(n+1)-k(k-1)]}}\leq\rho=0.5939157\ldots$$

then $g(\theta)$ is nonnegative; if on the other hand

$$\frac{\left(n+\frac{1}{2}\right)[n-2k(k-1)]}{2[n(n+1)-k(k-1)]}>\rho^2$$

then there are integers n and k for which $g(\theta)$ assumes positive and negative values.

To prove statement (D) we need the following lemma

Lemma 3. Let

$$P_s(x)=\int_x^1(1-t^2)^{n-1}t^{2s}dt \text{ for } s=0, 1 \quad (20)$$

and

$$Q(x, \zeta)=P_1(x)-\zeta^2P_0(x). \quad (21)$$

The polynomial $Q(x, \zeta)$ is nonnegative in the interval $-1\leq x\leq 1$ if and only if

$$\zeta\leq z_n. \quad (22)$$

Here z_n is the root of the equation

$$R(z)\equiv Q(-z, z)\equiv\int_{-z}^{1}(1-t^2)^{n-1}(t^2-z^2)\,dt=0, \quad (23)$$

which falls into the interval (0, 1).

Moreover let $w_n=\sqrt{n+\frac{1}{2}}\,z_n$.

Then $\lim_{n\to\infty} w_n=\rho$ exists and is the root of the equation

$$F(\rho)=\sqrt{\pi}\left(\frac{1}{2}-\rho^2\right)-2\rho^3\int_0^1(1-t^2)e^{-\rho^2t^2}\,dt=0, \quad (24)$$

which is located in the interval $\left(0, \sqrt{\frac{1}{2}}\right)$.

Some values of z_n as well as ρ were computed. The proof of this lemma is rather lengthy. In order to avoid interrupting the discussion of the various nonnegative trigonometric polynomials, this proof will be given in the last section of this paper.

We proceed now to the *proof* of statement (D).

According to lemma 2 $B(x)$ is a polynomial of the second degree. Since the b_i are all odd numbers $P'(x)$ and $B(x)$ are even functions of x so that one obtains from (13) and (2)

$$P'(x)=-(1-x^2)^{n-1}(a+cx^2)=\sum_{m=1}^{n}(-1)^m\Delta_m T'_{b_m}(x).$$

This relation permits us to determine a and c, and it is seen that

$$P'(x)=-2^{2n}(2n+1)\Delta_n(1-x^2)^{n-1}\left\{x^2-\frac{n-2k(k-1)}{2[n(n+1)-k(k-1)]}\right\},$$

If we use for brevity the notation

$$\gamma=2^{2n}(2n+1)\Delta_n \quad (25)$$

and

$$\zeta_{n,k}^2=\frac{n-2k(k-1)}{2[n(n+1)-k(k-1)]}, \quad (26)$$

we have

$$\left.\begin{aligned} P'(x) &= -\gamma(1-x^2)^{n-1}(x^2-\zeta_{n,k}^2) \\ P(x) &= \gamma\int_x^1 (1-t^2)^{n-1}(t^2-\zeta_{n,k}^2)dt \end{aligned}\right\}. \tag{27}$$

If (i) is satisfied we see that $\zeta_{n,k}^2 \leq 0$, so that from (27) $P'(x) \leq 0$ for $|x| \leq 1$. In this case $P(x)$ is non-increasing in the interval $-1 \leq x \leq +1$, since $P(1)=0$ this means $P(x) \geq 0$ for $|x| \leq 1$ so that also $g(\theta) \geq 0$.

We assume next that (ii) is satisfied, then $\zeta_{n,k}^2 > 0$. Since $\gamma > 0$ and $P'(x) = \gamma Q(x, \zeta_{n,k})$, we see that statement (D) follows immediately from lemma 3.

(E) If the numbers $b_1, \ldots, b_n$ are obtained from the first consecutive $(n+2)$ integers by omitting the two integers k and p where $1 \leq k \leq p-1 \leq n$, then $g(\theta)$ is nonnegative if and only if a certain polynomial $Q(x)$ of the second degree is nonnegative for $|x| \leq 1$. Here

$$Q(x) = 4x^2 + 4[n - L(n, k, p)]x + 2n^2 + (n-2) - 4nL(n, k, p) + N(n, k, p), \tag{28}$$

where

$$\left.\begin{aligned} L(n,k,p) &= \frac{(n+2)[(n+1)^2-k^2][(n+1)^2-p^2]}{[(n+2)^2-k^2][(n+2)^2-p^2]} \\ N(n,k,p) &= \frac{(n+2)(2n+3)(n^2-k^2)(n^2-p^2)}{[(n+2)^2-k^2][(n+2)^2-p^2]} \end{aligned}\right\} \tag{29}$$

Proof: In this case $b_n = n+2$, so that according to lemma 1 $A(x)$ is a polynomial of the second degree, $A(x) = ax^2 + bx + c$. From (12), (2) and (3) we have

$$\begin{aligned} P(x) &= (1-x)^n(ax^2+bx+c) \\ &= V_0 + \sum_{m=1}^{n}(-1)^m \Delta_m T_{b_m}(x). \end{aligned} \tag{30}$$

From this relation we can determine the coefficients a, b, and c. A somewhat tedious elementary computation shows that

$$A(x) = (ax^2+bx+c) = 2^{n-1}\Delta_n Q(x).$$

This completes the proof of statement (E) which follows immediately from (30).

Certain particular cases can be discussed easily.

(a) If $k = p-1 = n$ then $N(n, n, n+1) = L(n, n, n+1) = 0$ so that $Q(x) = 4x^2 + 4nx + 2n^2 + n - 2$. The discriminant of $Q(x)$ is then $-16(n-1)(n+2)$ and is negative for $n > 1$. Therefore, $Q(x) \geq 0$ for all x so that $g(\theta)$ must be nonnegative.

(b) If $k < n$ while $p = (n+1)$ then $L(n, k, n+1) = 0$ and

$$N(n, k, n+1) = -\frac{(n+2)(2n+1)(n^2-k^2)}{(n+2)^2-k^2}.$$

$Q(x)$ and its discriminant can be computed easily and it can be shown that $g(\theta)$ is nonnegative if and only if

$$k^2 > \frac{(n-1)(n+2)}{2n}.$$

(c) If $k = n-1$ and $p = n$ then $N(n, n-1, n) = 0$ and

$$L(n, n-1, n) = \frac{n(n+2)}{3(n+1)}.$$

The discriminant of $Q(x)$ is then

$$\frac{16}{9(n+1)^2}(-2n^4 - 5n^3 + 7n^2 + 27n + 18),$$

which is negative if $n \geq 3$ so that in this case $g(\theta) \geq 0$. If $n = 2$, $Q(x)$ has two roots in the interval $-1 \leq x \leq +1$ so that $g(\theta)$ assumes also negative values

We proceed to discuss a more complicated case by assuming that the $b_1, b_2, \ldots, b_n$ are obtained from the first $(n+2)$ odd integers by omitting two odd integers $(2k-1)$ and $(2p-1)$ where

$$1 \leq k \leq p-1 \leq n \tag{31}$$

so that $b_n = 2n+3$.

We see then from lemma 2 that $B(x)$ is a polynomial of degree four. By the procedure employed in case (C) it is possible to determine the coefficients of this polynomial.

We obtain

$$P'(x) = -\gamma(1-x^2)^{n-1}B(x) = -\gamma(1-x^2)^{n-1}(4x^4 + ax^2 - b) \tag{32}$$

Here

$$\left.\begin{aligned} \gamma &= 2^{2n}(2n+3)\Delta_n > 0, \\ a &= \frac{2\{-2(n+1)^2(3n+5) + (n+1)(2n+5)[k(k-1)+p(p-1)] - 4k(k-1)p(p-1)\}}{[(n+2)(n+1)-k(k-1)][(n+2)(n+1)-p(p-1)]} \\ b &= \frac{\{-(n+1)(3n+4) + 2(n+1)[k(k-1)+p(p-1)] - 4k(k-1)p(p-1)\}}{[(n+2)(n+1)-k(k-1)][(n+2)(n+1)-p(p-1)]} \end{aligned}\right\}. \tag{33}$$

The trigonometric polynomial $g(\theta)$ is nonnegative if and only if

$$P(x)=\gamma\int_x^1(1-t^2)^{n-1}(4t^4+at^2-b)\,dt\geq 0 \text{ for all } |x|\leq 1. \tag{34}$$

The nonnegativity of the polynomial $P(x)$ depends on the nature of the roots of the polynomial $R(x)=4x^4+ax^2-b$. This introduces the need to distinguish a number of cases. For this purpose we write

$$\left.\begin{aligned} h(\tau)&=4\tau^2+a\tau-b=4(\tau-\tau_1)(\tau-\tau_2) \text{ where}\\ \tau_1&=\frac{-a-\sqrt{a^2+16b}}{8} \qquad \tau_2=\frac{-a+\sqrt{a^2+16b}}{8}\end{aligned}\right\}. \tag{35}$$

We are now in a position to formulate statement (F).

(F) If the numbers $b_1, b_2, \ldots, b_n$ are obtained from the first consecutive $(n+2)$ odd integers by omitting the two integers $2k-1$ and $2p-1$ (where $1\leq k\leq p-1\leq n$) then the trigonometric polynomial $g(\theta)$ is nonnegative if and only if one of the following four, mutually exclusive, conditions is satisfied

(α) $a\geq 0$ and $b\leq 0$,

(β) $a<0$ and $a^2+16b\leq 0$,

(γ) $a\geq 0$ and $0<b<4+a$ and also
$R_2(\sqrt{\tau_2})-\tau_1R_1(\sqrt{\tau_2})\geq 0$.

(δ) $0>a>-4$ and $-\frac{a^2}{16}<b<a+4$ and also
$R_2(\sqrt{\tau_2})-\tau_1R_1(\sqrt{\tau_2})\geq 0$, and if $\tau_1>0$
$R_2(-\sqrt{\tau_1})-\tau_2R_1(-\sqrt{\tau_1})\geq 0$.

Here

$$R_i(z)=\int_{-z}^1(1-t^2)^{n-1}t^{2(i-1)}(t^2-z^2)dt \text{ for } i=1,2, \tag{36}$$

so that $R_1(z)=R(z)$ as given by (23).

Proof: If $h(\tau)=4\tau^2+a\tau-b\geq 0$ for $0\leq\tau\leq 1$, then $P'(x)=-\gamma(1-x^2)^{n-1}h(x^2)\leq 0$ for $-1\leq x\leq 1$. Since $P(1)=0$ we see that $P(x)\geq 0$ for $-1\leq x\leq+1$. Clearly $h(\tau)=\left(2\tau+\frac{a}{4}\right)^2-\frac{a^2}{16}-b$, therefore

$$h(\tau)\geq 0 \text{ in } 0\leq\tau\leq 1 \text{ if and only if} \tag{37}$$

$$\left(2\tau+\frac{a}{4}\right)^2\geq\frac{a^2+16b}{16} \text{ in } 0\leq\tau\leq 1. \tag{38}$$

If $a\geq 0$, (38) holds if and only if $b\leq 0$, but this is exactly condition (α).

We next derive the condition for the validity of (37) when $a<0$. Clearly $h'(\tau)=8\tau+a$, $h''(\tau)=8$, so that $h(\tau)$ has a minimum at $\tau=-a/8$.

We consider first the case $|a|/8=-a/8<1$, we have then

$$\min_{0\leq\tau\leq 1}h(\tau)=h\left(\frac{-a}{8}\right)=-\frac{a^2+16b}{16}.$$

Relation (37) is therefore satisfied if $-8<a<0$ and $a^2+16b\leq 0$. If $|a|/8\geq 1$ we see that $h'(\tau)\leq 8(\tau-1)\leq 0$ in $0\leq\tau\leq 1$, so that $\min_{0\leq\tau\leq 1}h(\tau)=h(1)=4+a-b$. The function $h(\tau)$ is nonnegative if $a\leq -8$ and $4+a-b\geq 0$. But $a^2+16b=(a+8)^2-16(4+a-b)$ for any a, hence if $a^2+16b\leq 0$ we always have $4+a-b>0$. The alternatives discussed for case $a<0$ can therefore be joined so that condition (β) is established. To complete the discussion we must consider the remaining cases, namely

(γ') $a\geq 0$ and $b>0$,

and

(δ') $a<0$ and $a^2+16b>0$.

In case (γ') we see from (35) that $\tau_1<0$ while $\tau_2>0$. Since $P(x)=4\gamma\int_x^1(1-t^2)^{n-1}(t^2-\tau_1)(t^2-\tau_2)\,dt$, it follows that $P(x)\leq 0$ if $\tau_2\geq 1$, that is if $\sqrt{a^2+16b}\geq a+8$, but this occurs if and only if $b\geq 4+a$.

Thus $P(x)\leq 0$ for $-1\leq x\leq 1$ if $a\geq 0$ and $b\geq 4+a$, therefore (γ') reduces to the case

(γ'') $a\geq 0$ and $0<b<4+a$.

In this case both roots τ_1 and τ_2 are real and a simple computation shows that $\min_{-1\leq x\leq 1}P(x)=P(-\sqrt{\tau_2})$, hence $P(x)\geq 0$ in $|x|\leq 1$ if and only if

$$P(-\sqrt{\tau_2})=4\gamma\int_{-\sqrt{\tau_2}}^1(1-t^2)^{n-1}(t^2-\tau_1)(t^2-\tau_2)\,dt\geq 0.$$

That is if

$$\int_{-\sqrt{\tau_2}}^1(1-t^2)^{n-1}(t^2-\tau_2)t^2dt-\tau_1\int_{-\sqrt{\tau_2}}^1(1-t^2)^{n-1}(t^2-\tau_2)\,dt\geq 0$$

or, written in a more concise notation

$$R_2(\sqrt{\tau_2})-\tau_1R_1(\sqrt{\tau_2})\geq 0,$$

so that (γ) is established.

We proceed with the discussion of the last case (δ') $a<0$ and $a^2+16b>0$ and show first that always $a+4>0$. From (33) we obtain easily

$$\frac{(a+4)}{2}=\frac{2(n+1)^2(n^2+n-1)+(n+1)[k(k-1)+p(p-1)]-2k(k-1)p(p-1)}{[(n+2)(n+1)-k(k-1)][(n+2)(n+1)-p(p-1)]}.$$

On account of (31) this fraction has always a positive denominator so that its sign is determined by the sign of the numerator which we denote by $M(n,k,p)$. We have then

$$M(n,k,p)=p(p-1)[(n+1)-2k(k-1)]+(n+1)k(k-1)+2(n+1)^2(n^2+n-1)$$

$$=k(k-1)[(n+1)-2p(p-1)]+(n+1)p(p-1)+2(n+1)^2(n^2+n-1).$$

If $(n+1)-2k(k-1)\geq 0$ then $M(n,k,p)>0$. If on the other hand $(n+1)-2k(k-1)<0$ then also $(n+1)-2p(p-1)<0$. Therefore $M(n,k,p)$ decreases for fixed k and increasing p as well as for fixed p and increasing k. Hence $M(n,k,p)$ attains its minimum value if k and p are as large as possible, that is

$$M(n,k,p)\geq M(n,n,n+1)$$

$$=2(n+1)^2(n^2+n-1)-2n^2(n+1)(n-2)$$

$$\geq 2n^2(n+1)^2-2n^2(n+1)(n-2) \text{ if } n\geq 1.$$

Therefore $M(n,k,p)\geq 6n^2(n+1)>0$ if $n\geq 1$ so that also $a+4>0$. It is therefore no restriction if we write the case (δ') in the form

$$(\delta') \qquad 0>a>-4 \text{ and } a^2+16b>0.$$

We must first consider the case

$$(\delta_1) \qquad 0>a>-4 \text{ and } b\geq a+4.$$

We have then $a^2+16b>0$ so that $h(\tau)$ has two real roots; from (35) we see that $\tau_1<0$ while $\tau_2\geq 1$. Therefore

$$P(x)=4\gamma\int_x^1(1-t^2)^{n-1}(t^2-\tau_1)(t^2-\tau_2)dt\leq 0$$

for $-1\leq x\leq 1$ so that (δ_1) does not yield nonnegative trigonometric polynomials. We finally have to investigate the possibility that

$$(\delta_2) \qquad 0>a>-4 \text{ and } -\frac{a^2}{16}<b<4+a$$

holds. Again $a^2+16b>0$ and $h(\tau)$ has two real roots τ_1 and τ_2. It follows then from (35) that $1\geq\tau_2>\tau_1>-1$.

Assume first that $\tau_1>0$.

By a simple computation it is seen that $P(x)$ has the two minima $+\sqrt{\tau_1}$ and $-\sqrt{\tau_2}$ inside the interval $(-1,+1)$. $P(x)$ is therefore nonnegative for $-1\leq x\leq 1$ if and only if $P(\sqrt{\tau_1})\geq 0$ and $P(-\sqrt{\tau_2})\geq 0$. According to (34) and (35) this means that

$$\int_{-\sqrt{\tau_2}}^1(1-t^2)^{n-1}t^2(t^2-\tau_2)dt-\tau_1\int_{-\sqrt{\tau_2}}^1(1-t^2)^{n-1}(t^2-\tau_2)dt\geq 0$$

and

$$\int_{\sqrt{\tau_1}}^1(1-t^2)^{n-1}t^2(t^2-\tau_1)dt-\tau_2\int_{\sqrt{\tau_1}}^1(1-t^2)^{n-1}(t^2-\tau_1)dt\geq 0$$

or, using the notation of (36)

$$R_2(\sqrt{\tau_2})-\tau_1R_1(\sqrt{\tau_2})\geq 0$$

and simultaneously $R_2(-\sqrt{\tau_1})-\tau_2R_1(-\sqrt{\tau_1})\geq 0$.

If $\tau_1\leq 0$ then there is only one minimum for $P(x)$, and therefore only the first condition remains. This establishes condition (δ) and completes the proof of statement (F).

In this section we give proof of lemma 3, which was stated on page 141. We write

$$P_s(x)=\int_x^1(1-t^2)^{n-1}t^{2s}dt \qquad (s=0,1) \qquad (39)$$

and want to determine the conditions which ζ has to satisfy in order that the polynomial

$$Q(x,\zeta)=P_1(x)-\zeta^2P_0(x) \qquad (40)$$

should be nonnegative for $-1\leq x\leq+1$.

Clearly $0<P_1(x)<P_0(x)$ for $-1\leq x<+1$. Therefore $Q(x,\zeta)<0$ for $|x|<1$ if $\zeta\geq 1$. If for some value ζ_0 such that $|\zeta_0|<1$ the function $Q(x,\zeta_0)\geq 0$ for $|x|\leq 1$ then also $Q(x,\zeta)\geq 0$ for $|x|\leq 1$ and $|\zeta|\leq|\zeta_0|$.

To obtain a criterion for the nonnegativity of $Q(x,\zeta)$ in $|x|\leq 1$ we have to determine the greatest possible ζ such that $|\zeta|<1$ and $Q(x,\zeta)\geq 0$ for $|x|\leq 1$.

An elementary computation shows that the function $Q(x,\zeta)$ has exactly one minimum in the interval $-1<x<+1$ which is located at $x=-\zeta$.

We consider next the equation $R(z)\equiv Q(-z,z)=0$ or, written in greater detail,

$$\int_{-z}^1(1-t^2)^{n-1}(t^2-z^2)dt=P_1(-z)-z^2P_0(-z)=0. \qquad (41)$$

Clearly $R(0)>0$ while $R(1)=P_1(-1)-P_0(-1)<0$ so that the equation (41) has at least one root in $(0,1)$. Moreover

$$\frac{dR}{dz}=-2z\int_{-z}^1(1-t^2)^{n-1}dt$$

so that dR/dz vanishes in the interval $0\leq z<1$ only at the point $z=0$, therefore the equation (41) has exactly one root z_n in the interval $(0,1)$.

Since $\min_{-1\leq x\leq 1}Q(x,z_n)=R(z_n)=0$ we see that $Q(x,z_n)\geq 0$ in $|x|\leq 1$ and therefore $Q(x,\zeta)\geq 0$ in $|x|\leq 1$ if $\zeta\leq z_n$.

If however $\zeta>z_n$ then

$$Q(-z_n,\zeta)=P_1(-z_n)-\zeta^2P_0(-z_n)=-(\zeta^2-z_n^2)P_0(-z_n)<0$$

that $G(x,\zeta)$ assumes also negative values. This establishes the first part of lemma 3. We still have to discuss the asymptotic behaviour of the solution of equation (41).

We derive first a useful inequality. By definition $-z_n$ is a root of equation (41), therefore

$$\int_{-1}^{+1}(1-t^2)^{n-1}(t^2-z_n^2)dt=\int_{-1}^{-z_n}(1-t^2)^{n-1}(t^2-z_n^2)dt>0.$$

If we set

$$w_n=\sqrt{n+\frac{1}{2}}\,z_n \tag{42}$$

then we see that

$$2\int_0^1(1-t^2)^{n-1}\left(t^2-\frac{w_n^2}{n+\frac{1}{2}}\right)dt\geq 0.$$

or

$$\int_0^1(1-t)^{n-1}t^{\frac{1}{2}}dt-\frac{w_n^2}{n+\frac{1}{2}}\int_0^1(1-t)^{n-1}t^{-\frac{1}{2}}dt\geq 0.$$

We see therefore that

$$\frac{\Gamma(n)\Gamma\left(\frac{3}{2}\right)}{\Gamma\left(n+\frac{3}{2}\right)}-\frac{w_n^2}{n+\frac{1}{2}}\frac{\Gamma(n)\Gamma\left(\frac{1}{2}\right)}{\Gamma\left(n+\frac{1}{2}\right)}\geq 0$$

so that

$$w_n^2\leq\frac{1}{2}\text{ or }z_n^2\leq\frac{1}{2n+1}. \tag{43}$$

In order to derive an asymptotic estimate for w_n we rewrite (41) by dividing the interval of integration into two parts $(-z,0)$ and $(0,1)$. The integrals over the second interval may be easily expressed in terms of gamma functions. A simple computation yields:

$$R(z)=\frac{1}{2}\frac{\Gamma\left(\frac{1}{2}\right)\Gamma(n)}{\Gamma\left(n+\frac{1}{2}\right)}\left(\frac{1}{2n+1}-z^2\right)$$

$$-z^3\int_0^1(1-z^2t^2)^{n-1}(1-t^2)dt.$$

If we write

$$L(z)=\frac{2\left(n+\frac{1}{2}\right)\Gamma\left(n+\frac{1}{2}\right)}{\Gamma(n)}R(z)$$

and

$$I_n(z)=\int_0^1(1-z^2t^2)^{n-1}(1-t^2)\,dt, \tag{44}$$

we have

$$L(z)=\frac{1}{2}\sqrt{\pi}[1-(2n+1)z^2]-\frac{2\Gamma\left(n+\frac{1}{2}\right)}{\Gamma(n)}\left(n+\frac{1}{2}\right)z^3I_n.$$

From the asymptotic formula for $\log\Gamma(x)$ it is seen that

$$\frac{\Gamma\left(n+\frac{1}{2}\right)}{\left(n+\frac{1}{2}\right)^{\frac{1}{2}}\Gamma(n)}=\exp\left[-\frac{3}{8n}+o(n^{-1})\right]=e^{o(n^{-1})}$$

hence

$$L(z)=\frac{\sqrt{\pi}}{2}[1-(2n+1)z^2]-2e^{o(n^{-1})}\left(n+\frac{1}{2}\right)^{\frac{3}{2}}z^3I_n. \tag{45}$$

We next transform the integral I_n. Let $0<x<1$ then $(1-x)e^x<1$ and $(1-x)^{n-1}<e^{-(n-1)x}$, therefore

$$0<1-[(1-x)e^x]^{n-1}<(n-1)[1-(1-x)e^x].$$

Since $e^x>1+x$ we have also $(1-x)e^x>1-x^2$ and $1-(1-x)e^x<x^2$ so that finally $0<1-(1-x)^{n-1}e^{(n-1)x}<(n-1)x^2$ or $0<e^{-(n-1)x}-(1-x)^{n-1}<(n-1)x^2$. We replace here x by z^2t^2 and see that $0<e^{-(n-1)z^2t^2}-(1-z^2t^2)^{n-1}<(n-1)z^4t^4$ for $z^2t^2<1$, so that

$$(1-z^2t^2)^{n-1}=e^{-(n-1)z^2t^2}-(n-1)\theta_n z^4t^4\text{ for }z^2t^2<1$$

with $0<\theta_n<1$.

We substitute this into the expression (44) for I_n and obtain

$$I_n=\int_0^1 e^{-(n-1)z^2t^2}(1-t^2)dt-\frac{2\delta_n}{35}(n-1)z^4 \tag{46}$$

for $z^2<1$ with $0<\delta_n<1$.

We have

$$0<e^{-(n-1)z^2t^2}-e^{-\left(n+\frac{1}{2}\right)z^2t^2}=e^{-(n-1)z^2t^2}\left[1-e^{-\frac{3}{2}z^2t^2}\right]$$

Since $0<1-e^{-\frac{3}{2}z^2t^2}<\frac{3}{2}z^2t^2$ we see that $\left(1-e^{-\frac{3}{2}z^2t^2}\right)$ $=\eta\,z^2t^2$ with $0<\eta<3/2$ and hence

$$e^{-(n-1)z^2t^2}=e^{-\left(n+\frac{1}{2}\right)z^2t^2}+\eta e^{-(n-1)z^2t^2}z^2t^2$$

therefore

$$\int_0^1 e^{-(n-1)z^2t^2}(1-t^2)dt=\int_0^1 e^{-\left(n+\frac{1}{2}\right)z^2t^2}(1-t^2)dt$$

$$+\frac{2\lambda}{15}z^2e^{-(n-1)z^2\sigma}$$

with $0<\sigma<1$ and $0<\lambda<\frac{3}{2}$.

Substituting this into (46) we have

$$I_n = \int_0^1 e^{-\left(n+\frac{1}{2}\right)z^2t^2}(1-t^2)dt + \frac{2\lambda z^2}{15} e^{-(n-1)z^2\sigma} - \frac{2\delta_n(n-1)z^4}{35} \tag{47}$$

with $0<\delta_n<1$, $0<\sigma<1$, $0<\lambda<\frac{3}{2}$.

We introduce next a new variable $w_n=\sqrt{n+\frac{1}{2}}\,z$, using (45) and (47) we see that w_n satisfies the equation

$$\left.\begin{aligned}\sqrt{\pi}\left(\frac{1}{2}-w_n^2\right)-2w_n^2\,e^{O(n^{-1})}\int_0^1 e^{-w_n^2t^2}(1-t^2)dt \\ -2w_n^2\,e^{O(n^{-1})}\left[\frac{2\lambda}{15}\frac{w_n^2}{n+\frac{1}{2}}\,e^{-\frac{n-1}{n+\frac{1}{2}}\sigma w_n^2}-\frac{2\delta_n w_n^4}{35}\frac{(n-1)}{\left(n+\frac{1}{2}\right)^2}\right]=0\end{aligned}\right\} \tag{48}$$

For each value of n this equation has a root w_n, by (43) we see that the set of these roots is bounded. We consider any accumulation point ρ of this set and a subsequence $\{w_{n_i}\}$ of the sequence $\{w_n\}$ such that $\lim_{i\to\infty} w_{n_i}=\rho$. From (48) it is seen that ρ satisfies the equation

$$F(\rho)=\sqrt{\pi}\left(\frac{1}{2}-\rho^2\right)-2\rho^3\int_0^1 e^{-\rho^2t^2}(1-t^2)dt=0 \tag{49}$$

and by transforming the integral we obtain finally for ρ the equation

$$F(\rho)=\sqrt{\pi}\left(\frac{1}{2}-\rho^2\right)-\int_0^\rho(\rho^2-x^2)e^{-x^2}dx=0 \tag{50}$$

To complete the proof of lemma 3 we have only to show that the sequence $\{w_n\}$ converges. We demonstrate this by showing that $\{w_n\}$ has only one accumulation point, and this follows if we show that $F(\rho)=0$ has only one root in $\left(0,\sqrt{\frac{1}{2}}\right)$.

We see easily that $F(0)>0$ and $F\left(\sqrt{\frac{1}{2}}\right)<0$ so that there is at least one root in the interval.

From (50) we see that

$$F'(\rho)=-2\rho\left[\sqrt{\pi}+2\int_0^\rho e^{-x^2}dx\right]$$

so that $F'(\rho)<0$ for $\rho>0$. This shows that $F(\rho)$ has exactly one root.

The equation (41) has been evaluated for certain values of n, similarly the asymptotic solution ρ has been found from (50). This was done in part at the Computation Laboratory of the National Bureau of Standards, Washington, D. C., and in part at the computation department of the Institute for Numerical Analysis in Los Angeles, Calif. The results are given in the following table, which shows also the values of w_n.

n	z_n	w_n
2	.38197	.60394
3	.32114	.60079
4	.28244	.59915
5	.25505	.59814
6	.23434	.59745
7	.21798	.59696
8	.20463	.59659
9	.19346	.59630
10	.18395	.59606
15	.15122	.59536
20	.13141	.59500
$\rho=0.5939157$		

WASHINGTON, May 25, 1951

Journal of Research of the National Bureau of Standards Vol. 48, No. 2, February 1952 Research Paper 2298

Measurement of Cesium-137 and Cobalt-60 Gamma Radiation With a Pressure Ionization Chamber

G. R. Grove [1]

The characteristics of the pressure ionization chamber at the National Bureau of Standards have been studied for the gamma radiation from a cesium-137 source (0.6614 Mev) and from a cobalt-60 source (1.1715 and 1.3316 Mev). The dosage rates produced in air by these sources were measured with this chamber with an accuracy of about 2 percent. Dosage rates obtained with an extrapolation chamber and a Victoreen thimble chamber agreed with the values measured by the pressure chamber within the limits of the experimental errors.

1. Introduction

A study of the charactristics of the pressure ionization chamber at the National Bureau of Standards for X-rays up to 400 kv has been discussed by Taylor, Singer, and Charlton [1][2]. The results of their study showed that it was possible to measure accurately the dosage rates of high-voltage X-rays in accordance with the international definition of the roentgen. Taylor and Singer [2] also used this chamber to measure the ionization of the gamma radiation from a radium source and determined a value for the emission constant of radium. At that time it was not feasible to investigate completely the chamber response with quantum energies in the million-volt region. However, Taylor and Singer believed their measurements were accurate to within ± 0.4 percent.

Radioactive materials of sufficient radioactivity intensity and particularly suited for use with the pressure chamber have become available only recently. The study of the characteristics of the chamber with isotopes having gamma radiation in the energy regions of 0.6 and 1.3 Mev was undertaken to determine the reliability of the chamber for measuring the dosage rates produced by radiation energies up to 1.3 Mev. An extrapolation chamber and a Victoreen thimble chamber were also tested so that their readings could be compared with that of the pressure chamber.

Cesium-137 and cobalt-60 isotopes were obtained from the Oak Ridge National Laboratory for use with the chamber. The cesium isotope emits a gamma ray of 0.6614 Mev [3], and cobalt-60 emits 2 quanta in cascade per disintegration with energies of 1.1715 and 1.3316 Mev [4]. The activities of the cesium and cobalt samples were about 8 and 1.5 curies, respectively.

2. Apparatus and Procedure

2.1. Pressure Chamber

The diaphragm system and chamber are shown schematically in figure 1. The source is housed in an aluminum cylindrical spool, which can be moved

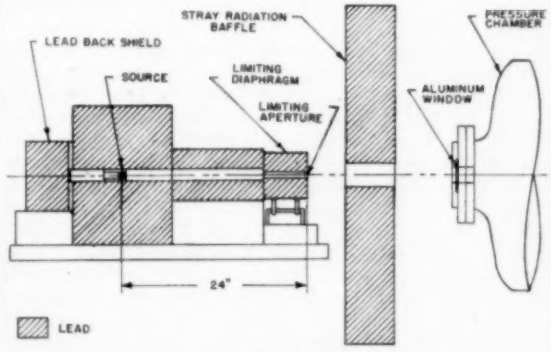

FIGURE 1. *Diaphragm system.*

axially inside a 1½-in. diameter aluminum tube to vary the distance between the diaphragm and the source. The diameter of the aluminum tube is twice as large as the diameter of the diaphragm aperture and about three times as large as the diameters of the sources used. The aluminum tubing is supported in containers that are filled with lead shot to reduce the radiation intensity in all directions except along the axis of the tube. A lead wall across the back of the tubing confines the radiation to a forward direction.

The gamma-ray beam defined by the diaphragm passes through an aluminum window 0.8 mm thick and 5.2 cm in diameter into the chamber. The cylindrical pressure chamber has an inside length of 7 ft and a diameter of 30 in. Collecting electrodes are arranged in the chamber on a pair of rails in such a way that they can be moved from the outside along the axis of the tank over a range of about 125 cm. The spacing of the electrodes also can be smoothly adjusted from 7.2 cm up to about 39 cm. These electrodes consist of aluminum plates 75 cm long and 40 cm in height. An insulated aluminum collecting plate 25.4 cm wide and 35 cm high is located at the center of the grounded electrode. The sections of the grounded electrode around the collecting plate act as guard plates. Equal potential planes are provided in the sensitive ionization volume by means 0.4-mm aluminum guard wires located in planes

[1] Present address, Mound Laboratory, Miamisberg, Ohio.
[2] Figures in brackets indicate the literature references at the end of this paper.

parallel to the electrodes. Each of these wires completely surrounds the volume defined by the plates. These guard wires, which are 2 cm apart with adjacent wires connected by 2-megohm metalized resistors, produce a uniformly graded potential between the high-voltage electrode and the grounded guard plates.

Air is pumped into the chamber through a filter and a calcium chloride drier, and in addition, several trays of drier are kept inside the pressure tank to keep the moisture content of the air at a minimum. The pressure of the gas can be read directly from a Bourdon gage with an accuracy of about 0.2 percent, and the temperature of the gas can be determined from a thermometer fastened to the electrode assembly, which can be read through a thick glass window in the rear of the tank with an accuracy of about 0.4 percent.

The potential applied to the high-voltage electrode is supplied by a group of about 500 B batteries (45 v per battery). Potentials from 500 to 20,000 v are available in steps varying from about 500 to 2,500 v. Using a 100-μa meter with appropriate multipliers, the plate potential can be measured with an accuracy of about 0.5 percent. A General Electric Co. FP–54 electrometer tube is used in a conventional detector circuit with a galvanometer of approximately 10^{-9} amp/mm sensitivity. A Rubicon potentiometer connected to the collecting plate through a S. S. White resistor supplies the necessary current through the resistor to buck out the current from the collecting plate and maintain it at ground potential. With the grid of the electrometer tube also connected to the collecting electrode, the compensation current can be adjusted to exactly neutralize the ionization current as indicated by a balance of the galvanometer.

The dosage rate supplied to the ionization chamber under saturation conditions can then be determined from a knowledge of the effective volume of air defined by the collecting plate and the diaphragm aperture along with the values of the grid resistor and the potentiometer voltage necessary to balance the detector.

If the response of the pressure chamber with plate voltage and plate separation at various pressures is internally consistent and is in agreement with the expected characteristic response of a parallel plate chamber, the values measured can be relied upon as representing the true dosage rates.

Using the cesium-137 source and a constant plate separation of 35.14 cm, the ionization current was measured as a function of the plate voltage for several different pressures ranging from 4.81 to 8.90 atm corrected to standard temperature and pressure (see fig. 2). The values of the ionization currents per unit volume of standard air obtained by the extrapolation of the saturation curves to an infinite electric field by the technique of Jaffe and Zanstra [5] and making the corrections due to air absorption, agreed within 1 percent with their average value. With a constant pressure of 8.93 atm, the ionization current response to plate voltage was measured for

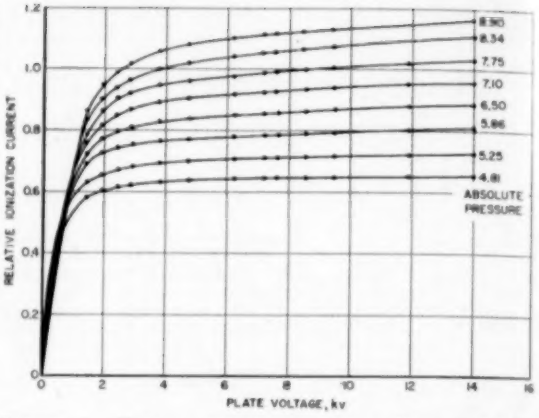

FIGURE 2. *Voltage saturation curves for different chamber pressures.*

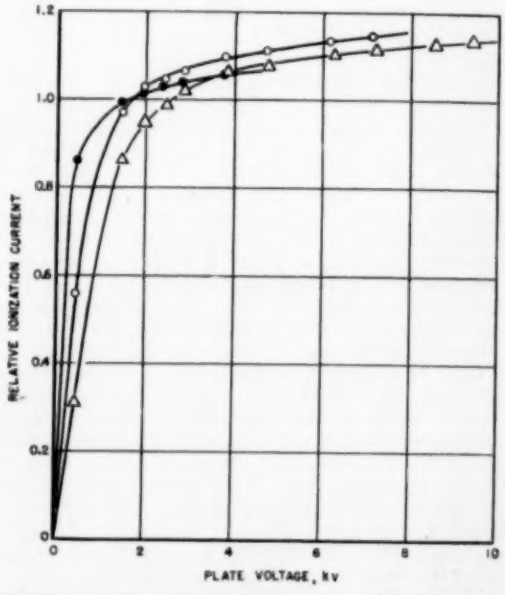

FIGURE 3. *Voltage saturation curves for different plate separations.*

●, 9.98 cm; ○, 23.96 cm; △, 35.14 cm.

different plate separations ranging from 7.18 to 37.94 cm. The saturation curves for three of the plate separations are shown in figures 3 and 4. With the smaller plate separations, the ionization current increases more rapidly in the lower plate voltage range than does the current from a larger plate separation, due to the greater field strength. When the plate separation is not large enough, as is the case of 9.98 cm at 8.93 atm (fig. 3), some electrons are collected by the electrodes before they expend all of their recoil energies by ionization. From the complete family of saturation curves at a constant pressure, a curve

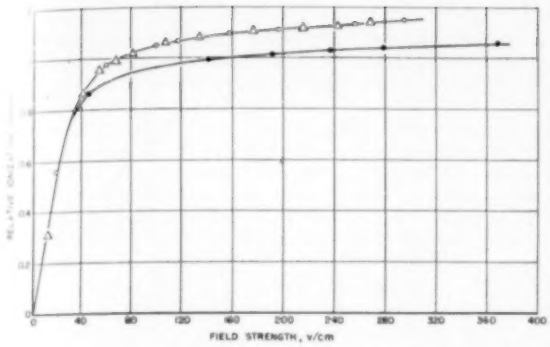

FIGURE 4. *Field saturation curves for different plate separations.* ●, 9.98 cm; ○, 23.96 cm; △, 35.14 cm.

of the ionization current versus the plate separation with constant electric field was determined. The ionization current was found to fall off for plate separations less than about 150 cm of equivalent standard air. When corrected for the diameter of the gamma-ray beam and the chamber pressure, a minimum sufficient plate separation of about 120 cm for 0.661-Mev radiation was found.

A similar procedure was followed in measuring the radiation intensity from the cobalt-60 source. For these quantum energies a minimum plate separation of about 400 cm of standard air was found necessary to obtain the maximum collecting rate of the ions with a constant electric field. This corresponds to a plate separation of about 335 cm of equivalent standard air when corrected for the beam diameter.

The dosage rates at the limiting diaphragm surface for the particular cesium and cobalt sources measured in the manner just described were 6.91 ± 0.07 and 5.10 ± 0.05 r/hr, respectively. These values need to be corrected only for the air and aluminum absorption and for the diaphragm leakage.

A test of the inverse-square response was made with the pressure chamber for the two sources. The distance, F, between the center of the source and the limiting diaphragm surface was varied, and the concomitant ionization current was measured. These data are shown in figure 5, from which it is seen that F is very nearly equal to the effective source-diaphragm distance.

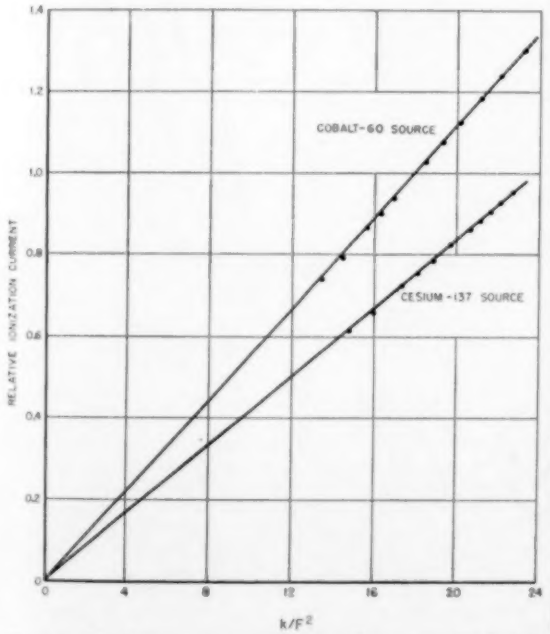

FIGURE 5. *Inverse-square plot for the source-diaphragm distance (F).*

2.2. Extrapolation Chamber

A parallel-plate extrapolation chamber [6] also was used to measure the dosage rates of the two sources. This chamber consists of two Lucite disks, the inner surfaces of which are painted with a conducting aquadag dispersion. Around each disk there is a concentric guard ring (fig. 6). The Lucite disks are supported in, but insulated from, brass rings, one of which is threaded into the other so that the plate separation can be varied. A complete revo-

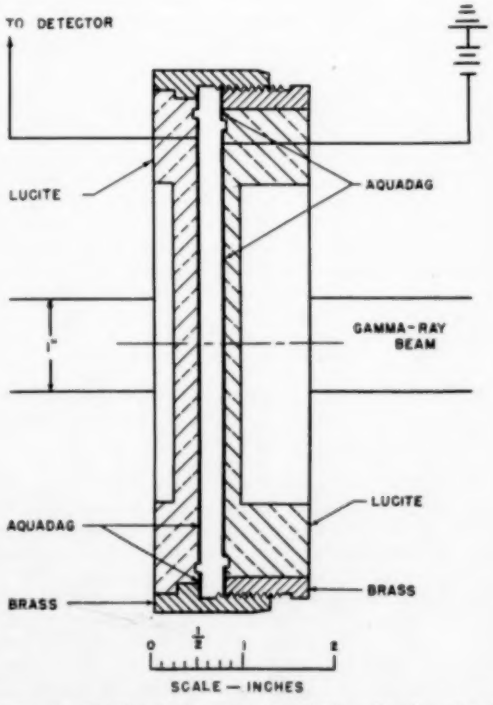

FIGURE 6. *Sectional view of extrapolation chamber showing approximate size of gamma-ray beam.*

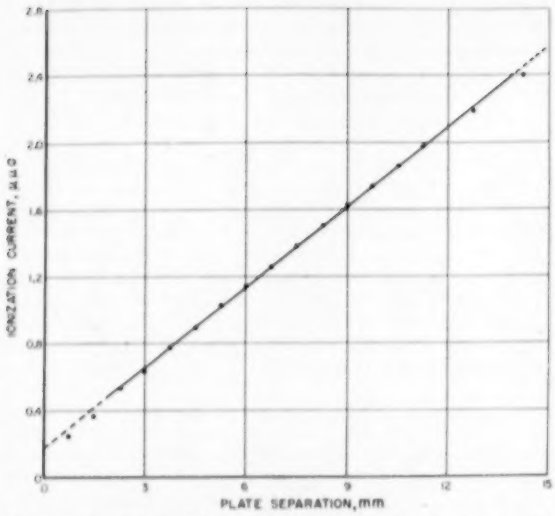

FIGURE 7. *Extrapolation chamber curve for the cesium-137 source.*

lution of one of the plates changes the plate separation by 0.150 cm, which is about 8 percent of the maximum plate separation.

By the use of this chamber with a shielded condenser-potentiometer circuit and a vibrating-reed electrometer as an indicator, the ionization current was measured as a function of the plate separation. A curve for the cesium source is shown in figure 7. From the slope of the straight line determined by the most points, the average ionization current per centimeter can be found. This quantity, together with the values of the temperature, pressure, and the area of the diaphragm aperture, determines a dosage rate at the limiting diaphragm surface. For the cesium and cobalt sources, dosage rates of 6.72 $\pm$0.13 and 5.20$\pm$0.10 r/hr, respectively, were calculated. These values need to be corrected only for air and Lucite absorption and for the diaphragm leakage.

2.3. Thimble Chamber

A 25-*r* Victoreen thimble chamber was also used to measure the dosage rates of the two isotopes. This chamber and charger unit had been previously calibrated for radium radiation, and a scale correction was determined with an accuracy of about 2 percent. With this chamber the dosage rates were measured for the two sources at a sufficient distance from the diaphragm, such that the largest dimension of the sensitive volume of the chamber was less than one-half the diameter of the umbra portion of the radiation. With the same geometry, readings were taken with different thicknesses of Lucite shells around the sensitive volume. The rate of ionization in the chamber at first increased with shell thickness due to the approach to electronic equilibrium, and then decreased with additional shell thickness due to absorption in the Lucite. By extrapolating the slope of the line due to absorption to zero shell thickness, a dosage rate was determined. This value is taken to be a good approximation to the ionization rate with electronic equilibrium and no Lucite absorption. The shell thicknesses necessary for electronic equilibrium were estimated to be about 1.0 mm for 0.661-Mev radiation and 1.3 mm for 1.3-Mev radiation. The extrapolated values were about 8.8 percent for cesium and 4.5 percent for cobalt higher than the respective values with electronic equilibrium shell thicknesses. Extrapolated values of 7.04$\pm$0.21 and 5.20$\pm$0.15 r/hr were calculated for the cesium and cobalt sources, respectively. These values are corrected for temperature and pressure and are for the same source-limiting aperture distance used with the other two chambers. These values can then be compared directly with the pressure-chamber results.

3. Corrections and Results

The sensitive volume of the pressure ionization chamber is determined by the length of the collector plates and the area of the limiting aperture. However, there is an error involved in considering only the radiation that passes through this aperture, as the thickness of the diaphragm is not small compared to its distance from the source of radiation, and thus some of the radiation will pass through the edge of the diaphragm and enter the chamber. To estimate the magnitude of this error it was necessary to determine what fraction of the total radiation producing ionization in the chamber was transmitted through the edge of the diaphragm. This was done by considering the activity of the source to be distributed uniformly over the surface of a thin disk located at the center of the source (fig. 8). If ρ and θ are the polar coordinates of a point on the surface of the disk and r is the distance from the source-diaphragm-chamber axis in a fixed direction at a distance D along the axis from the source, where D is equal to or greater than the distance d between the source and the outer diaphragm surface, then the total amount of radiation received by the ionization chamber is given by

$$2\pi \int_0^{r_{max}} \int_0^{\rho_{max}} \int_0^{2\pi} e^{-\mu\delta(r,\rho,\theta)} \rho r dr \rho d\theta,$$

where δ is the thickness of lead traversed by gamma rays emitted at ρ, θ, which pass through the point r, and μ is the linear absorption coefficient of lead for the radiation in question. The maximum value of ρ is equal to the radius of the source, and the maximum value of r is taken to be that radius at which the radiation intensity is negligible for all values of ρ and θ. The absorber thickness δ is given by

$$\delta = d - \frac{D\left\{\rho(r\cos\theta-\rho)+\sqrt{\rho^2(\rho-r\cos\theta)^2+(a^2-\rho^2)(r^2+\rho^2-2r\rho\cos\theta)}\right\}}{r^2+\rho^2-2r\rho\cos\theta}$$

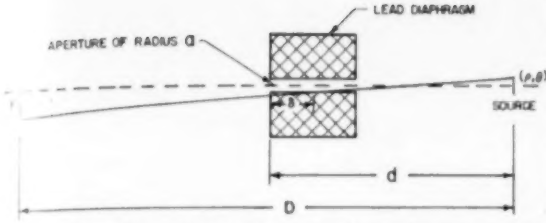

FIGURE 8. *Schematic indication of the variables required for determination of the diaphragm leakage correction.*

for all positive values of the right-hand term. When the right-hand term becomes negative, δ is equal to zero. This triple integral was evaluated by numerical integration, and the resulting intensity was compared with the intensity that was passed through the unobstructed aperture for the cesium and cobalt sources. In the case of cesium the correction was 2.40 percent, for cobalt it was 4.85 percent. These values are believed to be accurate to about 10 percent.

The resistance of the S. S. White resistor used in the grid circuit of the electrometer was measured during the course of the experiment and found to have a value of 3.003×10^9 ohms at 26° C and 3.161×10^9 ohms at 23° C. The precise temperature of the resistor during a set of measurements was not known but was taken to be the average value of the temperature of the air in the tank and room temperature. The maximum error due to this resistor is estimated to be about 1 percent.

By the application of the corrections due to air, aluminum, and Lucite absorptions [7], and that due to the diaphragm leakage, the correct dosage rates measured with the pressure and the extrapolation chambers were calculated. These values are tabulated in table 1, along with the thimble-chamber values. The cobalt source had been calibrated on June 1, 1949. The calibrated value corrected to the approximate date of this experiment was 5.05 ± 0.15 r/hr at a distance equal to the source-diaphragm distance. The errors assigned to the various values have been estimated and consist largely of the errors already discussed.

TABLE 1. *Comparative values of the dosage rates at the limiting diaphragm surface*

	Cesium-137	Cobalt-60
	r/hr	*r/hr*
Pressure chamber	7.17±0.14	5.15±0.10
Extrapolation chamber	7.03±0.21	5.17±0.15
Thimble chamber	7.04±0.21	5.20±0.15

Using the pressure chamber, the absorption coefficients for the gamma rays of cesium and cobalt were measured for lead, copper, and tin. Sets of standard absorbers ranging in thickness from 0.050 to about 3 cm were used in this determination. The values of the measured linear absorption coefficients are listed in table 2, along with the best available theoretical values [8]. The theoretical values are believed to be accurate within a few percent. The lower energy values are the most inaccurate because of the error in determining the more prominent photoelectric absorption coefficient.

TABLE 2. *Linear absorption coefficients*

	Cesium-137			Cobalt-60		
	Lead	Tin	Copper	Lead	Tin	Copper
	cm^{-1}	*cm*$^{-1}$	*cm*$^{-1}$	*cm*$^{-1}$	*cm*$^{-1}$	*cm*$^{-1}$
Measured	1.210	0.535	0.635	0.464	0.372	0.465
Calculated	1.302	.542	.644	.674	.371	.466

4. Conclusion

The response of the pressure ionization chamber for radiation energies below 1.3 Mev indicates that absolute dosage rates can be determined within a few percent in accordance with the international definition of the roentgen. The accuracy of the values obtained with this pressure chamber are limited mainly by three factors: (1) the error in the measurement of the ionization current, (2) the determination of the saturation current obtained by a Jaffe-Zanstra extrapolation, and (3) the accuracy of the determination of the area of the diaphragm aperture, with the correction factor due to leakage of radiation through the edge of the diaphragm. A consideration of these factors, together with the inherent tolerances of the chamber, led to an estimated error of 2 percent for the over-all accuracy of the results.

It appears that it is possible to get an accuracy that will allow dosage-rate measurements to be made with somewhat less than 1 percent error by minimizing the uncertainties arising from the sources listed above.

The dosage rates measured with the extrapolation and thimble chambers are in good agreement with the values determined with the pressure chamber. This is especially gratifying in the case of the thimble chamber, as it is used extensively and there has been some question regarding energy dependence for radiation in the million-electron-volt region. The Victoreen thimble chamber was not designed to measure the dose resulting from high energy radiation; however, it was found that the dose due to collimated cesium-137 and cobalt-60 gamma-rays could be determined relatively accurately by placing Lucite shells around the thimble to provide electronic equilibrium for the radiation in question.

5. References

[1] L. S. Taylor, G. Singer, and A. L. Charlton, Am. J. Roentgenol. Radium Therapy **XLIV,** No. 3 (1940).
[2] L. S. Taylor and G. Singer, Am. J. Roentgenol. Radium Therapy **XLI,** No. 2 (1939).
[3] L. M. Langer and R. D. Moffat, Phys. Rev. **78, 74** (1950).
[4] D. A. Lind, J. R. Brown, and J. W. M. DuMond, Phys. Rev. **76,** 1838 (1949).
[5] H. Zanstra, Physica **2,** 817 (1935).
[6] G. Failla, Radiology **XXIX,** 262 (1937).
[7] J. A. Victoreen, J. Applied Phys. **20,** 1141 (1949).
[8] Gladys White, Tables of X-ray attenuation coefficients with introductory notes, NBS Report 1003 (May 7, 1951).

WASHINGTON, October 12, 1951.

Journal of Research of the National Bureau of Standards Vol. 48, No. 2, February 1952 Research Paper 229

Techniques for Growing and Mounting Small Single Crystals of Refractory Compounds

Fred Ordway [1]

An apparatus is described for growing single crystals in a small droplet of melt at temperatures up to 1,600° C. The droplet, held by capillarity at the junction of a thermocouple, can be observed during the process through a binocular microscope. The heating is by means of a high-frequency current that can be separated by a filter from the thermocouple electromotive force, allowing the electromotive force to be measured continuously. The apparatus is therefore suitable also for determining melting points.

The process of mounting and grinding the single-crystal specimens for X-ray diffraction and a simple but versatile micromanipulator to facilitate these procedures are described.

1. Introduction

A necessary preliminary to single-crystal X-ray diffraction studies is the procurement of a suitable single-crystal specimen. The ideal specimen should be pure, free from flaws or twinning, and well enough developed that the crystallographic axes can be found from the orientation of edges and faces. In spite of the strictness of these requirements, usable crystals of many substances can be found in natural minerals, or in products of manufacture, because large size is not necessary. Even a crystal that is only 0.05 to 0.1 mm in least dimension can be used with ordinary X-ray cameras. Furthermore, if the external development is poor, the crystal can be oriented by X-ray patterns.

It sometimes is found, however, that all available specimens of a mineral are either too impure or too finely crystallized and that synthetic melts of the proper composition, heated in a furnace, likewise form crystals that are too small. This is the situation among the calcium silicates amd aluminates of portland cement clinker, which are being studied at the Bureau.

Previous experience in preparing X-ray specimens, from melts at low temperatures [1, 13, 18],[2] indicated that the most convenient method is manually controlled cooling of the smallest droplet that will yield a crystal large enough to be used. The small size of the droplet minimizes the number of nuclei and the accidental temperature inequalities that lead to growth of unwanted crystals. More important, the droplets can be observed by means of a stereoscopic microscope during the entire process of crystallization. Twins or other extraneous crystals can be detected as soon as they form, and melted away so that growth of the desired crystal can be recommenced immediately. A much larger body of melt, which would be necessary if the crystals were to be grown for optical or piezoelectric use, is actually an inconvenience when they need be only large enough for X-ray diffraction. To take advantage of this fact, a special apparatus was assembled for recrystallizing small samples at high temperatures under the stereoscopic microscope.

In order that the subsequent operations of mounting the specimen and grinding off excessive glass or crystalline material might also be carried out conveniently under the microscope, a micromanipulator and certain accessories were constructed. The methods described are not claimed to be unique solutions of the problem, but they are felt to be improved in certain details over the techniques seen elsewhere.

[1] Research Associate at the National Bureau of Standards, representing the Portland Cement Association.

[2] Figures in brackets indicate the literature references at the end of this paper.

2. Apparatus for Crystal Growing

2.1 Hot-Wire Apparatus

Numerous publications have described small furnaces in which a sample can be placed [7, 15, 28, 30] and electric heaters on which the sample can be mounted directly [6, 12, 17, 21] for microscopic observation. In the latter form of apparatus, elaborate insulation is not necessary to protect the microscope objectives if the hot zone is made small enough. This fact makes possible simpler construction and less restriction on the angle from which the sample can be viewed. An apparatus of the directly heated type was therefore constructed. The heater consisted simply of a 5-cm length of 0.3-mm platinum wire bent to a sharp V and supported at the ends by suitable binding posts. The wire was heated by current from a 6.3-v transformer, the primary voltage of which was controlled by a continuously variable autotransformer or a foot-operated rheostat intended for use with sewing machines. The droplet of melt, held by capillarity at the point of the V, was observed through a stereoscopic microscope. A variable-density filter, originally intended for the eyepieces of a pair of binoculars, served to protect the observer from excessive glare.

This hot-wire apparatus, when protected from drafts, was convenient for controlled crystallization at temperatures up to 1,500° C. It provided no indication of the temperature, however, except the reading on an ammeter or voltmeter in the circuit and the behavior of the sample itself. The autotransformer settings or meter readings corresponding

the melting range could be found by experiment, when the temperature was high these settings gradually changed as the platinum wire volatilized. Furthermore, it was impossible without an independent measure of temperature to detect small fluctuations due to air currents or changes in line voltage.

2.2. Hot-Thermocouple Apparatus

a. Construction

In considering the addition of a device for measuring the sample temperature, a thermocouple was preferred over a resistance thermometer or radiation pyrometer because reasonable accuracy could be obtained without special calibration of the sensitive element, and suitable measuring instruments were already available.

Attempts to measure the sample temperature with a thermocouple were discouraging because it conducted heat from the sample. Even when made from wire only 0.08 mm in diameter it greatly lowered the temperature. The possibility of supplying heat to the thermocouple from a separate source in order to counteract conduction from the sample was considered. The more suitable procedure finally discovered, however, was to use high-frequency alternating current for the heating, so that the direct-current electromotive force produced by the thermocouple could be separated out by a filter and measured independently. If this is done, obviously the hot-wire arrangement need not be a four-terminal device. The thermocouple itself can also serve as a heating element and support for the sample.

The essential parts that were assembled for the hot-thermocouple apparatus are indicated in figure 1. The heater current is obtained from a 50-w audio amplifier of the type used in public address systems. The amplifier is fed by a Hewlett-Packard model 200BR audio oscillator through a 10-turn helical potentiometer, which is used as a voltage divider for fine control. This equipment, having been chosen primarily because it was readily available, is much more elaborate than necessary. As the output need be only 25 to 30 w and freedom from harmonics is not important, a power supply built specially for the purpose could be simple and inexpensive.

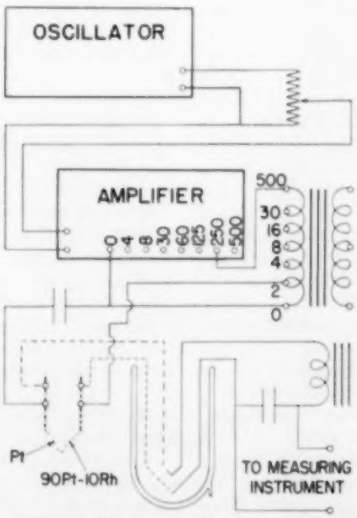

FIGURE 1. *Circuit diagram for hot-thermocouple apparatus.*

The power for heating the thermocouple is fed from the output terminals of the amplifier through an additional 50-w audio output transformer, whose secondary is used alone as an autotransformer. To prevent the transformer from acting as a short circuit for the thermocouple electromotive force, a blocking condenser must be inserted in series with the winding. The blocking condenser in use consists of three standard 10-μf oil-filled units connected in parallel.

The blocking condenser adds a considerable reactive component to the impedance of the amplifier load. For most efficient power transfer it is desirable to balance the capacitance by means of an equal inductive reactance in series with the load or reflected through the output transformer; that is, the load should be a series resonant circuit at the frequency used. In addition, the output transformer should of course have the proper turns ratio for the usual match of resistive impedances. These adjustments have not been accurately made in the present apparatus because it is found that sufficient heating can be obtained by the amplifier and transformer impedances shown in figure 1, with an oscillator frequency of about 4.7 kc. The resistance of the thermocouple is 0.1 to 0.4 ohm, depending on its temperature, and the reactance of the condenser is 1.1 ohms at the operating frequency. More careful matching to these values would be necessary if an amplifier of lower power were used. If a low-frequency power supply such as a 400-cycle rotary converter or a 60-cycle transformer were to be used, the impedance match would be extremely important because of the high reactance of the condenser at low frequencies. The use of 60-cycle power would probably be rendered impractical by the large size of the components required.

The thermocouple itself is mounted on an interchangeable four-prong plug-in assembly. The four-prong plug is made by cementing together two standard double banana plugs which fit into a pair of double banana jacks fastened permanently in position under the stereoscopic microscope, as shown in figure 2. In order to replace the thermocouple with a clean one for preparing a new melt, it is necessary merely to plug in a new assembly.

The portion of the thermocouple that is actually heated, at the junction, consists of 2-cm lengths of 0.25-mm platinum and platinum–10-percent rhodium wire. To reduce heating of the connectors these short lengths of fine wire are welded to 0.6-mm extension leads of the same metals, which in turn make contact with the banana plugs. Several of the interchangeable assemblies can be made up in advance by welding new lengths of fine thermo-

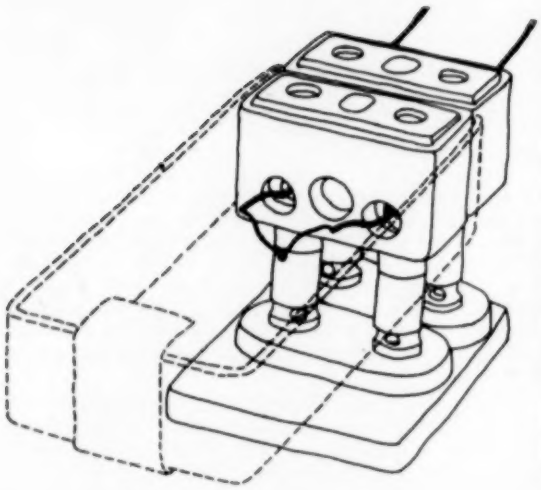

FIGURE 2. *Thermocouple assembly.*

couple wire onto the heavier leads. The leads need not be replaced, as they are not contaminated by contact with the melt; the amount of platinum used per sample is therefore only about 0.06 g.

The thermocouple is protected from drafts by two sheets of mica supported by a brass frame, which clips onto the Bakelite body of one of the double banana plugs, as shown by dotted lines in figure 2. Without the mica cover no special protection for the microscope is necessary if the vertical convection current from the hot wire is avoided, but with it even this danger to the objectives is eliminated.

The heater current reaches the thermocouple through the nearer pair of banana jacks shown in figure 2. The jacks farther from the thermocouple, which are less affected by the heat, can be used for the measuring circuit if convenient interchange of thermocouple assemblies is desired. For the most careful work two extension leads made of the thermocouple metals are connected directly to the thermocouple leads by means of the clamping screws in the second pair of banana plugs. This arrangement, which eliminates contact potentials between the leads and the banana plugs, is the one indicated in the figure.

The measuring circuit is conventional except for the inclusion of the low-pass filter (fig. 1) to protect the measuring instrument from the a-c potential across the thermocouple, which may be as high as 3 v. The filter must not be interposed between the thermocouple and the cold junction, of course, if the extension leads are to serve their purpose. In order that a millivoltmeter pyrometer that requires a low d-c resistance may be used for temperature measurements, the primary of a 100-w radio power transformer, having an inductance of 0.6 h and a resistance of 13 ohms, is employed as the filter choke. The filter condenser consists of two 2-μf oil-filled units in parallel.

All condensers in the heating and measuring circuits must be of the nonelectrolytic type with essentially zero conductance in either direction. The slight rectifying action of an electrolytic condenser could lead to a comparatively large error in the measurement of temperature.

b. Calibration

The convenience of the hot-thermocouple apparatus for its original purpose of growing small single crystals was immediately obvious when it was put into operation. In one of the first experiments a lime-alumina melt in the primary phase region for tricalcium aluminate produced a crystal of that compound better in size and perfection than had been found possible with any other method. The main value of the temperature measurement in growing crystals is for precise control during one experiment lasting up to 2 hr. Reproducibility of readings with duplicate samples on the same thermocouple or with duplicate thermocouples is less important. In view of the other possible uses for the apparatus, however, the absolute accuracy of the temperature measurements was tested as well as the precision of control.

For these tests the oscillator and amplifier were powered by a Sola constant-voltage transformer. A potentiometer whose smallest scale division is 0.001 mv and a Leeds & Northrup Speedomax recorder whose smallest scale division is 0.05 mv were connected so that either might be used at will. The recorder, which prints one point in 3 sec, follows more rapid fluctuations than the galvanometer used with the potentiometer. When the apparatus was carefully protected from drafts, with the thermocouple at about 1,000° C, the minimum fluctuation in the recorded electromotive force over 10-min periods was ± 0.02 mv. As the average potentiometer readings agreed with those of the recorder to within less than 0.02 mv at this and several lower temperatures, the thermocouple electromotive forces were read thereafter from the recorder chart.

Three of the interchangeable thermocouple assemblies were made from single lengths of wire 0.25 mm in diameter. These lengths were taken from 100-foot rolls that had been purchased by the Chemistry Division of the Bureau under strict specifications for homogeneity. Calibration certificates were available for couples made from each end of the original lengths of wire; their agreement within the limits of error of the calibration indicated the corrections to be valid for all couples made from this wire. The corrections amounted at most to +8.5 deg, at an electromotive force of 15 mv, over the temperatures read from a standard reference table of thermocouple potentials [23].

The three thermocouples were employed, with a correction chart, to determine the melting points of five inorganic compounds. The first two couples were used with barium disilicate and the third with potassium sulfate, sodium sulfate, potassium chloride, and sodium chloride, in that order. The barium

silicate was a sample synthesized as a melting-point standard by Eubank [8], and the other salts were of reagent grade. It was found most convenient in preparing for each determination to grind the substance in an agate mortar, moisten the powder slightly with reagent grade xylene, and transfer a small amount of the paste to the thermocouple junction with a microspatula. All the substances that have been tested adhere satisfactorily when treated in this way except potassium sulfate, which decrepitates at the β-α transition point.

The melting points were determined with the apparatus in a closed room but without the use of any shield against drafts except the two sheets of mica in their holder. Under these conditions the recorder showed random fluctuations up to ± 0.05 mv, or about 4 deg at 1,420° C. The results of the experiments, listed in table 1, indicate a maximum error of ± 5 deg C.

TABLE 1. *Melting-point determinations with the hot-thermocouple apparatus*

Compound	Melting point found	Melting point given in the literature [24]
	°C	°C
KCl	768	770
NaCl	795	800.4
Na_2SO_4	887	884
K_2SO_4	1,064	1,069.1
$BaO.2SiO_2$	1,423	1,418

The value listed for barium disilicate is an average of three determinations—two made with different thermocouples on samples with no preliminary heat treatment, and the third after holding the sample for 4 hr at 1,420° C. All three estimates agreed within 0.02 mv, or less than 2 deg.

c. Other Applications

The performance of the apparatus in these experiments indicated it to be satisfactory in the present form for determining melting points over the working range of the platinum and platinum-rhodium thermocouple wire, with an accuracy of ± 5 deg even at 1,420° C. If greater precision is desired, the high-frequency power supply can be equipped with automatic regulation to decrease the amplitude of the random fluctuations in temperature. Any of the well-known methods of regulating heater voltage or current, or the resistance of the heating element [20], is obviously applicable; perhaps the most desirable regulator would be one sensitive to the thermocouple electromotive force, using the methods of converting the direct to alternating current, and of amplifying minute a-c voltages, which are well established in industrial controller designs.

In considering the use of the hot-thermocouple apparatus for precise determination of a melting point or other transition temperature, several factors must be taken into account. Volatility of the substance renders the method useless if it causes the sample to disappear or to change significantly in composition during an experiment. Sodium chloride, for instance, vaporizes rapidly enough to necessitate some haste in the melting-point determination. Corrosion of the thermocouple by the molten sample also renders the method useless if the composition of the sample changes significantly. The effect of slight contamination on the electromotive force of the thermocouple is probably less important as there is little temperature gradient within the contaminated portion of the wire near the junction.

The thermocouple electromotive force is an accurate measure of the temperature at the center of the junction, but a comparatively large temperature gradient exists between the surface of the wire and the outer surface of the sample. This gradient is actually a help in growing single crystals, and causes no error in the determination of true melting points if the behavior of the material nearest the junction is observed. It may lead to segregation, however, if the solid and liquid have different compositions. For this reason the apparatus probably should be used in the investigation of multicomponent phase diagrams only for a rapid survey preliminary to detailed investigations by other methods. Bending the wire in such a way as to form a radiation shield [19] might well eliminate the temperature gradient within the sample, although probably at the cost of visibility.

A temperature gradient is to be expected from the center of the thermocouple wire to its surface. The maximum temperature difference within the wire may be calculated approximately by the formula [25]

$$\Delta T = qr^2/4k,$$

where q is the rate of heat generation per unit volume of the wire, r is the radius of the wire, and k is its heat conductivity. The least favorable values of these quantities in the present apparatus may be taken as $q = 3.9 \times 10^3$ cal/sec cm^3 (corresponding to the 8 w dissipated per centimeter of wire at 1,450° C), $r = 0.0125$ cm, and $k = 0.07$ cal/sec cm deg (reported by Barratt [3] for platinum–10-percent rhodium at room temperature). The temperature difference calculated from these values is 2.2 deg C. As this is less than the experimental error, the temperature gradient within the wire has been ignored in practice. The skin effect of alternating current tends to reduce the temperature gradient, but that effect is negligible at the frequency used in the present apparatus.

The principle used in this apparatus, heating a thermocouple by an alternating current that is filtered out so that the thermocouple electromotive force can be measured alone, has been described in the literature [5, 14] as long ago as 1919. The idea still seems to offer possibilities in untried applications, such as the measurement of surface temperatures [22], optical pyrometry [9], and elimination of errors caused by the heat conductivity of thermocouples [29].

3. Mounting Specimens

When a single crystal has been grown in a droplet of melt, the preparation is cooled to room temperature as rapidly as possible in order to minimize fur-

ther crystallization. The bead of glass is readily broken off the wire by bending the latter away from the bead with fine pliers. Then it is necessary to mount the specimen in proper orientation on the usual glass fiber attached to a brass pin that fits the goniometer head [32] of the X-ray apparatus.

Orienting of the crystal is facilitated by the visibility of faces and edges during crystallization. These often become more difficult to see after the specimen cools, but, if necessary, the interfering effect of refraction at the surface of the glass surrounding the crystal can be overcome by immersion in a suitable index liquid.

Before the crystal is mounted, the glass fiber is attached to the goniometer pin. The adhesive best suited for this purpose and for mounting crystals stable at fairly high temperatures is jewelers' shellac, which wets the surfaces readily when melted and hardens immediately on cooling. The fiber is cemented in place with the aid of a hand-held hot wire [26, p. 198].

It is desirable that the glass fiber be capable of some tilting relative to the goniometer pin in case the accidental misorientation of the crystal is not fully correctible by means of the movable arcs on the goniometer head. Frequently this has been done by softening the cement holding the fiber on the pin; another method has been the use of a goniometer pin with a thin, flexible section near the end [18, 27]. The method used is to solder on the goniometer pin a 15-mm length of 0.4-mm (0.016-in.) copper wire, as shown in figure 3. The wire is amply rigid to support the fiber and specimen, yet it can easily be bent with fine pliers or tweezers when necessary. The advantage of this arrangement is that tilting of the crystal can be done by displacing the lower end of the fiber, which is attached to the wire. Thus the crystal is not decentered while being tilted, as it is when the goniometer pin itself bends.

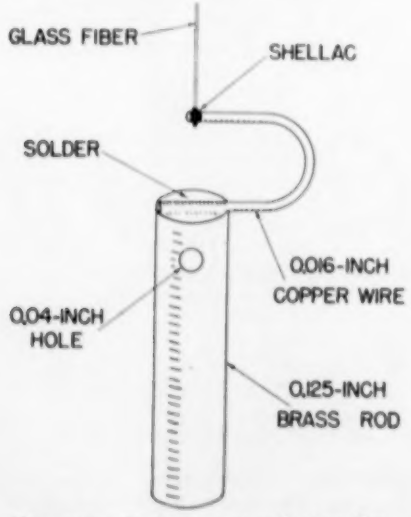

FIGURE 3. *Goniometer pin with glass fiber.*

When the fiber has been attached to the goniometer pin, a small amount of shellac is melted onto the upper end. The next step is then to hold this end of the fiber against the specimen in the proper orientation, heat until the shellac adheres, and allow to cool in the same position. The heating is done with a tiny hot-wire tool made from a 5-mm length of 0.015-mm platinum wire, which is connected to the 6.3-v transformer in series with a 22-ohm resistor.

4. Micromanipulator

To facilitate the procedure of mounting the specimen, some form of micromanipulator is desirable. Most of those described in the literature are either designed for use with a mono-objective microscope at high magnifications [2; 4; 10; 16, p. 62–72], and therefore delicate and limited in range, or adapted to coarser work but difficult to construct [11; 26, p. 202–4]. An attempt was therefore made to design an apparatus that would serve the purpose and yet require as little precise machining as possible in construction. The apparatus was intended for use with a stereoscopic microscope on a vertical-pillar stand with horizontal extension arm and weighted base. It will be described in detail in the hope that the description may be useful to others and stimulate improvements in the kinematic design [26, 31] of a simple manipulator.

The complete apparatus is shown in figure 4. It consists of a base plate, A; two manipulators, B; and a three-legged platform, C. The base plate and the other flat pieces are cut from a ½-inch steel plate, so that their weight insures stability.

Each of the manipulators, B, is in principle simply an ordinary laboratory tripod stand whose base is a 45° right triangle with leveling screws at the vertices. The ends of these adjusting screws are positioned by six small blocks bearing 90° V-grooves, mounted on the base plate. In each set of three blocks, two are turned so that their grooves are parallel, and the third has its groove perpendicular to the direction of the other two. Each manipulator is thereby constrained to a single definite position at all times.

Platform C is an equilateral triangle. When set in place on the base plate its legs are positioned by the three larger V-blocks so that the center of the triangle is almost directly above one of the adjusting screws of each manipulator. Objects can be placed on the platform and operated upon with microtools attached to the jointed column that is mounted on each of the manipulators.

The tools are usually moved by means of the adjusting screws at the sides and at the rear. Each screw causes its manipulator base to tilt about a line between the other two screws. The geometry of the arrangement is such that the tilts produced by the screws at the side and at the rear correspond to horizontal motions of the microtools suspended above the center of the triangular platform. As the screw below the center of the platform is at the 90° vertex of each manipulator base, the horizontal motions are at right angles. The screw at the rear moves

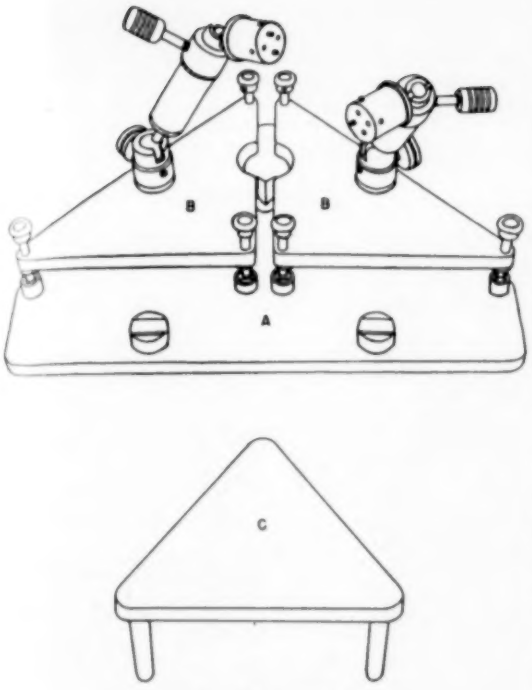

FIGURE 4. *Micromanipulator.*
A, Base plate; B, manipulator; C, platform.

the tool back and forth, and the one at the side moves it from side to side.

As the height of the tool above the base plate is approximately equal to each leg of the 45° right triangle, the motion of the tool is equal in sensitivity and maximum travel to the motion of the corresponding corner of the manipulator base along the adjusting screw. The present model has a sensitivity of 0.08 cm per turn and a maximum travel of about 2.5 cm.

Although the two horizontal motions are independent, a vertical movement requires simultaneous turning of all three adjusting screws. Therefore, it is ordinarily most convenient to adjust the height beforehand and use only the horizontal motions if possible.

The column for supporting the tools, which is mounted on each manipulator, has two ball-and-socket joints (tripod tilt tops, which may be obtained from most photographic supply houses). The two joints are connected by a length of 1-in. round aluminum rod, suitably threaded. At the upper end is a shorter length of the aluminum rod, drilled and equipped with setscrews to hold the ⅛-in. goniometer pins. All the tools used with the micromanipulator are mounted on ⅛-in. brass rods so that they can be attached in the same way.

The use of the ball-and-socket joints has the great advantage that tightening them does not displace the object being adjusted, and the chance of accidental damage to delicate specimens is minimized. As they are loosened during adjustment, there is no tendency to spring back out of position as with friction joints. It is desirable that all four ball joints be capable of turning to any direction within a complete hemisphere. Two of those in the present model are not, and the resulting limitation in flexibility is occasionally inconvenient, even though they are used in the lower positions.

The adjusting screws, which are ¼ in. in diameter and have 32 threads per inch, are made with a conical recess in the lower end. This 90° cone rests on a steel ball ¼ in. in diameter, which is positioned by the V-block. The combination provides a kinematic design in which the smooth, hard surface of the steel ball minimizes chattering when the screws are turned. Furthermore, if this surface becomes worn or damaged the steel ball can be replaced very cheaply. A short piece of flexible plastic tubing is slipped over each V-block to prevent the steel balls from rolling off when one of the manipulators is lifted from the base plate.

The adjusting screws were cut on a lathe to insure that the screw threads would be coaxial with the conical surface; this was the only precise machining used in constructing the assembly. The corresponding threads in the manipulator bases were made by hand with a standard tap.

The screw arrangement has disadvantages, being kinematically over-specified and therefore tending to allow lateral movement unless made to a very fine tolerance. This tendency was overcome to a considerable extent by preloading each screw with the simple device shown in figure 5, consisting of a leaf of 1/16-in. phosphor bronze with two tapped holes and a pointed setscrew. The tool can still be moved laterally by almost 0.001 in. if a horizontal force is deliberately exerted on one of the adjusting knobs, but the force required is great enough so that in practice no accidental motion occurs. Pos-

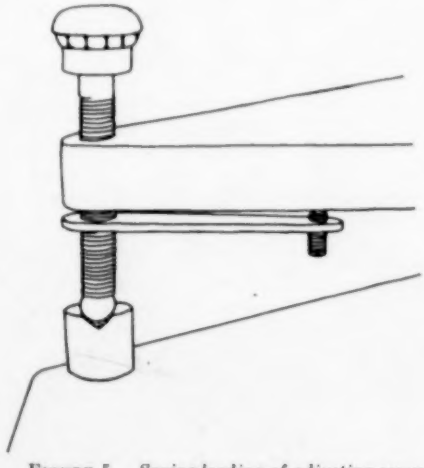

FIGURE 5. *Spring loading of adjusting screw.*

sibly other methods can be devised to eliminate the lateral movement entirely.

The manipulator has been used for almost a year as a permanent adjunct to the stereoscopic microscope. It has proved versatile and convenient for magnifications from ×5.4 to ×90. On one occasion, a standard petrographic microscope was set on the triangular table, and the manipulator was used to operate an implement on its stage at about ×150. Even under these conditions the precision and freedom from vibration were satisfactory, although the increased height made the arrangement cumbersome.

The present model is less sensitive to vibration than the manipulator described by Strong [26, p. 202–4], probably because of the rigidity of the 1-in. aluminum rod used for the jointed column. Furthermore, the strength of the ball-and-socket joint when clamped makes it capable of supporting much heavier objects; even a small electric-motor grinder weighing more than 200 g has been used as an implement.

It is believed that the simplicity, ruggedness, and cheapness of this apparatus make it valuable in many uses for which more elaborate equipment is not absolutely necessary, in addition to the mounting of crystals.

5. Grinding

The specimen containing a desired crystal may also contain extra crystals or excessive amounts of glass. If so, it is necessary to remove the undesirable portions of the specimen and leave the crystal undamaged. This can best be done by mounting the specimen as usual, in such a position that the undesirable portion is exposed, and then carefully removing that portion. A similar procedure of mounting and then removing the excess is necessary if cylindrical specimens are desired to simplify absorption corrections.

The slow removal of a part of the specimen is often done by hand with a solvent applied on a camel's-hair brush. In some cases no suitable solvent can be found, and mechanical removal becomes necessary. A small grinder to be used for this purpose on the micromanipulator was made from a miniature 27.5-v Alnico field motor, by fitting a simple adapter on the shaft so that standard abrasive tips with ⅛-in. shanks could be used. The motor operates satisfactorily on 120-v 60-cycle alternating current, with a 25-watt bulb and selenium rectifier in series and a 1,000-microfarad electrolytic condenser in parallel. The best grinding surface was obtained by stirring a pinch of 5-μ diamond powder into a few drops of thinned lacquer and coating a ⅛-in. polished steel shaft with the mixture. A surface thus prepared was found to cut many times faster than any other that has been tried. In addition, its relative smoothness caused much less vibration of the specimen than had previously been considered unavoidable, reducing considerably the chance of accidental breakage or loss. The use of diamond powder in other types of crystal-grinding apparatus, such as that of Sturdivant [27] for automatically producing a cylinder, would probably have similar advantages; its added convenience makes the effort of procurement worthwhile, and its cost per specimen is slight.

6. References

[1] S. C. Abrahams, R. L. Collin, W. N. Lipscomb, and T. B. Reed, Rev. Sci. Instr. **21,** 396 (1950).
[2] R. Barer and A. E. Saunders-Singer, Quart. J. Microscopical Sci. **89,** 439 (1948).
[3] T. Barratt and H. R. Nettleton, Int. Crit. Tables **5,** 226 (1929).
[4] M. Cailloux, Rev. Can. Biol. **2,** 528 (1943).
[5] L. W. Chubb and R. De S. Brown, U. S. Patent 1,291,409 (1919).
[6] A. L. Day and E. S. Shepherd, Am. J. Sci. **22,** 265–302 (1906).
[7] C. Doelter, Z. Elektrochem. **12,** 617–21 (1906).
[8] W. R. Eubank and R. H. Bogue, J. Research NBS **40,** 225 (1948) RP1867.
[9] C. O. Fairchild and W. H. Hoover, J. Opt. Soc. Am. **7,** 543 (1923).
[10] P. de Fonbrune, Recherches et Inventions **16** (No. 252), 433 (1935).
[11] Rack-and-pinion micromanipulator, Pamphlet number G1/21 (Gamma Instrument Co., Inc., 263 Great Neck Road, Great Neck, L. I., N. Y., June 1948).
[12] J. Joly, Proc. Roy. Irish Acad. **2,** 38 (1891).
[13] H. S. Kaufman and I. Fankuchen, Rev. Sci. Instr. **20,** 733 (1949).
[14] J. W. L. Köhler, Philips Tech. Rev. **3,** 165 (1938).
[15] A. J. Lambeth, Australian J. Sci. **7,** 118 (1945).
[16] C. E. McClung, ed., Handbook of microscopical technique, 2d ed., (Paul B. Hoeber, Inc., New York, N. Y., 1937).
[17] C. Milton and H. C. Spicer, Am. Mineralogist **31,** 401 (1946).
[18] F. Ordway, PhD Thesis, California Institute of Technology (1949).
[19] M. v. Pirani, Physik. Z. **13,** 753 (1912).
[20] H. S. Roberts, Automatic control of laboratory furnaces by the Wheatstone bridge method, p. 604–10 of Temperature, its measurement and control (Reinhold Pub. Co., Inc., New York, N. Y., 1941).
[21] H. S. Roberts and G. W. Morey, Rev. Sci. Instr. **1,** 576 (1930).
[22] N. Sasaki, Rev. Sci. Instr. **21,** 1 (1950).
[23] H. Shenker, J. I. Lauritzen, Jr., and R. J. Corruccini, Reference Tables for Thermocouples, NBS circular 508 (1951).
[24] A. Silverman, H. Insley, G. W. Morey, and F. D. Rossini, Data on chemicals for ceramic use, Bul. Nat. Research Council No. 118 (1949).
[25] H. Streintz, Poggendorf's Ann. Phys. Chem. **236** (Series 2, Vol. **160**), 409 (1877).
[26] J. Strong, Procedures in experimental physics (Prentice-Hall, New York, N. Y., 1945).
[27] J. H. Sturdivant, California Institute of Technology (unpublished work).
[28] T. Swinden, T. W. Howie, and J. H. Chesters, Trans. Brit. Ceram. Soc. **38,** 245 (1939).
[29] M. Tanaka and K. Okada, Electrotech. J. **1,** 42 (1937).
[30] J. White, D. D. Howat, and R. Hay, J. Roy. Tech. Coll., Glasgow **3,** 231 (1934).
[31] T. N. Whitehead, The design and use of instruments and accurate mechanisms (Macmillan & Co. Inc., New York, N. Y., 1934).
[32] R. W. G. Wyckoff, The structure of crystals, p. 108 (The Chemical Catalog Co., New York, N. Y., 1931).

WASHINGTON, February 15, 1951

Journal of Research of the National Bureau of Standards Vol. 48, No. 2, February 1952 Research Paper 2300

Crystal Forms of Chromium Orthophosphate

Barbara M. Sullivan and Howard F. McMurdie

There is no evidence for the existence of any crystalline hydrate of chromium orthophosphate other than the hexahydrate. This breaks down near 130°C to an amorphous material. If the unstrained and coarse hexahydrate is heated, it recrystallizes at 1,014° C to an unstable, fine-grained compound ($\beta CrPO^4$). If the original hydrate is ground and thus strained, it will form a stable compound ($\alpha CrPO^4$) at 972° C. X-ray diffraction powder patterns are given for the three crystalline forms, and the general relation of chromium orthophosphate hexahydrate to other hydrates is discussed.

1. Introduction

A study of the forms of chromium orthophosphate was suggested by the National Institutes of Health. They needed a radioactive material that was insoluble and nontoxic. Chromium orthophosphate with radioactive phosphorus had been used in similar work [1].[1] They found, however, that it was difficult to prepare a uniform anhydrous compound by heating the hexahydrate, inasmuch as the temperature of dehydration was very critical.

There are only a few previous studies of the compound reported in the literature. Joseph and Rae [2] in 1917 reported a violet hexahydrate, as well as a crystalline tetra- and dihydrate. In 1948 Clark and Tai [3] made X-ray powder patterns of the hexa- and tetrahydrates and found them identical, whereas patterns of the dihydrate and anhydrous forms indicated amorphous material.

2. Materials and Equipment

The samples studied here were given to the Bureau by the National Institutes of Health. They were prepared as hexahydrate ($CrPO_4.6H_2O$), using a modification of the method of Joseph and Rae [2] described in detail by Ness, Smith, and Evans [4]. Differential thermal-analysis studies were made by standard methods [5], using a program controller, a direct-current amplifier, and automatic recording. X-ray patterns were made on a North American Philips High-Angle Geiger Counter Spectrometer, using the techniques described by Swanson and Tatge [6] to obtain accurate spacings and intensities. In some cases patterns were made with the sample at high temperatures in the furnace described by Van Valkenburg and McMurdie [7]. CuKα radiation was used in all cases (λ=1.5405).

3. Chromium Orthophosphate Hexahydrate

The hexahydrate, as shown in figure 1, is violet in color, prismatic and twinned in habit, biaxial negative with α=1.568, β=1.591, γ=1.599, $2V$=13°. The d spacings and relative intensities of the powder pattern are shown in table 1.

[1] Figures in brackets indicate the literature references at the end of this paper.

FIGURE 1. *Chromium orthophosphate hexahydrate; ×150.*

TABLE 1. *d-Spacings and relative intensities of chromium orthophosphate hexahydrate*

d	I	d	I	d	I	d	I
5.76	6	3.46	30	2.57	12	1.924	12
5.63	28	3.33	7	2.48	9	1.903	4
5.35	11	3.29	6	2.47	8	1.874	6
5.27	24	3.05	8	2.43	4	1.808	8
4.87	40	2.95	9	2.38	4	1.701	10
4.78	22	2.87	8	2.24	10	1.677	4
4.23	100	2.82	24	2.22	7	1.527	2
4.07	26	2.80	22	2.18	7	1.488	3
3.85	42	2.79	21	2.12	4	1.450	3
3.75	8	2.69	10	2.04	3		

The chromium orthophosphate hexahydrate, when heated, begins to lose water at about 100° C and loses approximately 95 percent of the total between 100° and 400° C. It is not completely dehydrated until about 800° C. The details of the losses have been discussed by Ness, Smith, and Evans [4].

They showed that while most of the loss is near 130° C, the vapor-pressure curve indicates no sharp breaks, and there is considerable loss, even up to 800° C. With the initial loss of water, the material changes first to a bright-green color and then becomes dark brown. The X-ray powder pattern of material heated up to 130° C becomes gradually weaker but is otherwise unchanged. Above 130° C the pattern indicates amorphous material. No evidence was found here for the existence of the crystalline tetrahydrate reported by others [2, 3]. It was reported as being produced by boiling the hexhydrate in H_2O for half an hour. Material treated in this manner was bright green and showed a weak X-ray pattern of the hexahydrate. Under the microscope it appeared as a mixture of the crystalline hexahydrate and amorphous material. Weight-loss determinations of the boiled material indicated the loss of approximately 1 molecule of water.

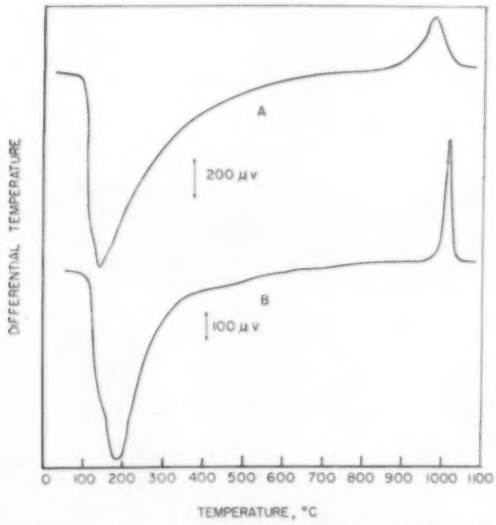

FIGURE 2. *Differential thermal analysis curves of* $CrPO_4.6H_2O$ *heated at 12½°/minute.*

A, Sample heated after grinding. $\alpha CrPO_4$ forms at 972° C. B, Sample heated unground. $\beta CrPO_4$ forms at 1,014° C.

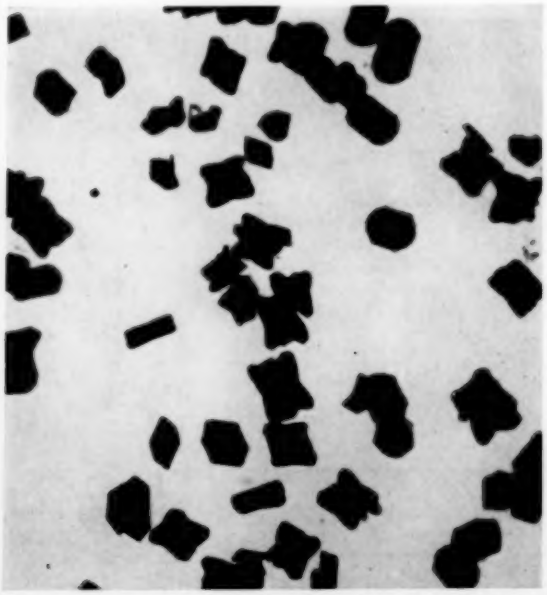

FIGURE 3. *Amorphous material obtained by heating chromium orthophosphate hexahydrate at 600° C for 66½ hours;* ×150.

The differential thermal analysis patterns of chromium orthophosphate hexahydrate, both ground and unground, heated at 12½ deg/min, are given in figure 2. The large endothermic break near 130° C is caused by the loss of water and the breakdown of the crystal structure. Above that temperature the material appears dark brown and almost opaque in the microscope, and the X-ray diffraction pattern indicates that it is amorphous. Figure 3 shows a sample that has been held at 600° C for 66½ hours. It may be noted that the external shape of the original hexahydrate is retained. This is typical of material heated in this temperature range.

4. Anhydrous Chromium Orthophosphate

The exothermic breaks on the differential thermal-analysis curves (fig. 2) near 1,000° C indicate the crystallization of anhydrous chromium orthophosphate. Two different crystal forms exist, one of which is stable. The stable high-temperature form is designated α, and the lower, unstable form, β. The β form is produced when unground material is heated and its formation produces the sharp break at 1,014° C. At higher temperatures this form gradually changes to α chromium orthophosphate. Although the X-ray pattern does not show the α form until it has been heated to 1,400° C, microscopic examination indicates its formation in small amounts as low as 1,200° C. Fairly pure β chromium orthophosphate can be formed when the unground hexahydrate is heated a short time between 1,000° and 1,100° C, but prolonged heating near 1,100° C results in the formation of a noticeable amount of the α form. When the hexahydrate is ground before heating, the α form crystallizes with no intermediate step. At a heating rate of 12½ deg/min this takes place with an exothermic break at 972° C. In the high-temperature X-ray furnace [7] only the α form was found, as it was necessary to grind the sample to hold it in position.

Tables 2 and 3 list the d spacings and relative intensities of the two anhydrous forms. A typical example of the β form is shown in figure 4. The very fine highly birefringent particles show no extinction positions and have an average index of 1.908. The α form (fig. 5) is strongly pleochroic, changing from bright green to deep blue. It is biaxial positive with a very large $2V$, and with α=1.761 (blue), and γ=1.844 (green). The presence of small amounts

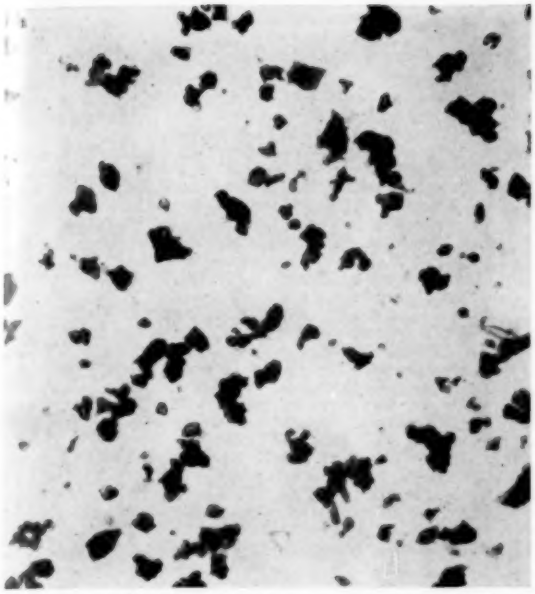

FIGURE 4. *Anhydrous chromium orthophosphate (β form) obtained by heating the unground hexahydrate to 1,100° C in the differential thermal-analysis furnace; ×150.*

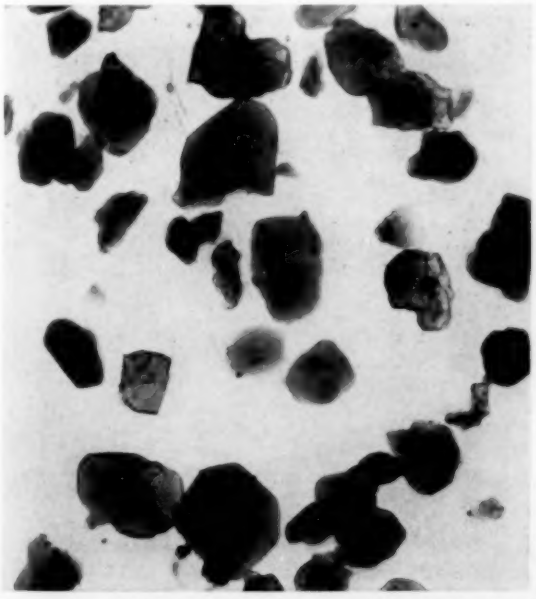

FIGURE 5. *Anhydrous chromium orthophosphate (α form) obtained by heating the hexahydrate at 1,500° C for 2 hours; ×140.*

of the α form is readily detected by the microscope because of its unusual pleochroism.

The α form was stable and unmelted up to 1,800° C, the limit of available furnaces.

TABLE 2. *d-Spacings and relative intensities of anhydrous chromium orthophosphate—β form*

d	*I*	*d*	*I*	*d*	*I*	*d*	*I*
4.30	74	2.03	5	1.621	5	1.337	6
3.88	41	1.975	37	1.531	12	1.319	6
3.51	95	1.938	20	1.502	5	1.290	10
3.27	51	1.845	4	1.484	4	1.268	14
2.58	50	1.808	6	1.473	16	1.202	12
2.48	100	1.760	28	1.443	7		
2.31	54	1.681	2	1.433	10		
2.15	5	1.637	20	1.383	37		

TABLE 3. *d-Spacings and relative intensities of anhydrous chromium orthophosphate—α form*

d	*I*	*d*	*I*	*d*	*I*	*d*	*I*
6.45	17	3.04	22	2.03	13	1.575	6
5.67	45	2.77	13	1.925	5	1.553	3
5.40	100	2.74	51	1.796	3	1.528	8
5.20	48	2.69	40	1.760	8	1.519	6
4.14	4	2.60	26	1.703	13	1.507	3
3.83	3	2.49	7	1.686	3	1.447	3
3.55	7	2.17	18	1.629	4	1.443	2
3.15	9	2.07	5	1.612	5		

5. Discussion

No evidence was found in this investigation for the existence of any crystalline hydrate of chromium orthophosphate other than the hexahydrate. The dehydration is not completed below 800° C because of the formation of an amorphous material that has an extremely large absorbing surface. The dehydration curves of Ness, Smith, and Evans [4] do not show sharp breaks as do compounds that form new crystal phases immediately following dehydration, but are much more gradual, which, it is believed, is typical of conditions when amorphous phases exist for some time before recrystallization.

The formation of an amorphous phase that exists over a wide temperature range is of special interest here. It is known that kaolinite forms such a phase between its decomposition at about 550° C and the formation of γAl_2O_3 at 980° C [8], and that certain other silicates, such as pyrophyllite [9], pass through an amorphous state. These compounds differ in two distinct ways from chromium orthophosphate hexahydrate. In these silicates the "water" is in the form of OH groups and is lost above 500° C, and the silicate groups are linked together with shared O atoms. In the case of $CrPO_4 \cdot 6H_2O$, however, it is reasonable to expect that the water is present as molecular water surrounding the Cr atoms, and the PO_4 groups are discrete unlinked groups.

Aluminum and iron orthophosphates have inversions and structures similar to those of silica [10]. It was at first thought that chromium orthophosphate was related to silica in an analogous manner, but no evidence was found to support this.

The formation of an unstable form of the anhydrous compound, when unground material is used, is evidence that the β form is more closely allied to the original structure than is the α form. When

the starting material is ground with an attendant increase in surface, it approaches equilibrium more rapidly and the β form is not obtained. It is apparent that the β form is not stable above 973° C.

The formation of a preliminary unstable phase is not an unusual occurrence; the formation of γAl_2O_3 in kaolinite is such a case [8]. When $3CaO.Al_2O_3.6H_2O$ is dehydrated, the first crystal phases formed are $12CaO.7Al_2O_3$ and CaO, whereas the final equilibrium compound is the single phase $3CaO.Al_2O_3$ [11]. Grim and Bradley [9] have noted the occurrence of various unstable phases in dehydration of clays and other silicates.

6. Summary

There is a single crystalline hydrate of chromium orthophosphate ($CrPO_4.6H_2O$) that is violet, platy, biaxial negative with $\alpha=1.568$, $\beta=1.591$, $\gamma=1.599$, and $2V=13°$.

This hydrate breaks down near 130° C to an amorphous material that retains some water up to 800° C.

If the original material is unstrained and coarse, it will recrystallize on heating at about 1,020° C to an unstable fine-grained $\beta CrPO_4$ with an average index of refraction of 1.908.

If the original hydrate is ground and thus strained, the material will form a stable compound ($\alpha CrPO_4$) that is highly pleochroic, biaxial negative with $\alpha=1.761$, $\gamma=1.844$, and $2V$ large.

7. References

[1] H. Allen, L. H. Hempelmann, Jr., and N. A. Womack, The effect of insoluble radiophosphorus (chromium phosphate) when applied interstitially in the treatment of adenocarcinoma of the mamma in mice, Cancer Research **5**, 239 (1945).

[2] A. F. Joseph and W. N. Rae, Chromium phosphate, J. Chem. Soc. **III**, 196 (1917).

[3] G. L. Clark and A. P. Tai, Phosphate coating of aluminum and polymorphism of chromium phosphate, Science **107**, 505 (1948).

[4] A. T. Ness, R. E. Smith, and R. L. Evans, The preparation and some properties of normal and radioactive chromic phosphate, J. Am. Chem. Soc. (publication pending).

[5] S. Speil, L. H. Berkelhamer, J. Pask, and B. Davies, Differential thermal analysis, U. S. Bureau of Mines Tech. Pap. 664 (1945).

[6] H. E. Swanson and E. Tatge, Standard X-ray diffraction patterns, J. Research NBS **46**, 318 (1951) RP2202.

[7] A. Van Valkenburg, Jr., and H. F. McMurdie, High-temperature X-ray diffraction apparatus, J. Research NBS **38**, 415 (1947) RP1782.

[8] H. Insley and R. H. Ewell, Thermal behavior of kaolin minerals, J. Research NBS **14**, 615 (1935) RP792.

[9] W. F. Bradley and R. E. Grim, High-temperature thermal effects of clay and related materials, Am. Mineral. **36**, 182 (1951).

[10] M. J. Buerger, Crystals based on the silica structure, Am. Mineral. **33**, 751 (1948).

[11] W. G. Schneider and T. Thorvaldson, The dehydration of tricalcium aluminate hexahydrate, Can. J. Research **19** [B], 123 (1941).

WASHINGTON, October 10, 1951.